

1 **Spatiotemporal variability and contribution of different aerosol**  
2 **types to the Aerosol Optical Depth over the Eastern Mediterranean**

3  
4 **Aristeidis K. Georgoulas<sup>1,2,3,\*</sup>, Georgia Alexandri<sup>4,5</sup>, Konstantinos A. Kourtidis<sup>5</sup>,**  
5 **Jos Lelieveld<sup>3,6</sup>, Prodromos Zanis<sup>1</sup>, Ulrich Pöschl<sup>2</sup>, Robert Levy<sup>7</sup>, Vassilis**  
6 **Amiridis<sup>8</sup>, Eleni Marinou<sup>4,8</sup>, Athanasios Tsikerdekis<sup>1</sup>**

7  
8 [1] Department of Meteorology and Climatology, School of Geology, Aristotle University of  
9 Thessaloniki, 54124, Thessaloniki, Greece

10 [2] Multiphase Chemistry Department, Max Planck Institute for Chemistry, D-55128, Mainz,  
11 Germany

12 [3] Energy, Environment and Water Research Center, The Cyprus Institute, Nicosia, Cyprus

13 [4] Laboratory of Atmospheric Physics, Physics Department, Aristotle University of  
14 Thessaloniki, 54124, Thessaloniki, Greece

15 [5] Laboratory of Atmospheric Pollution and Pollution Control Engineering of Atmospheric  
16 Pollutants, Department of Environmental Engineering, Democritus University of Thrace,  
17 67100, Xanthi, Greece

18 [6] Atmospheric Chemistry Department, Max Planck Institute for Chemistry, D-55128,  
19 Mainz, Germany

20 [7] Earth Science Division, NASA Goddard Space Flight Center, MD 20771, Greenbelt, USA

21 [8] Institute for Astronomy, Astrophysics, Space Application and Remote Sensing, National  
22 Observatory of Athens, 15236 Athens, Greece

23 *\* current address: Laboratory of Atmospheric Pollution and Pollution Control Engineering of*  
24 *Atmospheric Pollutants, Department of Environmental Engineering, Democritus University of*  
25 *Thrace, 67100, Xanthi, Greece*

26  
27 Correspondence to: A. K. Georgoulas (argeor@env.duth.gr)

28  
29 **Abstract**

30 This study characterizes the spatiotemporal variability and relative contribution of different  
31 types of aerosols to the Aerosol Optical Depth (AOD) over the Eastern Mediterranean as  
32 derived from MODIS Terra (3/2000-12/2012) and Aqua (7/2002-12/2012) satellite  
33 instruments. For this purpose, a 0.1° x 0.1° gridded MODIS dataset was compiled and

1 validated against sunphotometric observations from the AErosol RObotic NETwork  
2 (AERONET). The high spatial resolution and long temporal coverage of the dataset allows for  
3 the determination of local hot spots like megacities, medium sized cities, industrial zones, and  
4 power plant complexes, seasonal variabilities, and decadal averages. The average AOD at 550  
5 nm ( $AOD_{550}$ ) for the entire region is  $\sim 0.22 \pm 0.19$  with maximum values in summer and  
6 seasonal variabilities that can be attributed to precipitation, photochemical production of  
7 secondary organic aerosols, transport of pollution and smoke from biomass burning in Central  
8 and Eastern Europe, and transport of dust from the Sahara Desert and the Middle East. The  
9 MODIS data were analyzed together with data from other satellite sensors, reanalysis projects  
10 and a chemistry-aerosol-transport model using an optimized algorithm tailored for the region  
11 and capable of estimating the contribution of different aerosol types to the total  $AOD_{550}$ . The  
12 spatial and temporal variability of anthropogenic, dust and fine mode natural aerosols over  
13 land and anthropogenic, dust and marine aerosols over the sea is examined. The relative  
14 contribution of the different aerosol types to the total  $AOD_{550}$  exhibits a low/high seasonal  
15 variability over land/sea areas, respectively. Overall, anthropogenic aerosols, dust and fine  
16 mode natural aerosols account for  $\sim 51\%$ ,  $\sim 34\%$  and  $\sim 15\%$  of the total  $AOD_{550}$  over land,  
17 while, anthropogenic aerosols, dust and marine aerosols account  $\sim 40\%$ ,  $\sim 34\%$  and  $\sim 26\%$   
18 of the total  $AOD_{550}$  over the sea, based on MODIS Terra and Aqua observations.

19

## 20 **1 Introduction**

21 For more than fifteen years, two MODIS (Moderate Resolution Imaging Spectroradiometer)  
22 satellite sensors monitor tropospheric aerosols at a global scale on a daily basis. The retrieved  
23 aerosol optical properties have been used in numerous air quality studies as well as studies  
24 related to the effect of airborne particles on various climatic parameters (e.g. radiation, clouds,  
25 precipitation, etc.). The  $1^\circ \times 1^\circ$  daily gridded level-3 dataset is primarily used for global as well  
26 as regional studies while the single pixel level-2 data with a 10 km resolution (at nadir) are  
27 mostly used for regional and local scale studies. Nevertheless, the use of the coarse resolution  
28 MODIS data has predominated even in regional studies. The reasons for this could be the  
29 smaller file size which makes their processing and storage easier or the fact that they are easily  
30 accessible through user-friendly data bases which also allow for a very basic analysis like e.g.  
31 NASA's GIOVANNI website (<http://giovanni.gsfc.nasa.gov/giovanni/>) (Acker and Leptoukh,  
32 2007).

1 The same holds for studies focusing on the Mediterranean Basin, an area which is considered of  
2 particular sensitivity as far as air pollution and climate change is concerned (Lelieveld et al.,  
3 2002; Giorgi, 2006). The Mediterranean basin is one of the regions with highest aerosol optical  
4 depths (AODs) in the world (Husar et al., 1997; Ichocku et al., 2005; Papadimas et al., 2008),  
5 causing significant climate forcing especially in summer, which is characterized by low  
6 cloudiness and high incoming solar radiation levels (Papadimas et al., 2012; Alexandri et al.,  
7 2015). The Mediterranean is also recognized as a crossroads between three continents where  
8 aerosols of various types accumulate (Lelieveld et al., 2002). Marine aerosols from the  
9 Mediterranean Sea and even the Atlantic Ocean combine with aerosols from continental Europe  
10 (urban and rural), dust particles transported from the Sahara Desert and Middle East as well as  
11 biomass burning aerosols from occasional wild fires and agricultural burning (Lelieveld et al.,  
12 2002). Specifically, as discussed in Hatzianastassiou et al. (2009), Eastern Mediterranean, the  
13 region under investigation here, is located at a "key" point of this crossroads. There is a  
14 significant number of ground and satellite-based studies on the abundance and optical properties  
15 of tropospheric aerosols in the area; however, these studies are either focused on specific spots  
16 or used a coarse spatial and temporal resolution.

17 The ground-based instrumentation used in studies focusing on the aerosol load and optical  
18 properties over the Eastern Mediterranean includes active and passive sensors such as Lidars  
19 (e.g. Papayannis and Balis, 1998; Balis et al., 2004; Papayannis et al., 2005, 2009; Amiridis et  
20 al., 2005, 2009; Mamouri et al., 2013; Kokkalis et al., 2013; Nisantzi et al., 2015), Cimel  
21 sunphotometers (e.g. Israelevich et al., 2003; Kubilay et al., 2003; Derimian et al., 2006;  
22 Kalivitis et al., 2007; Kelektsoğlu and Rapsomanikis, 2011; Nikitidou and Kazantzidis, 2013),  
23 Brewer spectrophotometers (e.g. Kazadzis et al., 2007; Koukouli et al., 2010), Multi-Filter  
24 Radiometers (e.g. Gerasopoulos et al., 2009, 2011; Kazadzis et al., 2014), ceilometers (e.g.  
25 Tsaknakis et al., 2011), Microtops sunphotometers (e.g. El-Metwally and Alfaro, 2013), etc.  
26 However, these and other studies not referenced here either refer to specific spots with the  
27 majority of the ground stations being situated in large urban centers (e.g. Athens, Thessaloniki,  
28 Cairo) or to specific events (e.g. Sahara dust intrusions, biomass burning events, etc.).

29 On the other hand, AOD and other aerosol optical properties have been studied over the greater  
30 Eastern Mediterranean region based on data from Meteosat (Moulin et al., 1998), SeaWIFS  
31 (Koren et al., 2003; Antoine and Nobileau, 2006; Mélin et al., 2007; Nabat et al., 2013), TOMS  
32 (Alpert and Ganor, 2001; Israelevich et al., 2002; Koukouli et al. 2006; Hatzianastassiou et al.,  
33 2009; Koukouli et al., 2010, Israelevich et al., 2012, Kaskaoutis et al., 2012a; Nabat et al., 2013;

1 Gkikas et al., 2013, 2014; Varga et al., 2014), MODIS Terra and Aqua (Barnaba and Gobbi,  
2 2004; Papayannis et al., 2005; Kaskaoutis et al., 2007, 2008, 2010, 2011, 2012a,b,c,d;  
3 Kosmopoulos et al., 2008; Papadimas et al., 2008, 2009; Rudich et al., 2008; Carmona and  
4 Alpert, 2009; Karnieli et al., 2009; Gkikas et al., 2009, 2013; Hatzianastassiou et al., 2009; El-  
5 Metwally et al., 2010; Koukouli et al., 2010; Kanakidou et al., 2011; Gerasopoulos et al., 2011;  
6 de Meij and Lelieveld, 2011; Marey et al., 2011; de Meij et al., 2012; Nabat et al., 2012, 2013;  
7 Nikitidou and Kazantzidis, 2013; Athanasiou et al., 2013; Benas et al., 2011, 2013; Sorek-  
8 Hamer et al., 2013; Kabatas et al., 2014; Kourtidis et al., 2014; Mishra et al., 2014; Flaounas et  
9 al., 2015; Kloog et al., 2015), OMI/AURA (Kaskaoutis et al., 2010; El-Metwally et al., 2010;  
10 Marey et al., 2011; Kaskaoutis et al., 2012b,c, Gkikas et al., 2013, 2014; Sorek-Hamer et al.,  
11 2013; Varga et al., 2014; Flaounas et al., 2015), CALIOP/CALIPSO (Amiridis et al., 2009,  
12 2013, Mamouri et al., 2009; Marey et al., 2011; Kaskaoutis et al., 2012c; de Meij et al., 2012;  
13 Nabat et al., 2012, 2013; Mamouri and Ansmann, 2015), MISR/Terra (Kanakidou et al., 2011;  
14 Marey et al., 2011; de Meij and Lelieveld, 2011; de Meij et al., 2012; Nabat et al., 2013;  
15 Kabatas et al., 2014; Abdelkader et al., 2015) as well as NOAA/AVHRR, MERIS/ENVISAT,  
16 AATSR/ENVISAT, PARASOL/POLDER, MSG/SEVIRI, and Landsat satellite data (see  
17 Retalis and Sifakis, 2010; Nabat et al., 2013; Benas et al., 2013; Sifakis et al., 2014). To our  
18 knowledge, these studies comprise the majority of work focusing on tropospheric aerosols over  
19 the Eastern Mediterranean by means of satellite remote sensing, published in peer reviewed  
20 journals the last ~ 15 years. As shown in Fig. 4 of this work, the publication rate of satellite-  
21 based studies focusing on the Eastern Mediterranean aerosols nearly doubled every three years  
22 during the period 1997-2014 which is indicative of the increasing scientific interest in the area.  
23 In a very large fraction of the satellite-based studies referenced above, the used data are either of  
24 coarse mode (usually  $1^\circ$  which is ~ 100 km for the mid-latitudes) or focus on specific spots for  
25 validation purposes. In a few cases, high resolution data were used in spatiotemporal studies;  
26 however, either these studies are restricted over surfaces covered by water or examine a short  
27 period only. For example, Moulin et al. (1998) investigated the dust AOD patterns over the  
28 oceanic areas of the Mediterranean Basin at a resolution of  $35 \times 35 \text{ km}^2$  for a period of 11 years  
29 (1984-1994) using Meteosat observations. A 7-year climatology (1998-2004) of total and dust  
30 AOD for the same regions at a resolution of  $0.16^\circ \times 0.16^\circ$  was compiled by Antoine and  
31 Nobileau (2006) using observations from SeaWIFS. Mélin et al. (2007) merged SeaWIFS and  
32 MODIS data and presented high resolution AOD patterns ( $2 \times 2 \text{ km}^2$ ) for May 2003. As far as  
33 MODIS is concerned, only Barnaba and Gobbi (2004) presented a high resolution ( $0.1^\circ \times 0.1^\circ$ )

1 spatiotemporal analysis for a period of 1 year (2001) over sea only. In a recent paper,  
2 Athanasiou et al. (2013) presented in detail a method for compiling a 0.5-degree resolution  
3 AOD gridded dataset using level-2 MODIS Terra data for the greater region of Greece (2000-  
4 2008). However, the spatial resolution they used ( $\sim 50$  km) is not high enough to reveal local  
5 sources (e.g. cities, islands, river banks, etc.). Overall, there has not been so far any detailed  
6 high resolution spatiotemporal study of the AOD over the Eastern Mediterranean.

7 In this paper, the  $AOD_{550}$  spatiotemporal variability over the Eastern Mediterranean ( $30^{\circ}N$ -  
8  $45^{\circ}N$ ,  $17.5^{\circ}E$ - $37.5^{\circ}E$ ) is presented at a high spatial resolution ( $0.1^{\circ} \times 0.1^{\circ}$ ) based on MODIS  
9 Terra and Aqua observations. Level-2 MODIS data are used for the compilation of a 0.1-degree  
10 gridded dataset which is validated against ground-based observations. In order to calculate the  
11 contribution of different aerosol types to the total AOD, the MODIS data were analyzed  
12 together with other satellite data, ERA-Interim reanalysis data and the Goddard Chemistry  
13 Aerosol Radiation and Transport (GOCART) model using an algorithm optimized for the  
14 surface properties of the Eastern Mediterranean region. The different datasets used in this  
15 research are presented in detail in Sect. 2 while a detailed description of the method is given in  
16 Sect. 3. Sect. 4 includes the results from the MODIS validation procedure, the annual and  
17 seasonal variability of  $AOD_{550}$  over the region with a discussion on the local aerosol sources  
18 and the differences between Terra and Aqua, and the annual and seasonal contribution of  
19 different aerosol types to the total  $AOD_{550}$ . Finally, in Sect. 5, the main conclusions of the paper  
20 are presented along with a short discussion on how these results could contribute to future  
21 studies in the area.

22

## 23 **2 Observations, reanalysis data and model simulations**

### 24 **2.1 MODIS Terra and Aqua satellite observations**

25 The main data used in this work come from the level-2 MODIS Terra (MOD04\_L2) and  
26 MODIS Aqua (MYD04\_L2) Collection 051 dataset and have been acquired through NASA's  
27 Level 1 and Atmosphere Archive and Distribution System (LAADS)  
28 (<http://ladsweb.nascom.nasa.gov>). The fact that MODIS Terra and Aqua have a daytime  
29 equator crossing time at 10:30 LT (morning) and 13:30 LT (noon), respectively. MODIS  
30 instruments with a viewing swath of 2330 km measure backscattered radiation at 36 spectral  
31 bands between 0.415 and 14.235  $\mu m$  with a spatial resolution of 250, 500 and 1000 m,  
32 providing a nearly global coverage on a daily basis. Aerosol optical properties for the  
33 standard MODIS aerosol product are retrieved using two different "Dark Target" (DT)

1 algorithms. The one is used over land surfaces (Kaufman et al., 1997; Levy et al., 2007a, b;  
2 Remer et al., 2005; Levy et al., 2010) and the other over oceanic regions (Tanré et al., 1997;  
3 Levy et al., 2003; Remer et al., 2005). The "Deep Blue" algorithm (DB) (Hsu et al., 2004;  
4 Hsu et al., 2006) has been used for retrievals over bright land surfaces (e.g. deserts) where the  
5 DT algorithm fails. Only recently, updates to the algorithm allowed for extending the spatial  
6 coverage of the DB aerosol product over all land areas (Hsu et al., 2013; Sayer et al., 2013;  
7 2014). AERONET Cimel sunphotometric measurements have been extensively used for the  
8 validation of the MODIS over-land and over-ocean products (e.g. Chu et al., 2002; Remer et  
9 al., 2002; Remer et al., 2005; Levy et al., 2010; Shi et al., 2013).

10 In this work, AOD<sub>550</sub> over both land and sea and the Fine Mode Ratio (FMR<sub>550</sub>) over sea from  
11 Collection 051 were used at a spatial resolution of 10 km (at nadir). The uncertainty of the  
12 MODIS aerosol optical depth has been estimated at  $\pm(0.05+0.15AOD)$  over land (Chu et al.,  
13 2002; Levy et al., 2010) and  $\pm(0.03+0.05AOD)$  over ocean (Remer et al., 2002) relative to the  
14 AERONET AOD. Specifically, for the DT data used in this work only high quality retrievals  
15 are used over land. This means that the data have a Quality Assurance Confidence (QAC) flag  
16 equal to 3 (high confidence). For retrievals over sea we use data with a QAC flag of 1  
17 (marginally good), 2 (good) and 3 (see Levy et al., 2009 for details). The pre-launch  
18 uncertainty of FMR<sub>550</sub> is  $\pm 30\%$  over ocean (Remer et al., 2005) while over land this  
19 parameter is by no means trustworthy and should only be used in qualitative studies (e.g. see  
20 Georgoulias and Kourtidis, 2011). In cases where DT algorithm does not provide products  
21 over land, especially over bright arid and semi-arid regions of North Africa, AOD<sub>550</sub> values  
22 from the DB algorithm are used in our work. The expected uncertainty of the DB product  
23 used here is  $\pm(0.05+0.2AOD)$  relative to the AERONET AOD (Hsu et al., 2006). The  
24 analyzed datasets cover the period from 3/2000 to 12/2012 for Terra and from 7/2002 to  
25 12/2012 for Aqua MODIS covering the region of the Eastern Mediterranean. The Collection  
26 051 DB data for Terra are available only until 12/2007 due to calibration issues; nevertheless,  
27 these data are carefully used within our analysis to get a complete image of the aerosol load  
28 over the region.

29

## 30 **2.2 AERONET ground-based observations**

31 For the evaluation of the MODIS AOD<sub>550</sub>, data from 13 AERONET Cimel network ground  
32 stations in the region of the Eastern Mediterranean have been acquired  
33 (<http://aeronet.gsfc.nasa.gov>). The stations were selected such that their operation period

1 covers at least 2 years and there are at least 100 common days of co-localized AERONET and  
2 MODIS observations. AERONET Cimel sunphotometers measure solar radiation every 15  
3 minutes within the spectral range from 340 to 1020 nm (Holben et al., 2001). The spectral  
4 measurements allow for the retrieval of columnar aerosol properties (see Holben et al., 1998;  
5 Dubovik and King, 2000; Dubovik et al., 2000, 2002). The AERONET AOD uncertainty is in  
6 the order of 0.01-0.02 (Eck et al., 1999), being larger at shorter wavelengths. Here, we use  
7 quadratic fits on a log-log scale to interpolate the AERONET data (AODs at 440, 500, 675  
8 and 870 nm) to the MODIS band-effective wavelength of 550 nm (Eck et al., 1999; Levy et  
9 al., 2010). So, we can directly compare the MODIS AOD<sub>550</sub> retrievals against AERONET  
10 observations. Simultaneous measurements of the Ångström Exponent (AE) for the spectral  
11 range 440-870 nm (AE<sub>440-870</sub>) from the 13 AERONET stations mentioned above were also  
12 utilized in this work in order to account for days with dust dominance. The uncertainty of the  
13 AE is significantly higher than the AOD uncertainty, especially under low-AOD conditions.  
14 Li et al. (2014) found that the uncertainty for a typical Northern Hemispheric AERONET  
15 station (GSFC) is  $\sim 0.6$  during winter when AODs are significantly lower compared to  
16 summer ( $\sim 0.15$ ).

17

### 18 **2.3 LIVAS CALIOP/CALIPSO dust climatology**

19 Dust aerosol optical depths at 532 nm (AOD<sub>532</sub>) from CALIOP/CALIPSO (Cloud-Aerosol  
20 Lidar with Orthogonal Polarization instrument aboard Cloud-Aerosol Lidar and Infrared  
21 Pathfinder Satellite Observations satellite) at a resolution of  $1^\circ \times 1^\circ$  are also used here for the  
22 period 2007-2012. CALIPSO measures cloud and aerosol properties flying at a 705 km sun  
23 synchronous polar orbit with a 16 day repeat cycle and an equator-crossing time close to that  
24 of the Aqua satellite (13:30 LT). The dust product used here comes from a Saharan-dust-  
25 optimized retrieval scheme that was developed within the framework of the LIVAS (Lidar  
26 Climatology of Vertical Aerosol Structure for Space-Based LIDAR Simulation Studies)  
27 project (Amiridis et al. 2015) and has been presented in detail in Amiridis et al. (2013). In  
28 brief, the LIVAS dust product is optimized for Europe by applying a lidar ratio of 58 sr  
29 instead of 40 sr to Level 2 dust related backscatter products. This correction results to an  
30 improvement of the AOD<sub>532</sub> product. Comparison against spatially and temporally co-located  
31 AERONET observations (Amiridis et al., 2013) returned an absolute bias of  $\sim -0.03$ . The  
32 corresponding reported biases for the original CALIPSO data are significantly higher ( $\sim -$   
33 0.10). The bias is even lower when compared against MODIS satellite-based observations.

1 Other improvements of this product are related to the use of a new methodology for the  
2 calculation of pure dust extinction from dust mixtures and the application of an averaging  
3 scheme that includes zero extinction values for the non-dust aerosol types detected. Overall,  
4 this product (hereafter denoted as LIVAS dust product) exhibits better agreement with  
5 observations from MODIS and AERONET and simulations from the BSC-DREAM8b dust  
6 model over North Africa and Europe than the standard CALIPSO data hence being an ideal  
7 tool for the evaluation of other satellite-based products.

8

#### 9 **2.4 Earth Probe TOMS and OMI satellite observations**

10 For this work, UV Aerosol Index (AI) data (Herman et al., 1997) from the Earth Probe TOMS  
11 (Total Ozone Mapping) spectrometer aboard Earth Probe for the period 1/2000-9/2004 at a  
12 resolution of  $1^\circ$  (latitude)  $\times$   $1.25^\circ$  (longitude) and the OMI (Ozone Monitoring Instrument)  
13 sensor aboard EOS AURA for the period 10/2004-12/2012 at a resolution of  $1^\circ \times 1^\circ$  were  
14 acquired through the GIOVANNI web database (<http://giovanni.gsfc.nasa.gov/giovanni/>).  
15 Earth Probe TOMS continued the record of the first three TOMS instruments aboard Nimbus-  
16 7, Meteor-3 and ADEOS flying in a sun synchronous orbit at an altitude of 740 km with an  
17 instantaneous field of view size of  $39 \times 39 \text{ km}^2$  at nadir. The instrument had an ascending  
18 node equator crossing time at 12:00 LT covering 85 % of the globe on a daily basis from  
19 7/1996 until 12/2005. The satellite was originally set to a 500 km sun synchronous orbit but  
20 was set to its final orbit after the failure of ADEOS satellite in 6/1997. OMI is a UV/VIS  
21 nadir solar backscatter spectrometer (Levelt et al., 2006) that continues the long TOMS  
22 record. OMI flies in a sun synchronous polar orbit at an altitude of 705 km with an ascending  
23 node equator crossing time at 13:45 LT. Its 2600 km viewing swath allows for almost daily  
24 global coverage while the spatial resolution of the instrument is  $13 \times 24 \text{ km}^2$  at nadir. The AI  
25 (also known as Absorbing Aerosol index) which is calculated by the two instruments  
26 constitutes a qualitative indicator of the presence of UV absorbing aerosols in the atmosphere  
27 such as biomass burning and dust (Torres et al., 1998). Positive AI values generally represent  
28 absorbing aerosols while small or negative values represent non-absorbing aerosols. The  
29 Version 8 algorithm is applied to spectral measurements from both TOMS and OMI sensor to  
30 produce a consistent long-term AI timeseries (Li et al., 2009). AI is calculated from the  
31 difference in surface reflectivity derived from the 331.2 and 360 nm measurements exhibiting  
32 an uncertainty of  $\pm 30 \%$  (Torres et al., 2007).

33



## 2.5 ERA-Interim reanalysis data

Wind speed (ws) data at 10 m above surface from the ERA-Interim reanalysis (Dee et al., 2011) are used for 9:00 and 12:00 UTC on a daily basis for the period 2000-2012. We use 9:00 and 12:00 UTC data in order to be closer to the Terra and Aqua overpass time in the area, respectively. The various ERA-Interim reanalysis fields are produced by ECMWF's Integrated Forecast System (IFS) assimilating satellite and ground-based observations. The system includes a 4-D variational analysis with a 12-hour analysis window. The spatial resolution of the ERA-Interim data is  $\sim 79$  km with 60 vertical levels from the surface up to 0.1 hPa while the data can be acquired at various resolutions (in this work  $1^\circ \times 1^\circ$ ) through ECMWF's website (<http://apps.ecmwf.int/datasets/data/interim-full-daily/>). Over ocean, the 10 m ERA-interim wind speed exhibits a bias of less than -0.5 m/s compared to quality-controlled in situ observations on a global scale (Dee et al., 2011). Specifically, for the region of the Eastern Mediterranean examined here, the 10 m ERA-interim wind speed exhibits a bias of -0.96 m/s (-16 %) compared to satellite-based observations from QuikSCAT (Hermann et al., 2011).

## 2.6 MACC reanalysis data

The daily MACC total and dust AOD<sub>550</sub> data for the period 2003-2012 come from the aerosol analysis and forecast system of ECMWF which consists of a forward model (Morcrette et al., 2009) and a data-assimilation module (Benedetti et al., 2009). AOD<sub>550</sub> measurements from the two MODIS instruments aboard Terra and Aqua are assimilated by the MACC forecasting system through a 4D-Var assimilation algorithm to produce the aerosol analysis, leading to an improved AOD representation compared to observations (see Benedetti et al., 2009; Mangold et al., 2011). Five aerosol species are included within MACC, namely, mineral dust, sea salt, sulfates, black carbon and organic matter. Three different size bins are used for mineral dust and sea salt particles while the black carbon and organic material are distributed to a hydrophilic and a hydrophobic mode. Dust and sea salt emissions are given as a function of surface wind speed, while the emissions of the other species are taken from inventories. The spatial resolution of the MACC reanalysis data is  $\sim 79$  km with 60 vertical levels from the surface up to 0.1 hPa and can be acquired through: <http://apps.ecmwf.int/datasets/data/macc-reanalysis/> for the period 2003-2012. The MACC total and dust AODs have been evaluated against ground and satellite-based observations (see Elguindi et al., 2010; Bellouin et al., 2013; Inness et al., 2013; Cesnulyte et al., 2014; Cuevas et al., 2015) showing that the MACC

1 aerosol products generally capture well the daily, seasonal and interannual variability of  
2 aerosols. As discussed in Bellouin et al. (2013) the uncertainties of MACC total AOD<sub>550</sub> (~  
3 0.03) and dust AOD<sub>550</sub> (~ 0.014) arise from uncertainties in the MODIS retrievals which are  
4 assimilated into the model and errors in the forward modeling of total and component AODs.  
5

## 6 **2.7 GOCART data**

7 Daily total and dust AOD<sub>550</sub> data from the GOCART chemistry-aerosol-transport model  
8 simulations (version 006) are used in this study for the period 2000-2007. The GOCART  
9 model (see Chin et al., 2000, 2002, 2004, 2007; Ginoux et al., 2001, 2004) uses the  
10 assimilated meteorological fields of the Goddard Earth Observing System Data Assimilation  
11 System (GEOS DAS) which are generated by the Goddard Global Modeling and Assimilation  
12 Office (GMAO). The data which are used were acquired from an older version of NASA's  
13 GIOVANNI web database (<http://disc.sci.gsfc.nasa.gov/giovanni/>) and come from a  
14 simulation implemented at a spatial resolution of 2° (latitude) x 2.5° (longitude) with 30  
15 vertical sigma layers (Chin et al., 2009). The model includes physicochemical processes of  
16 major tropospheric aerosol components (sulfates, dust, black carbon, organic carbon, sea salt)  
17 and precursor gases (SO<sub>2</sub> and dimethylsulfide) incorporating various atmospheric processes.  
18 The total AOD<sub>550</sub> from GOCART compared to ground-based observations from the  
19 AERONET exhibits a relative mean bias [mean(GOCART)/mean(AERONET)] of 1.120,  
20 1.135 and 0.959 over Europe, North Africa and for the whole globe, respectively.  
21

## 22 **2.8 Ancillary data**

23 Apart from the primary datasets presented above, three additional datasets were used in order  
24 to support our findings. OMI/AURA daily gridded (Bucsela et al., 2013) tropospheric NO<sub>2</sub>  
25 columnar data (OMNO2d version 2.1) at a spatial resolution of 0.25° x 0.25° were acquired  
26 from NASA's GIOVANNI web database (<http://giovanni.gsfc.nasa.gov/giovanni/>) for the  
27 period 2005-2012. The quality checked data used in this work correspond to sky conditions  
28 where cloud fraction is less than 30 %. Planetary boundary layer (PBL) SO<sub>2</sub> daily gridded  
29 columnar data (OMSO2e version 1.1.7) were also acquired from GIOVANNI for the same  
30 period. The OMSO2e gridded data (0.25° x 0.25°) used in this work are produced from best  
31 level-2 pixel data, screened for OMI row anomaly and other data quality flags. The PBL SO<sub>2</sub>  
32 column retrievals are produced with an algorithm based on principal component analysis  
33 (PCA) of the OMI radiance data (Li et al., 2013). Finally, monthly precipitation data from the

1 3B43 TRMM and Other Sources Monthly Rainfall Product (version 7) at a spatial resolution  
2 of  $0.25^\circ \times 0.25^\circ$  for the period 2000-2012 were obtained from GIOVANNI. This dataset is  
3 derived from 3-hourly precipitation retrievals from the Precipitation Radar (PR), the TRMM  
4 Microwave Imager (TMI) and the Visible and Infrared Scanner (VIRS) aboard the TRMM  
5 (Tropical Rainfall Monitoring Mission) satellite merged with other satellite-based  
6 precipitation data and the Global Precipitation Climatology Centre (GPCC) rain gauge  
7 analysis (Huffman et al., 2007).

### 8 9 **3 Methodology**

#### 10 **3.1 Compiling a MODIS $0.1^\circ \times 0.1^\circ$ gridded dataset**

11 To investigate the spatial and temporal variability of aerosols over the Eastern Mediterranean  
12 we first created a  $0.1^\circ \times 0.1^\circ$  daily gridded aerosol dataset using single pixel level-2 AOD<sub>550</sub> and  
13 FMR<sub>550</sub> data from MODIS Collection 051. The same resolution has been utilized in previous  
14 studies (e.g. Barnaba and Gobbi, 2004) in the region; however, without reporting on the  
15 gridding methodology followed. In this work we present a gridding methodology that could be  
16 used as a reference for future regional studies. The methodology has been successfully applied  
17 in the past on level-2 MODIS Terra data in different cases studies, e.g. in order to examine the  
18 weekly cycle patterns of AOD<sub>550</sub> over the region of Central Europe and the aerosol load  
19 changes observed over a cement plant in Greece due to changes in the deposition practices of  
20 the primary materials (see Georgoulas and Kourtidis, 2012; Georgoulas et al., 2012; Kourtidis  
21 et al., 2014). In the following lines we proceed to a detailed description of the method  
22 underlining the potential of being used in detailed quantitative studies like this one.

23 First, a  $0.1^\circ \times 0.1^\circ$  resolution grid covering the Eastern Mediterranean ( $30^\circ\text{N}$ - $45^\circ\text{N}$ ,  $17.5^\circ\text{E}$ -  
24  $37.5^\circ\text{E}$ ) is defined which corresponds to 30000 grid cells. As already mentioned in Sect. 2.1,  
25 only level-2 single pixel AOD<sub>550</sub> measurements with a QAC flag of 3 and a QAC flag greater  
26 than 0 were used over land and over sea, respectively, to ensure the high quality of the data.  
27 Pixels are attributed to a specific grid cell if their center falls within a  $25 \times 25 \text{ km}^2$  square  
28 window around the grid cell (see Fig. S1 in the Supplement). These pixels are then used for the  
29 calculation of daily averages. As shown in Figure S1, a grid cell of  $0.1^\circ$  ( $\sim 10 \text{ km}$ ) is as big as  
30 the centre of a large Mediterranean city like Thessaloniki, Northern Greece ( $\sim 1$  million  
31 inhabitants). The procedure was followed separately for MODIS Terra and Aqua data. In cases  
32 of grid cells with no DT MODIS observations, data from the DB algorithm were used (over

1 bright arid and semi-arid regions of North Africa) constituting only a small part of the gridded  
2 dataset.

3 The size of the gridding window was selected following Koukouli et al. (2007). They used both  
4 10 and 25-km windows showing that the latter allows for the inclusion of more data points  
5 without undermining the ability of monitoring accurately the aerosol load over a specific spot.  
6 In addition, in cases of urban sites, a window of 25 km allows for the inclusion of pixels from  
7 the surrounding non-urban surfaces where the MODIS surface reflectance parameterization is  
8 better (Levy et al., 2010). The size of each MODIS pixel is 10 km at nadir, but at the swath  
9 edges, it may become 2-3 times larger. Hence, ideally the maximum number of pixels that could  
10 be used in the daily averaging is nine. The overlap between the windows of neighbouring grid  
11 cells does not affect the representativeness of the dataset over each grid cell. Aerosols are  
12 transported by air masses throughout the day and thus the aerosol load in neighbouring grid  
13 cells is not expected to be completely independent.

14 In order to make sure that the use of a 25-km gridding window is optimal for capturing local  
15 pollution sources we repeated the same procedure for bigger gridding windows (50-km, 75km  
16 and 100-km) using MODIS Terra AOD<sub>550</sub> data for the year 2004. Numerous aerosol hot spots  
17 cannot be seen as the gridding window becomes bigger and there is a significant smoothing of  
18 the aerosol patterns mainly over land (Fig. S2). The use of the MODIS gridded dataset in the  
19 detection of local aerosol hot spots is discussed in more detail in Sect. 4. In addition, we  
20 conducted a detailed validation of the MODIS data against sunphotometric data from a total of  
21 13 AERONET stations in the region (see Fig. 1). The validation procedure was repeated several  
22 times for different spatial collocation windows which were equal to the windows used for the  
23 gridding procedure (i.e. 25, 50, 75 and 100-km) and for different data quality criteria. The  
24 results of the validation procedure are presented in Sect. 4.1 while part of them is given in the  
25 Supplement of this manuscript (see Table S2). Overall, it is shown that the gridding  
26 methodology followed here offers the best compromise for studying the spatial variability of  
27 aerosols on a regional or local scale, preserving at the same time the representativeness of the  
28 real aerosol load over each specific spot.

29 In order to generalize our results, nine different sub-regions (Fig. 1) were selected apart from  
30 the three basic regions of interest, namely, the whole Eastern Mediterranean (EMT) and the land  
31 (EML) and oceanic (EMO) areas of the region. The selection was done mainly taking into  
32 account geographical but also land type and land use criteria. The four sub-regions that  
33 correspond to the land regions of the Eastern Mediterranean are the Northern Balkans Land

1 (NBL), the Southern Balkans Land (SBL), the Anatolia Land (ANL) and the Northern Africa  
2 Land (NAL) region while the five sub-regions that correspond to the oceanic regions are the  
3 Black Sea Oceanic (BSO), the North-Western Oceanic (NWO), the South-Western Oceanic  
4 (SWO), the North-Eastern Oceanic (NEO) and the South-Eastern Oceanic (SEO) region. Mean  
5 values of the total  $AOD_{550}$  from the Terra and Aqua MODIS are reported for each one of the  
6 three basic regions of interest and their nine sub-regions in Sect. 4.

7

## 8 **3.2 Contribution of different aerosol types to $AOD_{550}$**

### 9 **3.2.1 Sea**

10 In order to quantify the contribution of different types of aerosols to the total  $AOD_{550}$  we  
11 followed a different approach for sea and land. This is due to the lack of reliable  $FMR_{550}$   
12 retrievals over land (e.g. see Levy et al., 2010; Georgoulias and Kourtidis, 2011) which are  
13 crucial for the algorithms used in this work. Over the sea we utilize wind speed data at 10 m  
14 above surface from the ERA-Interim reanalysis, AI data from TOMS and OMI along with  
15  $AOD_{550}$  and  $FMR_{550}$  from the MODIS Terra and Aqua gridded datasets presented above. All the  
16 datasets were brought to the same 0.1 degree spatial resolution as MODIS by using bilinear  
17 interpolation. In the case of TOMS and OMI we used monthly mean AI data following Bellouin  
18 et al. (2008) in order to avoid gaps especially during the TOMS period.

19 In general, the algorithm used over the oceanic regions (see Fig. 2) is similar with the one  
20 presented in Bellouin et al. (2008). First, the marine  $AOD_{550}$  ( $\tau_m$ ) is calculated from near surface  
21 wind speed using a linear relation which has been obtained from ground-based studies over  
22 pollution free oceanic regions. Bellouin et al. (2008) use the linear relation of Smirnov (2003).  
23 Then, if  $\tau_m$  is greater or equal than  $AOD_{550}$  it is assumed that there are marine particles only  
24 over this region. If  $\tau_m$  is smaller than  $AOD_{550}$  a decision tree is followed which is first based on  
25  $FMR_{550}$  and then on AI in order to reach a conclusion about the type of aerosols that account for  
26  $AOD_{550}$ . If  $FMR_{550}$  is smaller than the critical value of 0.35 and AI is greater than or equal to a  
27 critical value it is assumed that there are both marine aerosols ( $\tau_m$ ) and dust ( $\tau_d=AOD_{550}-\tau_m$ )  
28 while if AI is smaller than this critical value it is assumed that there are marine aerosols only.  
29 The AI critical value is equal to 1 in Bellouin et al. (2008). If  $FMR_{550}$  is greater than or equal to  
30 0.83 it is assumed that there are both anthropogenic ( $\tau_a=AOD_{550}-\tau_m$ ) and marine aerosols ( $\tau_m$ ).  
31 In the occasion of having a  $FMR_{550}$  equal to 0.35 or greater than 0.35 but smaller than 0.83 one  
32 has to take again AI into consideration. If AI is less than the critical value it is assumed that  
33 there are marine aerosols ( $\tau_m$ ) only while in the opposite occasion it is assumed that all the three

1 types of aerosols that can be defined over oceanic regions by this algorithm, namely, dust  
2 [ $\tau_d=(1-FMR_{550})(AOD_{550}-\tau_m)$ ], anthropogenic [ $\tau_a=FMR_{550}(AOD_{550}-\tau_m)$ ] and marine aerosols ( $\tau_m$ )  
3 are present. One should keep in mind that all the biomass burning aerosols are classified as  
4 anthropogenic by this method.

5 In this work, we proceeded to a "fine-tuning" of the algorithm for the region of the Eastern  
6 Mediterranean. First, we applied the algorithm on MODIS Terra data using the same equations  
7 and critical values as in Bellouin et al. (2008). The results showed that the original Bellouin et  
8 al. (2008) method might be valid for global studies but for a "closed" sea like the Mediterranean  
9 the method leads to a large overestimation of sea salt AODs and therefore underestimation of  
10 dust and anthropogenic aerosol AODs. Indicative of this situation is Fig. S3 in the Supplement  
11 where we present the relative contribution of dust, marine and anthropogenic aerosols per  
12 month over the oceanic regions of the Eastern Mediterranean as calculated using the original  
13 Bellouin et al. (2008) method. It is shown that the marine contribution is several times higher  
14 than the values reported for the Mediterranean Basin in previous studies (e.g. see Nabat et al.,  
15 2012). Evaluation of the algorithm was done using dust AOD<sub>532</sub> data from the LIVAS  
16 CALIOP/CALIPSO product. From LIVAS we only use the high quality Sahara dust product as  
17 a reference and not other aerosol type retrievals (e.g. marine aerosols) since the dust retrievals  
18 from CALIOP/CALIPSO are by far the most reliable (e.g. Burton et al., 2013). We performed  
19 several tests by changing the linear relation that connects  $\tau_m$  with near surface wind speed and  
20 the AI critical values and compared each time the dust AOD<sub>550</sub> seasonal variability with the  
21 LIVAS AOD<sub>532</sub> seasonal variability for the sea covered sub-regions of the Eastern  
22 Mediterranean. Results from this algorithm-tuning procedure can be found in Figs. S4e-i of the  
23 Supplement where one can also see the underestimation of dust AOD<sub>550</sub> from the original  
24 Bellouin et al. (2008) algorithm.

25 The linear relation given in Kaufman et al. (2005) was finally selected ( $\tau_m=0.007ws+0.02$ ). The  
26 2000-2012 average wind speed over the sea for the region of the Eastern Mediterranean is  $\sim 5.3$   
27 m/s. Kaufman et al. (2005) reduced the offset in the linear relation of Smirnov (2003) from 0.06  
28 to 0.02 to fit the average baseline AOD of 0.06 for the typical wind speed of 6 m/s. In addition,  
29 our tests showed that an AI critical value of 1 performs well over the region of the Eastern  
30 Mediterranean. The results did not change significantly when using other AI thresholds (e.g. 0.5  
31 which is suggested in Jones and Christopher, 2011) and therefore we decided to adopt 1 as the  
32 AI critical value. Another test, following the example of other studies (see Lehahn et al., 2010),  
33 was to assume that for wind speed less than 5 m/s there is very little or no sea-spray particle

1 production (limited bursting of entrained air bubbles associated with whitecap formation). In  
2 this case,  $\tau_m$  is stable, equal to the offset of the linear relation between  $\tau_m$  and wind speed which  
3 is indicative of the background sea salt AOD<sub>550</sub>. However, this test reveals that the effect of  
4 assuming stable  $\tau_m$  for wind speed less than 5 m/s is insignificant and therefore we selected to  
5 follow the Kaufman et al. (2005) linear relationship for the whole wind speed range. As shown  
6 in Figs. S4e-i, the seasonal variability when applying our modified algorithm over oceanic  
7 regions is very close to the LIVAS dust AOD<sub>532</sub> especially for the months with lower dust load  
8 (June-January). It is also shown that dust AODs from this algorithm are closer to the LIVAS  
9 dust product than dust AODs from MACC reanalysis do. The slight overestimation of dust  
10 AOD or the shift of the maximum dust load we observe for the period of high dust loads in the  
11 region (February-May) is probably connected to the narrow swath and the 16-day time of  
12 CALIPSO which means that several dust events might be not observed by the CALIOP  
13 instrument contrary to MODIS which has a daily coverage.

14

### 15 **3.2.2 Land**

16 As already mentioned in the previous paragraph a different approach is followed over the land  
17 regions of the Eastern Mediterranean due the low confidence on the MODIS FMR<sub>550</sub> and  
18 Ångström exponent retrievals over land compared to that over ocean (e.g. see Levy et al., 2010;  
19 Georgoulas and Kourtidis, 2011). This limitation does not allow us to distinguish the  
20 contribution of fine and coarse mode aerosols in terms of AOD<sub>550</sub>. In this case, we choose to use  
21 daily model fields of the dust contribution to the total AOD (here MACC reanalysis and  
22 GOCART). We follow a method similar with the one presented in Bellouin et al. (2013).  
23 Specifically, we calculate the dust AOD<sub>550</sub> by scaling the MODIS AOD<sub>550</sub> data with the MACC  
24 or GOCART dust/total AOD<sub>550</sub> ratios [ $f_d = \tau_{d(model)}/\tau_{(model)}$ ] on a daily basis.

25 Since the MACC data are available only from 2003 to 2012, in order to take advantage of the  
26 full MODIS dataset (3/2000-12/2012), data from the GOCART model were used for the period  
27 2000-2002. The GOCART data were normalized in order to be consistent with the MACC data.  
28 Daily dust/total AOD<sub>550</sub> ratios ( $f_d$ ) from the common GOCART-MACC period 2003-2007 were  
29 first brought to a common 1° x 1° spatial resolution using bilinear interpolation and then we  
30 calculated the regression line for each grid cell on a seasonal basis. The linear relations were  
31 afterwards used in order to normalize the 2000-2002 GOCART ratios to have a homogeneous  
32 dataset. The slopes and offsets of these regression lines and the corresponding correlation  
33 coefficients (R) can be seen in Figs. S5, S6 and S7 of the Supplement, respectively. Overall, for

1 the whole time period, the MACC reanalysis  $f_d$  ratios are lower by  $\sim 26\%$  from the GOCART  $f_d$   
2 ratios and the linear relation connecting the two products is  $f_{d\text{MACC}}=0.4964f_{d\text{GOCART}}+0.0952$   
3 with a correlation coefficient  $R$  of 0.74. The  $f_d$  values of the merged GOCART-MACC (2000-  
4 2012) timeseries were checked using the Standard Normalized Homogeneity Test (SNHT) as  
5 described in Alexandersson (1986). The statistical significance was checked following Khaliq  
6 and Ouarda (2007) and the  $f_d$  timeseries were found to be homogeneous (see Fig. S8 of the  
7 Supplement). Hence, this test verifies that the use of the merged GOCART-MACC  $f_d$  dataset  
8 will not insert any artifacts (e.g. trends or breaks) in the algorithm. Finally, the  $f_d$  data were  
9 brought to the same spatial resolution with MODIS data ( $0.1^\circ \times 0.1^\circ$ ) using bilinear interpolation  
10 again.

11 After the calculation of  $\tau_d$  with the use of  $f_d$  values ( $\tau_d=f_d\text{AOD}_{550}$ ), we proceed to the calculation  
12 of the anthropogenic contribution to the total  $\text{AOD}_{550}$  ( $\tau_a$ ) by multiplying the non-dust part of  
13  $\text{AOD}_{550}$  with the anthropogenic fraction  $f_a$  for the region of Eurasia ( $0.77\pm 0.20$ ) given in  
14 Bellouin et al. (2013) [ $\tau_a=f_a(1-f_d)\text{AOD}_{550}$ ]. The rest of the total  $\text{AOD}_{550}$  is attributed to the fine  
15 mode natural aerosols [ $\tau_n=(1-f_a)(1-f_d)\text{AOD}_{550}$ ] (see Fig. 2). As discussed in Bellouin et al.  
16 (2013), the fine mode natural aerosols consist of sea salt, dimethyl sulfide from land and  
17 oceanic sources,  $\text{SO}_2$  from degassing volcanoes and secondary organic aerosols from biogenic  
18 emissions. It has to be highlighted that like in the case of oceanic regions the biomass burning  
19 aerosols are classified as anthropogenic by this algorithm. As shown in Figs. S4a-d, the seasonal  
20 variability of  $\tau_d$  over land covered regions is very close to the LIVAS dust  $\text{AOD}_{532}$  which is  
21 used as a reference.

22 Overall, the algorithm described above performs well as far as dust is concerned. This is further  
23 shown when comparing MODIS Terra and Aqua  $\tau_d$  values with collocated AERONET  
24 observations for dust dominated days (see Fig. S9 in the Supplement). The method followed for  
25 the collocation of the data is similar to the one presented in Sect. 4.1 while dust dominated days  
26 were days with an AERONET AE smaller than 1 (see Mateos et al., 2014) and a MODIS based  
27  $\tau_d$  greater than  $\tau_a$  and  $\tau_n$  or  $\tau_m$ . The uncertainties of the calculated  $\tau_a$ ,  $\tau_d$ ,  $\tau_n$  and  $\tau_m$  values which  
28 are inserted by the input data and the assumptions of the algorithm are expected to be similar  
29 with the ones presented in Bellouin et al. (2013). Bellouin et al. (2013) using a Monte-Carlo  
30 analysis indicated that  $\tau_a$  can be specified with an uncertainty of  $\sim 23\%$  over land and  $\sim 16\%$   
31 over the ocean,  $\tau_d$  can be specified with an uncertainty of  $\sim 19\%$  over land and  $\sim 33\%$  over the  
32 ocean,  $\tau_n$  can be specified with an uncertainty of  $\sim 41\%$  and  $\tau_m$  with an uncertainty of  $\sim 28\%$ .  
33 The results of the application of the algorithm described in the paragraphs above are presented



1 in the following section (Sect. 4) by means of maps, pie charts, plots and tables for each one of  
2 the three basic regions of interest and their nine sub-regions.

## 3 4 **4 Results and discussion**

### 5 **4.1 Validation of MODIS gridded data using ground-based observations**

6 As discussed in Sects. 2 and 3, the high quality (QAC: 3) DT level-2 Collection 051 MODIS  
7 data used in this work were validated in detail against data from 13 AERONET stations (see  
8 Fig. 1). The stations were selected to make sure that their version 2.0 level 2.0 high quality  
9 cloud screened Cimel sunphotometric observations were covering at least 2 years and there  
10 were at least 100 common days of AERONET and MODIS observations. The exact  
11 geolocation of the AERONET stations is given in Table 1 (see also Fig.1) along with the  
12 period of available data, the hosting country, the type of the station (e.g. urban/rural,  
13 coastal/continental, etc.) and the corresponding mean overpass time of Terra and Aqua  
14 MODIS. First, we collocated spatially and temporally the MODIS and AERONET  
15 observations by temporally averaging AERONET measurements within  $\pm 30$  min from the  
16 MODIS overpass time (see Levy et al., 2010) and spatially averaging MODIS measurements  
17 centered within a  $25 \times 25 \text{ km}^2$  window around each station (see Koukouli et al., 2010). The  
18 use of a collocation window equal to the one used for the gridding procedure, practically,  
19 allows us to validate at the same time the  $0.1^\circ \times 0.1^\circ$  MODIS gridded product.

20 The regression lines between MODIS and AERONET AODs are shown in Fig. 3 while  
21 details about the validation results can be found in Table 2. Overall, the MODIS Terra DT  
22 Collection 051 data overestimate  $\text{AOD}_{550}$  by 11.59 % (Normalized Mean Bias - NMB) with  
23 63.28 % of the data falling within the expected error (EE) envelope and 67.78% within the  
24 pre-launch expected error (pLEE) envelope. The expected error envelope is define as:  $\text{AOD} -$   
25  $|\text{EE}| \leq \text{AOD}_{\text{MODIS}} \leq \text{AOD} + |\text{EE}|$  with EE being  $\pm(0.05 \pm 0.15\text{AOD})$  (Levy et al., 2010) and  
26 pLEE being  $\pm(0.05 \pm 0.20\text{AOD})$  (Kaufman et al., 1997). On the other hand, the MODIS Aqua  
27 DT Collection 051 data overestimate  $\text{AOD}_{550}$  by 25.18 % (NMB) with 57.14 % of the data  
28 falling within the EE envelope and 61.87 % within the pLEE envelope. The percentage of the  
29 MODIS Terra and Aqua data falling within the EE envelope are close to the 57 % given in  
30 Remer et al. (2005) for the Eastern Mediterranean. The validation results for each station  
31 separately can be found in Table S1 of the Supplement. The results discussed in this  
32 paragraph are comparable to the ones appearing in previous studies focusing on the  
33 Mediterranean region (see Papadimas et al., 2009; Koukouli et al., 2010). In general, it is

1 shown here that the MODIS Terra Collection 051 data exhibit a better agreement with the  
2 ground-based observations from AERONET than MODIS Aqua data do.

3 To be in line with the global validation of the DT Collection 051 product by Levy et al.  
4 (2010) we also performed a validation with the specifications used in their work. We used a  
5  $50 \times 50 \text{ km}^2$  window for the spatial collocation of the MODIS and AERONET data while  
6 only days with at least 5 MODIS retrievals and 2 AERONET measurements were taken into  
7 account. The increased size of the collocation window improves the results of the validation.  
8 As shown in Table 2, MODIS Terra DT Collection 051 data overestimate  $\text{AOD}_{550}$  by 5.10 %  
9 (NMB) with 70.17 % of the data falling within the EE envelope and 74.64 % within the pLEE  
10 envelope. For MODIS Aqua, the NMB is 15.34%, while the percentage of the measurements  
11 falling within the EE and pLEE envelope is 66.76 % and 70.45 %, respectively. These results  
12 for the Eastern Mediterranean are close to the global ones presented in Levy et al. (2010).

13 As discussed in Sect. 3.1, data from the DB algorithm were used over bright arid and semi-  
14 arid regions of North Africa for the production of the  $0.1^\circ \times 0.1^\circ$  MODIS gridded dataset for  
15 grid cells with no DT data. Therefore, in this work we also perform a validation of the DB  
16 Collection 051 product over the region of the Eastern Mediterranean. In the case of DB data,  
17 we first make use of all the available DB observations without any quality filtering over the  
18 13 AERONET stations. A spatial window of 25-30 km has been typically used in the past for  
19 the collocation of MODIS DB data with the AERONET observations (see Shi et al., 2011;  
20 Ginoux et al., 2012; Sayer et al., 2013; 2014) which is in line with the  $25 \times 25 \text{ km}^2$  window  
21 used here. The MODIS Terra DB data overestimate  $\text{AOD}_{550}$  by 21.38 % (NMB) with 51.90 %  
22 of the data falling within the expected uncertainty (EU) envelope assuming a DB expected  
23 uncertainty of  $\pm 0.05 \pm 20\% \text{AOD}_{\text{AERONET}}$  (Hsu et al., 2006). The MODIS Aqua DB Collection  
24 051 data overestimate  $\text{AOD}_{550}$  by 33.03 % (NMB) with 55.30 % of the data falling within the  
25 expected uncertainty envelope. We repeated the validation procedure for DB data taking into  
26 account the highest quality data only. The sample of available measurements was diminished  
27 by a factor of 5 in the case of MODIS Terra and 6 in the case of MODIS Aqua but the results  
28 were pretty similar with the ones for the unfiltered data. Therefore, the use of unfiltered DB  
29 data during the gridding procedure does not insert any significant uncertainty. The DB results  
30 for the 13 AERONET stations examined here are not of the same agreement than the DT  
31 results and the ones presented in previous studies utilizing DB Collection 051 data for other  
32 stations and larger regions (see Shi et al., 2011; Ginoux et al., 2012). However, it has been  
33 reported that stations in the region (e.g. Sede Boqer in Israel) are among the ones with the

1 greatest discrepancies between MODIS DB and AERONET measurements (Ginoux et al.,  
2 2012). Nevertheless, as commented in Sect. 3.1, the DB data constitute only a small fraction  
3 of the data used for the production of the MODIS gridded dataset (~ 1 % only of the 30000  
4 grid cells covering the Eastern Mediterranean has only DB retrievals) and therefore they do  
5 not affect significantly its quality.

6 As discussed in Sect. 3.1 the gridding procedure was repeated four times using a gridding  
7 window of 25, 50, 75 and 100-km using MODIS Terra AOD<sub>550</sub> data for the year 2004 showing  
8 that the 25-km window is optimal for capturing local pollution sources. In order to see how the  
9 size of the gridding window affects the agreement between MODIS and AERONET data we  
10 also proceeded to a validation of MODIS DT data against AERONET measurements using  
11 different spatial collocation windows (25, 50, 75 and 100-km) and two quality criteria, a "strict"  
12 one: at least 2 AERONET measurements for each MODIS-AERONET pair and "stricter" one:  
13 at least 5 MODIS retrievals and 2 AERONET measurements for each MODIS-AERONET pair  
14 as in Levy et al. (2010). The results for the DT MODIS Terra and Aqua data are presented in  
15 Table S2 of the Supplement. In general, it is shown that the increased size of the spatial  
16 collocation window leads to an improvement of the bias between satellite and ground-based  
17 observations. This is probably due to the inclusion of more observations into the calculations  
18 which diminishes the noise of the MODIS observations. In addition, as expected, the stricter  
19 quality criteria lead to a better agreement between MODIS DT and AERONET data. Taking  
20 into account not only the NMB but also the regression lines and the other metrics appearing in  
21 Table 2S, it is concluded that the 50-km window is the best choice for the validation procedure  
22 in line with Ichoku et al. (2002). On the other hand, the 25-km validation results are close to the  
23 50-km ones (see Table S2) and at the same time the 25-km gridding window allows for a more  
24 efficient detection of local aerosol sources as shown in Sect. 3.1. Taking this into account, we  
25 suggest that the 25-km window used for the production of the 0.1° x 0.1° gridded MODIS  
26 dataset is the optimal selection for studying the spatial variability of aerosols, preserving at the  
27 same time the representativeness of the real aerosol load over each specific spot.

28

## 29 **4.2 Aerosol spatial variability and hot spots**

30 The AOD<sub>550</sub> spatial variability over the greater Eastern Mediterranean region for the period  
31 2000-2012 as seen from the Terra MODIS 0.1° x 0.1° dataset is presented in Fig. 4. Several  
32 aerosol hot spots that coincide with megacities (e.g. Cairo, Istanbul), large cities (e.g. Athens,  
33 Ankara, Alexandria, Izmir, Thessaloniki) or even medium sized cities (e.g. Larissa,

1 Limassol), industrial zones (e.g. OSTIM Industrial Zone in Ankara, Turkey), power plant  
2 complexes (e.g. Maritsa Iztok complex at the Stara Zagora Province in Bulgaria, Ptolemaida-  
3 Kozani power plants in Western Macedonia, Greece), river basins (e.g. Evros river Basin at  
4 the borders between Greece and Turkey), etc, can be detected on the map. Indicatively, in Fig  
5 4 we give a list of 35 local particle pollution sources in the region; however, careful  
6 inspection of this map and the seasonal maps presented in Fig. 6 allows for the detection of  
7 many more aerosol sources. The results from the analysis of Aqua MODIS data are pretty  
8 similar as shown in Fig. S10 of the Supplement. A significant number of the local aerosol  
9 sources can also be detected on the OMI 2004-2012 tropospheric NO<sub>2</sub> and PBL SO<sub>2</sub> maps  
10 given in Figs. 5a and b which reveals the origin of aerosols over these regions (e.g. traffic,  
11 industrial activities, etc). However, there are regions of high aerosol load which cannot be  
12 seen in Fig. 5a and b and vice versa which is indicative of the significant role of other  
13 anthropogenic or natural processes that contribute to the local aerosol load (e.g. fires, soil dust  
14 from agricultural activities or arid regions, Sahara dust transport).

15 The topography (Fig. 5c) and precipitation (see Fig. 5d for annual precipitation levels for the  
16 period 2000-2012 from TRMM) are also major determinants of the local AOD<sub>550</sub> levels. For  
17 example, regions with mountain ranges on the Balkan Peninsula (e.g. Pindus mountain range  
18 in Greece, Dinaric Alps that run through Albania and the former Yugoslav republics, the  
19 Balkan mountain range in Central Bulgaria) are characterized by low AODs (see Fig. 4). On  
20 the contrary, regions of low altitude are generally characterized by higher AODs because the  
21 majority of anthropogenic activities is usually concentrated there. Also, low altitude regions  
22 surrounded by high mountains are characterized by higher AODs as aerosols cannot be easily  
23 transported by the wind (e.g. the industrialized regions in Central Bulgaria which are confined  
24 between the high Balkan and Rodopi mountain ranges). As precipitation is the major removal  
25 mechanism of pollutants in the atmosphere, regions with high AOD<sub>550</sub> are in many cases  
26 connected to low precipitation levels and vice versa (see Figs. 4 and 5d). It has to be  
27 highlighted that the AOD<sub>550</sub> over these regions is high primarily due to the emissions and the  
28 atmospheric processes forming aerosol particles. The low removal rates from precipitation  
29 just preserve the AOD<sub>550</sub> levels high. A striking example is the region of Anatolia in Central  
30 Turkey which is characterized by lower precipitation levels and higher aerosol loads  
31 compared to the surrounding regions. Also, the low precipitation levels are partly responsible  
32 for the high aerosol loads appearing over Northern Africa.

1 Overall, the mean AOD<sub>550</sub> for the whole period of interest is estimated at  $0.215 \pm 0.187$  for  
2 Terra and  $0.217 \pm 0.199$  for Aqua MODIS for the Eastern Mediterranean region which is  $\sim 45$   
3 % higher than the global average appearing in recent studies (e.g. Kourtidis et al., 2015). Over  
4 land higher mean AODs are generally recorded ( $0.219 \pm 0.165$  for Terra and  $0.239 \pm 0.189$   
5 for Aqua MODIS) than over the sea ( $0.213 \pm 0.201$  for Terra and  $0.202 \pm 0.205$  for Aqua  
6 MODIS). All these values along with the mean AODs for the 9 sub-regions of interest  
7 covering the Eastern Mediterranean can be found in Table 3.

8 The AOD<sub>550</sub> spatial variability on a seasonal basis from MODIS Terra and Aqua is presented  
9 in Fig. 6 along with the difference between the two products. The majority of the local aerosol  
10 sources over land are more prominent in summer. The limited washout by precipitation (see  
11 also Papadimas et al., 2008) and also the enhanced photochemical production of secondary  
12 organic aerosols (Kanakidou et al., 2011 and references therein) contribute to the high AODs  
13 appearing over local sources. In addition, during summer, over the region, there is typically a  
14 significant transport of aerosols (e.g. see Kanakidou et al., 2011 and references therein) and  
15 gaseous pollutants like SO<sub>2</sub> and NO<sub>2</sub> (see Georgoulas et al., 2009; Zyrichidou et al., 2009)  
16 and biomass burning aerosols from Central-Eastern Europe. Over the sea, a profound  
17 maximum is observed in spring extending across the North African coast and the neighboring  
18 oceanic areas which is due to the well documented transport of significant amounts of dust  
19 from the Sahara Desert (see Barnaba and Gobbi., 2004 and the list of references given in the  
20 introduction). The seasonal variability of aerosols and the relative role of different aerosol  
21 types and various processes is discussed in more details in Sect 4.4.

22 The difference between MODIS Terra and Aqua Collection 051 AOD<sub>550</sub> over the Eastern  
23 Mediterranean is  $-0.002$  ( $-1.40$  %) for winter,  $-0.009$  ( $-3.27$  %) for spring,  $-0.011$  ( $-4.46$  %)  
24 for summer and  $0.008$  ( $4.40$  %) for autumn. AOD<sub>550</sub> levels from Terra MODIS are lower than  
25 that from Aqua MODIS over land for all seasons. Over the sea, Terra MODIS AOD<sub>550</sub> levels  
26 are lower than that of Aqua MODIS only in winter. The fact that Terra MODIS measurements  
27 are systematically higher than that from Aqua over the sea by  $\sim 0.01$  on an annual basis is in  
28 line with the findings of previous global studies for Collection 5 (e.g. Remer et al., 2006;  
29 2008). Locally, one can see regions with positive and negative differences between Terra and  
30 Aqua MODIS AOD<sub>550</sub>. The patterns of the Terra-Aqua difference per season are presented in  
31 Figs. 6c, f, i and l while the patterns of the percent difference are given in Fig. S11 of the  
32 Supplement. The largest part of the Terra-Aqua MODIS differences over land and sea which  
33 are observed here may be attributed to the known calibration and sensor degradation issues of

1 MODIS (for details see Levy et al., 2010; 2013; Lyapustin et al., 2014). A significant effort  
2 has been undertaken to address these issues in the new (Collection 6) MODIS product (e.g.  
3 Levy et al., 2013; Lyapustin et al., 2014) and a repetition of a similar analysis with Collection  
4 6 data in the future would be a valuable contribution. Taking into account the aforementioned  
5 issues and the retrieval uncertainty of MODIS it becomes more than obvious that the  
6 attribution of observed differences between Terra and Aqua to the diurnal variability of  
7 aerosol load (e.g. over biomass burning regions) in the region is a difficult task. It is shown in  
8 Fig. S12 of the Supplement that the diurnal variability of AOD<sub>550</sub> from AERONET ranges  
9 significantly from station to station. The average hourly departure from the daily mean for the  
10 total of the 13 stations ranges from ~ -5 % to ~ 5 %. Specifically, for the MODIS Terra and  
11 Aqua overpass times, the AERONET AOD<sub>550</sub> difference ranges from ~ -10 % to ~ 10 % (see  
12 Fig. S12b). The Terra-Aqua AOD<sub>550</sub> difference is negative for the total of the 13 stations  
13 ranging from ~ -25 % to ~ -5 %. It is shown in Fig. S12b that the two differences exhibit a  
14 similar variability from station to station which indicates that part of the observed Terra-Aqua  
15 difference is indeed due to the diurnal variability of aerosols. However, as mentioned above,  
16 the diurnal variability of aerosols is a very delicate issue and should be comprehensively  
17 addressed in a future study. The same stands for other kind of variabilities which could be  
18 connected to local and regional anthropogenic activities like e.g. the weekly cycle of aerosols  
19 (see Georgoulias and Kourtidis, 2011; Georgoulias et al., 2015).

20

### 21 **4.3 Contribution of different aerosol types to the total AOD<sub>550</sub>**

#### 22 **4.3.1 Annual contribution**

23 As mentioned above, we attempt to estimate in our work the contribution of different aerosol  
24 types to the total AOD<sub>550</sub> over the region of the Eastern Mediterranean was calculated  
25 following the methodology presented in Sect. 3.2. For the land covered areas, based on  
26 MODIS Terra observations, we estimate that 52 % (0.112±0.087) of the total AOD<sub>550</sub> is due  
27 to anthropogenic aerosols, 32 % (0.074±0.080) due to dust and 16 % (0.034±0.026) due to  
28 fine mode natural aerosols (see Fig. 7). For the oceanic areas, 41 % (0.086±0.085) of the total  
29 AOD<sub>550</sub> is due to anthropogenic aerosols, 34 % (0.076±0.185) due to dust and 25 %  
30 (0.054±0.018) due to marine aerosols (see Fig. 7). The results based on observations from  
31 MODIS Aqua are similar. Over land, 50 % (0.117±0.093) of the total AOD<sub>550</sub> is  
32 anthropogenic, 35 % (0.090±0.102) is due to dust and 15 % (0.035±0.028) due to fine mode  
33 natural aerosols, while, over the sea, 40 % (0.079±0.080) of the total AOD<sub>550</sub> is of

1 anthropogenic origin, 33 % ( $0.070\pm 0.181$ ) is due to dust and 27 % ( $0.054\pm 0.018$ ) due to  
2 marine aerosols (see Fig. 7). These results along with the relative contributions and the annual  
3  $\tau_a$ ,  $\tau_d$ ,  $\tau_n$  and  $\tau_m$  levels for each one of the nine sub-regions of interest (see Fig. 1) are given in  
4 Table 4.

5 For anthropogenic aerosols, the region with the highest relative contribution is NBL (59 % for  
6 both Terra and Aqua MODIS) while the region with the lowest relative contribution is SWO  
7 (32 % for both Terra and Aqua MODIS) (see also Table 4). The spatial variability of  $\tau_a$  is  
8 presented in Fig. 8a for Terra MODIS and Fig. S13a of the Supplement for Aqua MODIS, the  
9 patterns being similar in both cases. Over land, the annual  $\tau_a$  patterns are similar to the  
10 AOD<sub>550</sub> patterns, the highest values appearing over local particle pollution sources (cities,  
11 industrial zones, etc.). Over the sea,  $\tau_a$  is higher along the coasts, while it drops significantly  
12 towards other directions. An interesting feature here is that the oceanic region of Black Sea  
13 (BSO) presents higher relative anthropogenic contributions than the rest of the oceanic sub-  
14 regions but also than land areas with significant anthropogenic sources (e.g. ANL and NAL).  
15 This is indicative of the transport of atmospheric particles from Central Europe and biomass  
16 burning aerosols during the biomass burning seasons in April-May from Russia (across the  
17 latitudinal zone 45°N-55°N) and July-August from South-Western Russia and Eastern Europe  
18 (Amiridis et al., 2010). These aerosols are transported at much lower latitudes as shown in  
19 previous studies (e.g. Vrekoussis et al., 2005; Karnieli et al., 2009) reaching the Sahara Desert  
20 and the Middle East regions (Pozzer et al., 2015). The fact that  $\tau_a$  drops gradually from the  
21 coasts is also seen in Fig. 9 where the latitudinal variability of the optical depths of the  
22 different aerosol types ( $\tau_a$ ,  $\tau_d$ ,  $\tau_n$  and  $\tau_m$ ) is presented for four bands that cover the whole  
23 Eastern Mediterranean. An interesting feature is that  $\tau_a$  increases nearby the shoreline  
24 (particularly along the North African coastal zone) before it gradually decreases. Over land  
25 aerosols are located within the atmospheric boundary layer, close to the emission sources, and  
26 hence, their deposition and removal from the atmosphere is more efficient than over the sea.  
27 The particles which are transported over the sea on the other hand usually reach greater  
28 heights which prolongs their lifetime.

29 As shown in Fig. 9, the same feature is observed for dust. Indicatively,  $\tau_d$  and the relative  
30 contribution of dust to the total AOD<sub>550</sub> on an annual basis over the oceanic regions of SWO  
31 and SEO are in general higher or comparable to the ones over NAL (see Table 4 for more  
32 details). In Fig. 9, the MODIS-based  $\tau_d$  latitudinal variability is presented along with the  
33 latitudinal variability of dust AOD<sub>532</sub> and extinction coefficients of dust at 532 nm from

1 LIVAS. As expected, in all cases  $\tau_d$  decreases with distance from the large dust sources in the  
2 South and South-East (Sahara Desert, Middle East deserts) with local maxima over the  
3 latitudinal zone from 35°N to 40°N (especially for band 2 and band 3). The latitudinal  
4 variability of  $\tau_d$  is similar to the latitudinal variability of dust AOD<sub>532</sub> for all the four bands  
5 despite the fact that the MODIS-based data have a resolution 100 times higher (0.1° vs 1°) and  
6 therefore are more sensitive to local characteristics. Dust reaches heights up to ~ 4-5 km in the  
7 area; however, the largest fraction of dust mass is confined within the first 2-3 km of the  
8 troposphere (see Fig. 9). The annual  $\tau_d$  patterns are shown in Fig. 8b for Terra MODIS (Fig.  
9 S13b of the Supplement for Aqua MODIS). The main dust transport pathways over the  
10 oceanic areas of the Eastern Mediterranean can be seen along with various local maxima over  
11 land. The highest  $\tau_d$  values over land appear over the regions of NAL and ANL (see Table 4)  
12 and along the coasts. The high dust concentrations appearing over these regions are not only  
13 due to the transport of dust from the nearby deserts but also due to local dust sources. A  
14 recent study by Liora et al. (2015) reports various local sources of wind blown dust along the  
15 coastal regions of Greece and Turkey, over the region of Anatolia in Turkey, over the Greek  
16 islands, Crete, Cyprus and regions close to the coastal zone of Middle East. Their results are  
17 in good agreement with the  $\tau_d$  patterns presented in this work.

18 As shown in Fig. 7, fine mode natural aerosols exhibit the lowest contribution to the total  
19 AOD<sub>550</sub> compared to the other aerosol types over land. The spatial variability of  $\tau_n$  is very low  
20 compared to  $\tau_a$  and  $\tau_d$  as shown in Figs. 8c and 9. It is inferred from the values appearing in  
21 Table 4 that  $\tau_n$  increases slightly as one moves from North to South; however, the relative  
22 contribution of fine mode natural aerosols to the total AOD<sub>550</sub> slightly decreases (i.e. 17.67 %  
23 over NBL and 14.97 % over NAL according to Terra MODIS observations). The latitudinal  
24 variability and the percentages appearing in Table 4 are in accordance to the relative  
25 contributions of biogenic aerosols to the total AOD<sub>550</sub> appearing over the Eastern  
26 Mediterranean in a recent modeling study (Rea et., 2015).

27 Similar to fine mode natural aerosols over land, marine aerosols generally have the lowest  
28 contribution to the total AOD<sub>550</sub> compared to the other aerosol types over the sea (see Fig. 7  
29 and Table 4) except for BSO. The variability of  $\tau_m$  is very low compared to  $\tau_a$  and  $\tau_d$ . On an  
30 annual basis, high  $\tau_m$  values appear over the Aegean Sea and the oceanic area between Crete  
31 and the North African coast while slightly lower values appear along the coasts of the Eastern  
32 Mediterranean (see Figs. 8d and 9). The  $\tau_m$  patterns follow the near surface wind speed  
33 patterns in the region (see Fig. S14 of the Supplement) being in accordance to the  $\tau_m$ , marine



1 particulate matter concentration or sea salt emission patterns appearing in other studies (Im et  
2 al., 2012; Nabat et al., 2013; Rea et al., 2015; Liora et al., 2015).

### 4 **4.3.2 Seasonal contribution**

5 The contribution of different aerosol types to the total AOD<sub>550</sub> over the Eastern Mediterranean  
6 varies from season to season. The relative contribution of each aerosol type over EML and  
7 EMO for each season is shown in Fig. 10. Over land, the relative contribution of  $\tau_a$ ,  $\tau_d$  and  $\tau_n$   
8 to the total AOD<sub>550</sub> exhibits a low seasonal variability. The relative contribution of  
9 anthropogenic aerosols to the total AOD<sub>550</sub> ranges from 49 % in SON to 55 % in DJF based  
10 on Terra MODIS observations and from 48 % in MAM and SON to 52 % in JJA based on  
11 Aqua MODIS observations. In contrast, over the oceanic regions the relative contribution of  
12  $\tau_a$ ,  $\tau_d$  and  $\tau_m$  to the total AOD<sub>550</sub> exhibits a significant seasonal variability. The relative  
13 contribution of anthropogenic aerosols to the total AOD<sub>550</sub> ranges from 27 % / 27 % in DJF to  
14 50 % / 47 % in JJA based on Terra/Aqua MODIS observations. The percentages appearing  
15 here are in accordance to the values appearing in Hatzianastassiou et al. (2009) where a  
16 different satellite-based approach was followed. Indicatively, for the greater Athens area, an  
17 average summertime anthropogenic contribution of ~ 50 % was found here based on Terra  
18 MODIS data which is within the summer period range of 47-61 % indicated in the study by  
19 Hatzianastassiou et al. (2009). In addition, the corresponding values for the greater  
20 Thessaloniki area, Crete, Cairo and Alexandria are 53 %, 38 %, 48 % and 41 %, respectively,  
21 within the range of values (57-73 %, 36-52 %, 34-56 % and 23-60 %) shown in  
22 Hatzianastassiou et al. (2009). Only in the case of Ankara, our results suggest a lower  
23 anthropogenic contribution (52 % versus 71-84 %). Particularly for Athens, Gerasopoulos et  
24 al. (2011) following a different approach incorporating ground-based AOD observations and  
25 trajectory modeling reached similar results (annual contribution of ~ 62 % from local and  
26 regional sources and continental Europe which is expected to be mostly of anthropogenic  
27 origin). Similarly, for Crete, Bergamo et al. (2008) using a different approach, also utilizing  
28 ground-based data, found an annual anthropogenic contribution of ~ 43 %.

29 The seasonal patterns of the anthropogenic aerosols ( $\tau_a$ ) over the Eastern Mediterranean based  
30 on MODIS Terra observations are presented in Figs. 11a, e, i and m while the seasonal  
31 variability of  $\tau_a$  over the whole region, over the land covered part and the oceanic part and  
32 over the 9 sub-regions of interest is presented in Fig. 12. The results based on MODIS Aqua  
33 observations are similar and can be found in Figs. S15a, e, i and m and Fig. S16 of the

1 Supplement. Generally, the local hot spots are detectable throughout the year; however, they  
2 are becoming much more discernible in spring and especially in summer. As shown in Fig.  
3 12a,  $\tau_a$  nearly doubles during the warm period of the year (spring-summer) with the seasonal  
4 variability being stronger over the sea (Fig. 12c) than over land (Fig. 12b). A clear peak is  
5 observed in summer, August being the month with highest  $\tau_a$  levels. As discussed in Sect.  
6 4.3.1 the summer peak is mostly a result of three basic reasons. The first one is the deficiency  
7 of wet removal processes compared to the cold period. As shown in Fig. S17, based on the  
8 TRMM satellite observations, August and July are the months with the lowest precipitation  
9 levels over the land covered part (a drop of  $\sim 75\%$  compared to winter months) and over the  
10 oceanic part (a drop of  $\sim 90\%$  compared to winter months) of the Eastern Mediterranean,  
11 respectively. The second reason is the enhancement of the photochemical production of  
12 secondary organic aerosols in summer (Kanakidou et al., 2011) and the third reason is the  
13 transport of pollution aerosols from Central Europe and biomass burning aerosols from South-  
14 Western Russia and Eastern Europe during the biomass burning season in July-August  
15 (Amiridis et al., 2010). The Etesians, which are persistent northerly winds that prevail over  
16 the Eastern Mediterranean during summer, bring dry and cool air masses and aerosols from  
17 the regions mentioned above while blocking at the same time the transport of desert dust in  
18 the region and dispersing local pollution in urban areas to levels typical for rural areas (see  
19 Tyrllis and Lelieveld, 2013 and references therein). As seen in Figs. 12a-l, a smaller but  
20 distinct in most cases  $\tau_a$  peak appears in April mostly as a result of the transport of biomass  
21 burning aerosols from Russia (across the latitudinal zone  $45^\circ\text{N}$ - $55^\circ\text{N}$ ). This is in line with the  
22 findings of Sciare et al. (2008) who detected traces of these biomass burning aerosols at the  
23 island of Crete in Southern Greece.

24 As discussed above, the relative contribution of dust to the total  $\text{AOD}_{550}$  over land exhibits a  
25 low seasonal variability ranging from 29 % in DJF to 36 % in SON based on Terra MODIS  
26 observations and from 33 % in JJA to 38 % in SON based on Aqua MODIS observations (see  
27 Fig. 10). Over the oceanic regions the relative contribution of dust to the total  $\text{AOD}_{550}$  ranges  
28 significantly throughout a year from 26 % / 28 % in JJA to 42 % / 39 % in MAM based on  
29 Terra/Aqua MODIS observations. The percentages appearing here are in accordance to model  
30 and observational studies. For example, de Meij et al. (2012) using the atmospheric chemistry  
31 general circulation model EMAC (ECHAM/MESSy Atmospheric Chemistry) showed that  
32 dust contributes on an annual level  $\sim 30\%$  to the total  $\text{AOD}_{550}$  over stations located in the  
33 area of the Eastern Mediterranean. Gerasopoulos et al. (2011) found a  $\sim 23\%$  percent

1 contribution of North African dust to the total AOD over Athens using ground-based AOD  
2 observations and trajectory modeling. Taking into account that part of the  $\sim 39\%$  local and  
3 regional sources appearing in Gerasopoulos et al. (2011) is due to local dust sources,  
4 especially in summer, turns out that their results are in agreement with the  $\sim 33\%$  relative  
5 contribution found in this work for the greater Athens area based on Terra MODIS  
6 observations. The seasonal patterns of dust ( $\tau_d$ ) over the region based on Terra MODIS  
7 observations are shown in Figs. 11b, f, j and n while the seasonal variability of  $\tau_d$  over the  
8 whole region, over land, over the sea and over the 9 sub-regions of interest is shown in Fig.  
9 12. The corresponding results based on MODIS Aqua observations are pretty similar and can  
10 be found in Figs. S15b, f, j and n and Fig. S16 of the Supplement.

11 As seen in Fig. 11f, in spring, mostly due to the strong Sahara dust events, very high  $\tau_d$  values  
12 appear over land regions in North Africa, Middle East, Anatolia and oceanic areas across the  
13 Eastern Mediterranean (especially below  $35^\circ\text{N}$ ). Dust loading over the sea exhibits two  
14 maxima, one at the coastal zone of Libya and one across the coastal zone of Middle East. The  
15 same two maxima but with much lower  $\tau_d$  values appear in summer (Fig. 11j) and autumn  
16 (Fig. 11n). Over land, the  $\tau_d$  patterns are similar in summer and autumn, the maximum values  
17 appearing over the Anatolian Plateau and areas of North Africa and Middle East. During  
18 winter, dust maxima appear across the coastal zone of Northern Africa with relatively low  $\tau_d$   
19 values across the coastal zone of Middle East (Fig. 11b). In winter  $\tau_d$  levels are low over land  
20 compared to the other seasons (Figs. 11b, f, j and n) as precipitation levels (see Fig. S17 of the  
21 Supplement) and hence wet scavenging of aerosols peak. At the same time, the local  
22 emissions of dust are low for regions away from the large area sources in the South (Liora et  
23 al., 2015). In contrast, over the sea  $\tau_d$  levels in winter are similar or slightly higher for some  
24 areas than that in summer and autumn (see Figs. 11 and 12) as this is the season with the  
25 second highest frequency (after spring) of strong ( $\sim 21\%$ ) and extreme ( $\sim 26\%$ ) desert dust  
26 episodes in the region (see Gkikas et al., 2013 for details). February is by far the winter month  
27 with the highest  $\tau_d$  levels (see Fig. 12) in line with the findings of Pey et al. (2013) who  
28 showed that the intensity of African dust episodes over stations in Greece and Cyprus peaks  
29 in February. Dust exhibits a strong peak in spring, April being the month with the highest  $\tau_d$   
30 levels in line with other studies (e.g. Israelevic et al., 2012; Varga et al., 2014). The peak in  
31 April is a result of the high cyclonic activity over North Africa during this month as shown by  
32 Flaounas et al. (2015). According to the same study, low pressure systems are responsible for  
33  $\sim 10\text{-}20\%$  of moderate and  $\sim 40\text{-}50\%$  of high and extreme Sahara dust transport events over

1 the Eastern Mediterranean. North Africa (Sharav) cyclones develop mainly in spring and  
2 summer while Mediterranean cyclones develop in winter and autumn. The Mediterranean  
3 cyclones are more intense than Sharav cyclones. The region, is also affected by events  
4 bringing particles from dust source regions in the eastern part of the Mediterranean basin  
5 (Negev desert in Israel, Sinai in Egypt, Anatolian Plateau in Turkey) and the Arabian deserts  
6 (Basart et al. 2009; Pey et al., 2013; Abdelkader et al., 2015). Dust remains in the atmosphere  
7 for a period of 1-4 days undergoing chemical aging before being removed (see Abdelkader et  
8 al. 2015 and references therein). The seasonal variability of  $\tau_d$  is much stronger and the spring  
9 maxima much more prominent over the sea (see Fig. 12). This is expected, as dust is only  
10 occasionally transported over the sea during episodic events, while over land, local sources  
11 also contribute to the dust burden especially in summer due to the dryness of soil. For  
12 example, over NBL, a broad spring-summer peak is observed, June being the month with the  
13 highest  $\tau_d$  levels. As one moves south (SBL, ANL and NAL) the April peak becomes more  
14 prominent.

15 The relative contribution of fine mode natural aerosols to the total  $AOD_{550}$  over land exhibits  
16 a very low seasonal variability ranging from 15 % in MAM and SON to 16 % in DJF and JJA  
17 based on Terra MODIS observations and from 14 % in DJF and SON to 15 % in MAM and  
18 JJA based on Aqua MODIS observations (see Fig. 10). The seasonal variability is also very  
19 low, the highest values appearing in spring and summer (Fig. 12). Despite the generally low  
20 contribution of fine mode natural aerosols to the total  $AOD_{550}$  over the Eastern  
21 Mediterranean,  $\tau_n$  levels are similar to  $\tau_d$  levels during winter months over specific regions  
22 (NBL and SBL). The low seasonal variability can also be seen in Figs. 11c, g, k and o where  
23 the patterns of fine mode natural aerosols ( $\tau_n$ ) are presented.

24 The seasonal relative contribution of marine aerosols to the total  $AOD_{550}$  over the oceanic  
25 regions of the Eastern Mediterranean is shown in Fig. 10.  $\tau_m$  ranges from 20 % in MAM to 35  
26 % in DJF based on Terra MODIS observations and from 21 % in MAM to 36 % in DJF based  
27 on Aqua MODIS observations (see Fig. 10). Like in the case of fine mode natural aerosols,  
28 the seasonal variability is very low, but here the highest values appear in winter (Fig. 12). Due  
29 to the linear relation of  $\tau_m$  and near surface wind speed within our algorithm (see Fig. 2) the  
30  $\tau_m$  seasonal variability and patterns follow the wind speed ones (see Figs. 11d, h, l, p and  
31 S14). Marine aerosol concentrations are lower close to the coastlines while the highest  
32 concentrations (see Liora et al., 2015) and  $\tau_m$  values within the Eastern Mediterranean appear  
33 over the Aegean Sea (see Fig. 11). Overall, the  $\tau_m$  patterns are in accordance to the  $\tau_m$ , marine

1 particulate matter concentration and sea salt emission patterns from previous studies (Im et  
2 al., 2012; Nabat et al., 2013; Rea et al., 2015; Liora et al., 2015).

## 3 4 **5 Summary and conclusions**

5 In this work, satellite data from MODIS Terra (3/2000-12/2012) and Aqua (7/2002-12/2012)  
6 were analyzed separately in order to examine the spatial and temporal variability of aerosols  
7 over the Eastern Mediterranean. A high resolution ( $0.1^\circ \times 0.1^\circ$ ) MODIS gridded dataset was  
8 compiled using a method that could be used in future regional studies. A number of tests were  
9 implemented and the dataset was validated in detail using sunphotometric observations from  
10 13 AERONET stations. It is shown that the gridding method we use offers the best  
11 compromise for studying the spatial variability of aerosols on a regional or local scale,  
12 preserving at the same time the representativeness of the real aerosol load over each specific  
13 spot.

14 Based on MODIS observations the average  $AOD_{550}$  levels over the region of the Eastern  
15 Mediterranean are  $\sim 0.22 \pm 0.19$  which is  $\sim 45\%$  higher than the global mean. A number of  
16 aerosol hot spots that coincide with megacities, large and even medium size cities, industrial  
17 zones, power plant complexes, river basins, etc., can be detected on the AOD maps. A  
18 number of local aerosol sources can also be seen on satellite retrieved tropospheric  $NO_2$  and  
19 planetary boundary layer  $SO_2$  maps from OMI/AURA. This is indicative of the strong  
20 presence of anthropogenic aerosols over these regions. Topography and precipitation also  
21 play an important role. Generally, regions with mountain ranges are characterized by low  
22 AODs while regions of low altitude are characterized by higher AODs. Regions with high  
23  $AOD_{550}$  are in many cases connected to low precipitation levels and vice versa. Precipitation  
24 is the major washout mechanism of atmospheric pollutants., Low removal rates from  
25 precipitation contribute in preserving high the  $AOD_{550}$  levels which are a result of emissions  
26 and other atmospheric processes.

27 The  $AOD_{550}$  patterns over the Eastern Mediterranean exhibit a significant seasonal variability  
28 which is mostly driven by precipitation, photochemical production of secondary organic  
29 aerosols, transport of pollution and biomass burning aerosols from Central and Eastern  
30 Europe and transport of dust from the Sahara Desert and the Middle East. Differences  
31 between MODIS Terra and Aqua Collection 051  $AOD_{550}$  over the Eastern Mediterranean are  
32 generally small ( $\sim -8\%$  over land and  $\sim 5\%$  over the sea). The comparison of the Terra-Aqua

1 differences with diurnal variabilities from the AERONET stations showed that only a part of  
2 the observed differences is due to the diurnal variability of aerosols.

3 The MODIS data were combined with data from other satellites (Earth Probe TOMS,  
4 OMI/AURA), reanalysis projects (ERA-Interim, MACC) and a chemistry-aerosol-transport  
5 model (GOCART) to calculate the contribution of different types of aerosols to the total  
6  $AOD_{550}$ . The algorithm used was optimized for the Eastern Mediterranean through a number  
7 of tests and comparison with LIVAS CALIOP/CALIPSO dust retrievals and AERONET  
8 ground-based observations. A different approach is used for land and sea as there is not any  
9 reliable satellite retrieved quantity to separate the contribution of fine and coarse mode  
10 aerosols over water surfaces.

11 Overall, for the land areas, based on MODIS Terra observations, 52 % ( $0.112\pm 0.087$ ) of the  
12 total  $AOD_{550}$  is due to anthropogenic aerosols, 32 % ( $0.074\pm 0.080$ ) due to dust and 16 %  
13 ( $0.034\pm 0.026$ ) due to fine mode natural aerosols (see Fig. 7). For the oceanic areas, 41 %  
14 ( $0.086\pm 0.085$ ) of the total  $AOD_{550}$  is due to anthropogenic aerosols, 34 % ( $0.076\pm 0.185$ ) due  
15 to dust and 25 % ( $0.054\pm 0.018$ ) due to marine aerosols. The results based on observations  
16 from MODIS Aqua are in accord with previous studies.

17 Over land, the  $\tau_a$  maxima are detected over local particle pollution sources (cities, industrial  
18 zones, etc.). Over the sea,  $\tau_a$  is higher along the coasts being significantly lower at greater  
19 distance. Very high  $\tau_d$  values appear over land regions in North Africa, Middle East, Anatolia  
20 and oceanic areas across the Eastern Mediterranean, especially for latitudes below  $35^\circ N$ . Over  
21 the sea, dust loading exhibits two maxima, one at the coastal zone of Libya and one across the  
22 coastal zone of the Middle East.  $\tau_d$  decreases with distance from the large dust sources in the  
23 South and South-East. Generally, dust reaches heights up to  $\sim 4-5$  km in the area, the largest  
24 fraction of dust mass being confined within the first 2-3 km of the troposphere. The spatial  
25 variability of  $\tau_n$  and  $\tau_m$  is very low compared to  $\tau_a$  and  $\tau_d$ , following the total  $AOD_{550}$  patterns  
26 and the near surface wind speed patterns, respectively.

27 Over land, the relative contribution of anthropogenic aerosols, dust and fine mode natural  
28 aerosols to the total  $AOD_{550}$  exhibits a low seasonal variability, while over the sea the relative  
29 contribution of anthropogenic aerosols, dust and marine aerosols shows a significant seasonal  
30 variability.

31  $\tau_a$  nearly doubles during the warm period of the year (spring-summer), August and April  
32 being the months with the highest  $\tau_a$  levels. The summer peak is mostly the result of low  
33 precipitation levels, enhancement of the photochemical production of secondary organic

1 aerosols and transport of pollution aerosols from Central Europe and biomass burning  
2 aerosols from South-Western Russia and Eastern Europe during the biomass burning season  
3 in July-August. The spring maximum in April is mostly the result of transport of biomass  
4 burning aerosols from Russia in line with previous studies. Dust exhibits a strong peak in  
5 spring (April), especially over the southern regions. April is the month with the highest  $\tau_d$   
6 levels as a result of the high cyclonic activity over North Africa. The seasonal variability of  
7 dust is much stronger and the spring maxima much more prominent over the sea as dust is  
8 only occasionally transported there during episodic events, while over land, local sources  
9 contribute to the dust burden, especially in summer due to the soil dryness. The seasonal  
10 variability of fine mode natural aerosols is very low, the highest values appearing in spring  
11 and summer. Marine aerosols also present a very low seasonal variability, the highest values  
12 appearing in winter due to the high near surface wind speeds.

13 Overall, it is suggested that the  $AOD_{550}$ ,  $\tau_a$ ,  $\tau_d$ ,  $\tau_n$  and  $\tau_m$  high resolution gridded dataset which  
14 was compiled in this work could be used in a number of future atmospheric and biological  
15 studies focusing on the region of the Eastern Mediterranean (e.g. satellite and ground-based  
16 studies on aerosol-cloud-radiation interactions, experimental and field campaign studies on  
17 aerosols and clouds and research on the impact of aerosols on human health and nature). It is  
18 also acknowledged that a future update of the results presented here using more recent  
19 releases of MODIS aerosol data (e.g. Collection 6) and aerosol reanalysis datasets (e.g.  
20 NASA's Modern-Era Retrospective Analysis For Research And Applications Aerosol Re-  
21 analysis) would be a useful contribution.

22

## 23 **Acknowledgements**

24 This research received funding from the European Social Fund (ESF) and national resources  
25 under the operational programme Education and Lifelong Learning (EdLL) within the  
26 framework of the Action "Supporting Postdoctoral Researchers" (QUADIEEMS project),  
27 from the European Research Council under the European Union's Seventh Framework  
28 Programme (FP7/2007-2013)/ERC grant agreement no. 226144 (C8 project), from the FP7  
29 Programme MarcoPolo (grant number 606953, theme SPA.2013.3.2-01) and from the  
30 European Union's Horizon 2020 research and innovation programme under grant agreement  
31 no. 654109. The authors express their gratitude to the teams that developed the algorithms and  
32 produced the satellite products used in this study and to those who worked on the production  
33 of the model and reanalysis data used here. Special thanks are expressed to NASA Goddard

1 Space Flight Center (GSFC) Level 1 and Atmosphere Archive and Distribution System  
2 (LAADS) (<http://ladsweb.nascom.nasa.gov>) for making available the MODIS Terra and Aqua  
3 Collection 051 level-2 aerosol data and the principal investigators and staff maintaining the  
4 13 AERONET (<http://aeronet.gsfc.nasa.gov>) sites used in the present work. LIVAS has been  
5 financed under the ESA-ESTEC project LIVAS (contract no. 4000104106/11/NL/FF/fk). We  
6 thank the ICARE Data and Services Center ([www.icare.univ-lille1.fr](http://www.icare.univ-lille1.fr)) for providing access to  
7 NASA's CALIPSO data and acknowledge the use of NASA's CALIPSO data. Special thanks  
8 are expressed to ECMWF ([www.ecmwf.int](http://www.ecmwf.int)) for the provision of the ERA-Interim and MACC  
9 reanalysis data. NASA's GIOVANNI web database (<http://giovanni.gsfc.nasa.gov/giovanni/>)  
10 is highly acknowledged for the provision of Aerosol Index data from Earth Probe TOMS and  
11 OMI, aerosol data from the GOCART chemistry-aerosol-transport model (older version of  
12 GIOVANNI), tropospheric NO<sub>2</sub> and PBL SO<sub>2</sub> columnar data from OMI and precipitation data  
13 from 3B43 TRMM and Other Sources Monthly Rainfall Product. A.K.G. acknowledges the  
14 fruitful discussions with various colleagues from the Max Planck Institute for Chemistry and  
15 the Cyprus Institute (EEWRC) who indirectly contributed to this research.

16

## 17 **References**

18 Abdelkader, M., Metzger, S., Mamouri, R. E., Astitha, M., Barrie, L., Levin, Z., and  
19 Lelieveld, J.: Dust-air pollution dynamics over the eastern Mediterranean, *Atmos. Chem.*  
20 *Phys.*, 15, 9173-9189, doi:10.5194/acp-15-9173-2015, 2015.

21 Acker, J. G. and Leptoukh, G.: Online analysis enhances use of NASA Earth science data,  
22 *Eos Trans. AGU*, 88(2), 14-17, doi:10.1029/2007EO020003, 2007.

23 Alexandersson, H.: A homogeneity test applied to precipitation data, *J. Climatol.*, 6(6), 661-  
24 675, doi:10.1002/joc.3370060607, 1986.

25 Alexandri, G., Georgoulas, A. K., Zanis, P., Katragkou, E., Tsikerdekis, A., Kourtidis, K.,  
26 and Meleti, C.: On the ability of RegCM4 regional climate model to simulate surface solar  
27 radiation patterns over Europe: an assessment using satellite-based observations, *Atmos.*  
28 *Chem. Phys.*, 15, 13195-13216, doi:10.5194/acp-15-13195-2015, 2015.

29 Alpert, P. and Ganor, E.: Sahara mineral dust measurements from TOMS: Comparison to  
30 surface observations over the Middle East for the extreme dust storm, 14-17 March 1998, *J.*  
31 *Geophys. Res.*, 106, D16, doi:10.1029/2000JD900366, 2001.



1 Antoine, D. and Nobileau, D.: Recent increase of Saharan dust transport over the  
2 Mediterranean Sea, as revealed from ocean color satellite (SeaWiFS) observations, *J.*  
3 *Geophys. Res.*, 111, D12214, doi:10.1029/2005JD006795, 2006.

4 Amiridis V., Balis, D., Kazadzis, S., Giannakaki, E., Papayannis, A., and Zerefos, C.: Four  
5 years aerosol observations with a Raman lidar at Thessaloniki, Greece, in the framework of  
6 European Aerosol Research Lidar Network (EARLINET), *J. Geophys. Res.*, 110, D21203,  
7 doi:10.1029/2005JD006190, 2005.

8 Amiridis, V., Balis, D. S., Giannakaki, E., Stohl, A., Kazadzis, S., Koukouli, M. E., and  
9 Zanis, P.: Optical characteristics of biomass burning aerosols over Southeastern Europe  
10 determined from UVRaman lidar measurements, *Atmos. Chem. Phys.*, 9, 2431-2440,  
11 doi:10.5194/acp-9-2431-2009, 2009.

12 Amiridis, V., Giannakaki, E., Balis, D. S., Gerasopoulos, E., Pytharoulis, I., Zanis, P.,  
13 Kazadzis, S., Melas, D., and Zerefos, C.: Smoke injection heights from agricultural burning in  
14 Eastern Europe as seen by CALIPSO, *Atmos. Chem. Phys.*, 10, 11567-11576,  
15 doi:10.5194/acp-10-11567-2010, 2010.

16 Amiridis, V., Wandinger, U., Marinou, E., Giannakaki, E., Tsekeri, A., Basart, S., Kazadzis,  
17 S., Gkikas, A., Taylor, M., Baldasano, J., and Ansmann, A.: Optimizing CALIPSO Saharan  
18 dust retrievals, *Atmos. Chem. Phys.*, 13, 12089-12106, doi:10.5194/acp-13-12089-2013,  
19 2013.

20 Amiridis, V., Marinou, E., Tsekeri, A., Wandinger, U., Schwarz, A., Giannakaki, E.,  
21 Mamouri, R., Kokkalis, P., Biniotoglou, I., Solomos, S., Herekakis, T., Kazadzis, S.,  
22 Gerasopoulos, E., Proestakis, E., Kottas, M., Balis, D., Papayannis, A., Kontoes, C.,  
23 Kourtidis, K., Papagiannopoulos, N., Mona, L., Pappalardo, G., Le Rille, O., and Ansmann,  
24 A.: LIVAS: a 3-D multi-wavelength aerosol/cloud database based on CALIPSO and  
25 EARLINET, *Atmos. Chem. Phys.*, 15, 7127-7153, doi:10.5194/acp-15-7127-2015, 2015.

26 Athanassiou, G., Hatzianastassiou, N., Gkikas, A., Papadimas, C.D.: Estimating aerosol  
27 optical depth over the broader greek area from MODIS satellite, *Water Air Soil. Pollut.*, 224  
28 (7) doi:10.1007/S12270-013-1605-2, 2013

29 Balis, D., Amiridis, V., Nickovic, S., Papayannis, A., and Zerefos, C.: Optical properties of  
30 Saharan dust layers as detected by a Raman lidar at Thessaloniki, Greece, *Geoph. Res. Lett.*,  
31 31, doi:10.1029/2004GL019881, 2004.

1 Barnaba, F. and Gobbi, G. P.: Aerosol seasonal variability over the Mediterranean region and  
2 relative impact of maritime, continental and Saharan dust particles over the basin from  
3 MODIS data in the year 2001, *Atmos. Chem. Phys.*, 4, 2367-2391, doi:10.5194/acp-4-2367-  
4 2004, 2004.

5 Basart, S., Pérez, C., Cuevas, E., Baldasano, J. M., and Gobbi, G. P.: Aerosol characterization  
6 in Northern Africa, Northeastern Atlantic, Mediterranean Basin and Middle East from direct-  
7 sun AERONET observations, *Atmos. Chem. Phys.*, 9, 8265-8282, doi:10.5194/acp-9-8265-  
8 2009, 2009.

9 Bellouin, N., Jones, A., Haywood, J. and Christopher, S. A.: Updated estimate of aerosol  
10 direct radiative forcing from satellite observations and comparison against the Hadley Centre  
11 climate model, *J. Geophys. Res.*, 113(D10), D10205, doi:10.1029/2007JD009385, 2008.

12 Bellouin, N., Quaas, J., Morcrette, J.-J., and Boucher, O.: Estimates of aerosol radiative  
13 forcing from the MACC re-analysis, *Atmos. Chem. Phys.*, 13, 2045-2062, doi:10.5194/acp-  
14 13-2045-2013, 2013.

15 Benas, N., Hatzianastassiou, N., Matsoukas, C., Fotiadi, A., Mihalopoulos, N., and Vardavas,  
16 I.: Aerosol shortwave direct radiative effect and forcing based on MODIS Level 2 data in the  
17 Eastern Mediterranean (Crete), *Atmos. Chem. Phys.*, 11, 12647-12662, doi:10.5194/acp-11-  
18 12647-2011, 2011.

19 Benas, N., Beloconi, A., and Chrysoulakis, N.: Estimation of urban PM10 concentration ,  
20 based on MODIS and MERIS / AATSR synergistic observations, *Atmos. Environ.*, 79, 448-  
21 454, doi:10.1016/j.atmosenv.2013.07.012, 2013.

22 Benedetti, A., Morcrette, J.-J., Boucher, O., Dethof, A., Engelen, R. J., Fisher, M., Flentjes,  
23 H., Huneeus, N., Jones, L., Kaiser, J. W., Kinne, S., Mangold, A., Razinger, M., Simmons, A.  
24 J., Suttie, M., and the GEMS-AER team: Aerosol analysis and forecast in the ECMWF  
25 Integrated Forecast System. Part II: Data assimilation, *J. Geophys. Res.*, 114, D13205,  
26 doi:10.1029/2008JD011115, 2009.

27 Bergamo, A., Tafuro, A. M., Kinne, S., De Tomasi, F., and Perrone, M. R.: Monthly-averaged  
28 anthropogenic aerosol direct radiative forcing over the Mediterranean based on AERONET  
29 aerosol properties, *Atmos. Chem. Phys.*, 8, 6995-7014, doi:10.5194/acp-8-6995-2008, 2008.

30 Bucsela, E. J., Krotkov, N. A., Celarier, E. A., Lamsal, L. N., Swartz, W. H., Bhartia, P. K.,  
31 Boersma, K. F., Veefkind, J. P., Gleason, J. F., and Pickering, K. E.: A new stratospheric and

1 tropospheric NO<sub>2</sub> retrieval algorithm for nadir-viewing satellite instruments: applications to  
2 OMI, *Atmos. Meas. Tech.*, 6, 2607-2626, doi:10.5194/amt-6-2607-2013, 2013.

3 Burton, S. P., Ferrare, R. A., Vaughan, M. A., Omar, A. H., Rogers, R. R., Hostetler, C. A.,  
4 and Hair, J. W.: Aerosol classification from airborne HSRL and comparisons with the  
5 CALIPSO vertical feature mask, *Atmos. Meas. Tech.*, 6, 1397-1412, doi:10.5194/amt-6-  
6 1397-2013, 2013.

7 Carmona, I. and Alpert, P.: Synoptic classification of Moderate Resolution Imaging  
8 Spectroradiometer aerosols over Israel, *J. Geophys. Res.*, 114(D7), D07208,  
9 doi:10.1029/2008JD010160, 2009.

10 Cesnulyte, V., Lindfors, A. V., Pitkänen, M. R. A., Lehtinen, K. E. J., Morcrette, J.-J., and  
11 Arola, A.: Comparing ECMWF AOD with AERONET observations at visible and UV  
12 wavelengths, *Atmos. Chem. Phys.*, 14, 593-608, doi:10.5194/acp-14-593-2014, 2014.

13 Chin, M., Rood, R. B., Lin, S.-J., Müller, J.-F. and Thompson, A. M.: Atmospheric sulfur  
14 cycle simulated in the global model GOCART: Model description and global properties, *J.*  
15 *Geophys. Res.*, 105(D20), 24671, doi:10.1029/2000JD900384, 2000.

16 Chin, M., Ginoux, P., Kinne, S., Torres, O., Holben, B. N., Duncan, B. N., Martin, R. V.,  
17 Logan, J. A., Higurashi, A. and Nakajima, T.: Tropospheric Aerosol Optical Thickness from  
18 the GOCART Model and Comparisons with Satellite and Sun Photometer Measurements, *J.*  
19 *Atmos. Sci.*, 59(3), 461-483, doi:10.1175/1520-0469(2002)059<0461:TAOTFT>2.0.CO;2,  
20 2002.

21 Chin, M., Chu, A., Levy, R., Remer, L., Kaufman, Y., Holben, B., Eck, T., Ginoux, P. and  
22 Gao, Q.: Aerosol distribution in the Northern Hemisphere during ACE-Asia: Results from  
23 global model, satellite observations, and Sun photometer measurements, *J. Geophys. Res.*  
24 *Atmos.*, 109(D23), n/a-n/a, doi:10.1029/2004JD004829, 2004.

25 Chin, Mian, Diehl, T., Ginoux, P., and Malm, W.: Intercontinental transport of pollution and  
26 dust aerosols: implications for regional air quality, *Atmos. Chem. Phys.*, 7, 5501-5517,  
27 doi:10.5194/acp-7-5501-2007, 2007.

28 Chin, M., Diehl, T., Dubovik, O., Eck, T. F., Holben, B. N., Sinyuk, A., and Streets, D. G.:  
29 Light absorption by pollution, dust, and biomass burning aerosols: a global model study and  
30 evaluation with AERONET measurements, *Ann. Geophys.*, 27, 3439-3464,  
31 doi:10.5194/angeo-27-3439-2009, 2009.

1 Chu, D. A., Kaufman, Y. J., Ichoku, C., Remer, L. A., Tanre, D., and Holben, B. N.:  
2 Validation of MODIS aerosol optical depth retrieval over land. *Geophys. Res. Lett.*, 29, 8007,  
3 doi:10.1029/2001GL013205, 2002.

4 Cuevas, E., Camino, C., Benedetti, A., Basart, S., Terradellas, E., Baldasano, J. M.,  
5 Morcrette, J. J., Marticorena, B., Goloub, P., Mortier, A., Berjón, A., Hernández, Y., Gil-  
6 Ojeda, M., and Schulz, M.: The MACC-II 2007-2008 reanalysis: atmospheric dust evaluation  
7 and characterization over northern Africa and the Middle East, *Atmos. Chem. Phys.*, 15,  
8 3991-4024, doi:10.5194/acp-15-3991-2015, 2015.

9 De Meij, A. and Lelieveld, J.: Evaluating aerosol optical properties observed by ground-based  
10 and satellite remote sensing over the Mediterranean and the Middle East in 2006, *Atmos.*  
11 *Res.*, 99(3-4), 415-433, doi:10.1016/j.atmosres.2010.11.005, 2011.

12 De Meij, A., Pozzer, A., Pringle, K. J., Tost, H., Lelieveld, J.: EMAC model evaluation and  
13 analysis of atmospheric aerosol properties and distribution, *Atmos. Res.*, 114-115, 38-69,  
14 2012.

15 Dee, D. P., Uppala, S. M., Simmons, a. J., Berrisford, P., Poli, P., Kobayashi, S., Andrae, U.,  
16 Balmaseda, M. a., Balsamo, G., Bauer, P., Bechtold, P., Beljaars, a. C. M., van de Berg, L.,  
17 Bidlot, J., Bormann, N., Delsol, C., Dragani, R., Fuentes, M., Geer, a. J., Haimberger, L.,  
18 Healy, S. B., Hersbach, H., Hólm, E. V., Isaksen, L., Kállberg, P., Köhler, M., Matricardi, M.,  
19 McNally, a. P., Monge-Sanz, B. M., Morcrette, J. J., Park, B. K., Peubey, C., de Rosnay, P.,  
20 Tavolato, C., Thépaut, J. N. and Vitart, F.: The ERA-Interim reanalysis: Configuration and  
21 performance of the data assimilation system, *Q. J. R. Meteorol. Soc.*, 137(656), 553-597,  
22 doi:10.1002/qj.828, 2011.

23 Derimian, Y., Karnieli, A., Kaufman, Y. J., Andreae, M. O., Andreae, T. W., Dubovik, O.,  
24 Maenhaut, W., Koren, I. and Holben, B. N.: Dust and pollution aerosols over the Negev  
25 desert, Israel: Properties, transport, and radiative effect, *J. Geophys. Res.*, 111(D5), D05205,  
26 doi:10.1029/2005JD006549, 2006.

27 Dubovik, O., Smirnov, a., Holben, B. N., King, M. D., Kaufman, Y. J., Eck, T. F. and  
28 Slutsker, I.: Accuracy assessments of aerosol optical properties retrieved from Aerosol  
29 Robotic Network (AERONET) Sun and sky radiance measurements, *J. Geophys. Res.*,  
30 105(D8), 9791, doi:10.1029/2000JD900040, 2000.

1 Dubovik, O. and King, M. D.: A flexible inversion algorithm for retrieval of aerosol optical  
2 properties from Sun and sky radiance measurements, *J. Geophys. Res.*, 105(D16), 20673,  
3 doi:10.1029/2000JD900282, 2000.

4 Dubovik, O., Holben, B., Eck, T. F., Smirnov, A., Kaufman, Y. J., King, M. D., Tanré, D. and  
5 Slutsker, I.: Variability of Absorption and Optical Properties of Key Aerosol Types Observed  
6 in Worldwide Locations, *J. Atmos. Sci.*, 59(3), 590-608, doi:10.1175/1520-  
7 0469(2002)059<0590:VOAAOP>2.0.CO;2, 2002.

8 Eck, T. F., Holben, B. N., Reid, J. S., Dubovik, O., Smirnov, A., O'Neill, N. T., Slutsker, I.  
9 and Kinne, S.: Wavelength dependence of the optical depth of biomass burning, urban, and  
10 desert dust aerosols, *J. Geophys. Res.*, 104, 31333-31349, doi:10.1029/1999jd900923, 1999.

11 Elguindi, N., Clark, H., Ordóñez, C., Thouret, V., Flemming, J., Stein, O., Huijnen, V.,  
12 Moinat, P., Inness, A., Peuch, V.-H., Stohl, A., Turquety, S., Athier, G., Cammas, J.-P., and  
13 Schultz, M.: Current status of the ability of the GEMS/MACC models to reproduce the  
14 tropospheric CO vertical distribution as measured by MOZAIC, *Geosci. Model Dev.*, 3, 501-  
15 518, doi:10.5194/gmd-3-501-2010, 2010

16 El-Metwally, M., Alfaro, S. C., Abdel Wahab, M. M., Zakey, A. S., and Chatenet, B.:  
17 Seasonal and inter-annual variability of the aerosol content in Cairo (Egypt) as deduced from  
18 the comparison of MODIS aerosol retrievals with direct AERONET measurements, *Atmos.*  
19 *Res.*, 97, 14-25, doi:10.1016/j.atmosres.2010.03.003, 2010.

20 El-Metwally, M. and Alfaro, S. C.: Correlation between meteorological conditions and  
21 aerosol characteristics at an East-Mediterranean coastal site, *Atmos. Res.*, 132-133, 76-90,  
22 doi:10.1016/j.atmosres.2013.05.006, 2013.

23 Flaounas, E., Kotroni, V., Lagouvardos, K., Kazadzis, S., Gkikas, A. and Hatzianastassiou,  
24 N.: Cyclone contribution to dust transport over the Mediterranean region, *Atmos. Sci. Lett.*,  
25 16(4), 473-478, doi:10.1002/asl.584, 2015.

26 Georgoulas, A. K., Balis, D., Koukouli, M. E., Meleti, C., Bais, A. and Zerefos, C.: A study  
27 of the total atmospheric sulfur dioxide load using ground-based measurements and the  
28 satellite derived Sulfur Dioxide Index, *Atmos. Environ.*, 43(9), 1693-1701,  
29 doi:10.1016/j.atmosenv.2008.12.012, 2009.

- 1 Georgoulas, A. K. and Kourtidis, K. A.: On the aerosol weekly cycle spatiotemporal  
2 variability over Europe, *Atmos. Chem. Phys.*, 11, 4611-4632, doi:10.5194/acp-11-4611-2011,  
3 2011.
- 4 Georgoulas, A. K. and Kourtidis, K. A.: A high resolution satellite view of the aerosol  
5 weekly cycle variability over Central Europe, *Atmos. Res.*, 107, 145-160,  
6 doi:10.1016/j.atmosres.2012.01.003, 2012.
- 7 Georgoulas, A. K., Kourtidis, K. A., Kosmidis, E., Despotakis, T., and Symeonidis, P.:  
8 AMFIC-WSDB: a web data base for hosting and easy retrieval of atmospheric data from  
9 satellites, *Comput. Geosci.*, 48, 57-66, doi:10.1016/j.cageo.2012.05.001, 2012.
- 10 Georgoulas, A. K., Kourtidis, K. A., Alexandri, G., Rapsomanikis, S., and Sanchez-Lorenzo,  
11 A.: Common summertime total cloud cover and aerosol optical depth weekly variabilities  
12 over Europe: sign of the aerosol indirect effects?, *Atmos. Res.*, 153, 59-73,  
13 doi:10.1016/j.atmosres.2014.07.031, 2015.
- 14 Gerasopoulos, E., Kokkalis, P., Amiridis, V., Liakakou, E., Perez, C., Haustein, K.,  
15 Eleftheratos, K., Andreae, M. O., Andreae, T. W., and Zerefos, C. S.: Dust specific extinction  
16 cross-sections over the Eastern Mediterranean using the BSC-DREAM model and sun  
17 photometer data: the case of urban environments, *Ann. Geophys.*, 27, 2903-2912,  
18 doi:10.5194/angeo-27-2903-2009, 2009.
- 19 Gerasopoulos, E., Amiridis, V., Kazadzis, S., Kokkalis, P., Eleftheratos, K., Andreae, M. O.,  
20 Andreae, T. W., El-Askary, H., and Zerefos, C. S.: Three-year ground based measurements of  
21 aerosol optical depth over the Eastern Mediterranean: the urban environment of Athens,  
22 *Atmos. Chem. Phys.*, 11, 2145-2159, doi:10.5194/acp-11-2145-2011, 2011.
- 23 Ginoux, P., Chin, M., Tegen, I., Prospero, J. M., Holben, B., Dubovik, O. and Lin, S.-J.:  
24 Sources and distributions of dust aerosols simulated with the GOCART model, *J. Geophys.*  
25 *Res.*, 106(D17), 20255, doi:10.1029/2000JD000053, 2001.
- 26 Ginoux, P., Prospero, J., Torres, O. and Chin, M.: Long-term simulation of global dust  
27 distribution with the GOCART model: correlation with North Atlantic Oscillation, *Environ.*  
28 *Model. Softw.*, 19(2), 113-128, doi:10.1016/S1464-8152(03)00114-2, 2004.
- 29 Ginoux, P., Clarisse, L., Clerbaux, C., Coheur, P.-F., Dubovik, O., Hsu, N. C., and Van  
30 Damme, M.: Mixing of dust and NH<sub>3</sub> observed globally over anthropogenic dust sources,  
31 *Atmos. Chem. Phys.*, 12, 7351-7363, doi:10.5194/acp-12-7351-2012, 2012.

- 1 Giorgi, F.: Climate change hot-spots, *Geophys. Res. Lett.*, 33(8), 1-4,  
2 doi:10.1029/2006GL025734, 2006.
- 3 Gkikas, A., Hatzianastassiou, N., and Mihalopoulos, N.: Aerosol events in the broader  
4 Mediterranean basin based on 7-year (2000-2007) MODIS C005 data, *Ann. Geophys.*, 27,  
5 3509-3522, doi:10.5194/angeo-27-3509-2009, 2009
- 6 Gkikas, A., Hatzianastassiou, N., Mihalopoulos, N., Katsoulis, V., Kazadzis, S., Pey, J.,  
7 Querol, X., and Torres, O.: The regime of intense desert dust episodes in the Mediterranean  
8 based on contemporary satellite observations and ground measurements, *Atmos. Chem. Phys.*,  
9 13, 12135-12154, doi:10.5194/acp-13-12135-2013, 2013.
- 10 Gkikas, A., Houssos, E. E., Lolis, C. J., Bartzokas, A., Mihalopoulos, N., and  
11 Hatzianastassiou, N.: Atmospheric circulation evolution related to desert-dust episodes over  
12 the Mediterranean, *Q. J. Roy. Meteorol. Soc.*, 690, 1634-1645, 2014.
- 13 Hatzianastassiou, N., Gkikas, A., Mihalopoulos, N., Torres, O. and Katsoulis, B. D.: Natural  
14 versus anthropogenic aerosols in the eastern Mediterranean basin derived from multiyear  
15 TOMS and MODIS satellite data, *J. Geophys. Res. Atmos.*, 114(24),  
16 doi:10.1029/2009JD011982, 2009.
- 17 Herman, J. R., Bhartia, P. K., Torres, O., Hsu, C., Seftor, C. and Celarier, E.: Global  
18 distribution of UV-absorbing aerosols from Nimbus 7/TOMS data, *J. Geophys. Res. Atmos.*,  
19 102(D14), 16911-16922, doi:10.1029/96JD03680, 1997.
- 20 Herrmann, M., Somot, S., Calmanti, S., Dubois, C., and Sevault, F.: Representation of spatial  
21 and temporal variability of daily wind speed and of intense wind events over the  
22 Mediterranean Sea using dynamical downscaling: impact of the regional climate model  
23 configuration, *Nat. Hazards Earth Syst. Sci.*, 11, 1983-2001, doi:10.5194/nhess-11-1983-  
24 2011, 2011.
- 25 Holben, B. N., Eck, T. F., Slutsker, I., Tanré, D., Buis, J. P., Setzer, A., Vermote, E., Reagan,  
26 J. A., Kaufman, Y. J., Nakajima, T., Lavenu, F., Jankowiak, I. and Smirnov, A.:  
27 AERONET—A Federated Instrument Network and Data Archive for Aerosol  
28 Characterization, *Remote Sens. Environ.*, 66(1), 1-16, doi:10.1016/S0034-4257(98)00031-5,  
29 1998.
- 30 Holben, B. N., Tanré, D., Smirnov, A., Eck, T. F., Slutsker, I., Abuhassan, N., Newcomb, W.  
31 W., Schafer, J. S., Chatenet, B., Lavenu, F., Kaufman, Y. J., Castle, J. Vande, Setzer, A.,

1 Markham, B., Clark, D., Frouin, R., Halthore, R., Karneli, A., O'Neill, N. T., Pietras, C.,  
2 Pinker, R. T., Voss, K. and Zibordi, G.: An emerging ground-based aerosol climatology:  
3 Aerosol optical depth from AERONET, *J. Geophys. Res. Atmos.*, 106(D11), 12067-12097,  
4 doi:10.1029/2001JD900014, 2001.

5 Hsu, N. C., Tsay, S. C., King, M. D. and Herman, J. R.: Aerosol properties over bright-  
6 reflecting source regions, *IEEE Trans. Geosci. Remote Sens.*, 42(3), 557-569,  
7 doi:10.1109/TGRS.2004.824067, 2004.

8 Hsu, N. C., Tsay, S. C., King, M. D. and Herman, J. R.: Deep Blue retrievals of Asian aerosol  
9 properties during ACE-Asia, *IEEE Trans. Geosci. Remote Sens.*, 44(11), 3180-3195,  
10 doi:10.1109/TGRS.2006.879540, 2006.

11 Hsu, N. C., Jeong, M.-J., Bettenhausen, C., Sayer, A. M., Hansell, R., Seftor, C. S., Huang, J.  
12 and Tsay, S.-C.: Enhanced Deep Blue aerosol retrieval algorithm: The second generation, *J.*  
13 *Geophys. Res. Atmos.*, 118(16), 9296-9315, doi:10.1002/jgrd.50712, 2013.

14 Huffman, G. J., Bolvin, D. T., Nelkin, E. J., Wolff, D. B., Adler, R. F., Gu, G., Hong, Y.,  
15 Bowman, K. P., and Stocker, E. F.: The TRMM Multisatellite Precipitation Analysis  
16 (TMPA): quasiglobal, multiyear, combined-sensor precipitation estimates at fine scales, *J.*  
17 *Hydrometeorol.*, 8, 38-55, doi:10.1175/JHM560.1, 2007.

18 Husar, R. B., Prospero, J. M., and Stowe, L. L.: Characterization of tropospheric aerosols over  
19 the oceans with the NOAA advanced very high resolution radiometer optical thickness  
20 operational product, *J. Geophys. Res.*, 102, 16889-16909, 1997.

21 Ichoku, C.: A spatio-temporal approach for global validation and analysis of MODIS aerosol  
22 products, *Geophys. Res. Lett.*, 29(12), 8006, doi:10.1029/2001GL013206, 2002.

23 Ichoku, C., Remer, L. A., and Eck, T. F.: Quantitative evaluation and intercomparison of  
24 morning and afternoon Moderate Resolution Imaging Spectroradiometer (MODIS) aerosol  
25 measurements from Terra and Aqua, *J. Geophys. Res.-Atmos.*, 110, D10S03,  
26 doi:10.1029/2004JD004987, 2005.

27 Im, U., Markakis, K., Koçak, M., Gerasopoulos, E., Daskalakis, N., Mihalopoulos, N.,  
28 Poupkou, A., Kindap, T., Unal, A. and Kanakidou, M.: Summertime aerosol chemical  
29 composition in the Eastern Mediterranean and its sensitivity to temperature, *Atmos. Environ.*,  
30 50, 164-173, doi:10.1016/j.atmosenv.2011.12.044, 2012.



1 Inness, A., Baier, F., Benedetti, A., Bouarar, I., Chabrillat, S., Clark, H., Clerbaux, C.,  
2 Coheur, P., Engelen, R. J., Errera, Q., Flemming, J., George, M., Granier, C., Hadji-Lazaro,  
3 J., Huijnen, V., Hurtmans, D., Jones, L., Kaiser, J. W., Kapsomenakis, J., Lefever, K., Leitão,  
4 J., Razinger, M., Richter, A., Schultz, M. G., Simmons, A. J., Suttie, M., Stein, O., Thépaut,  
5 J.-N., Thouret, V., Vrekoussis, M., Zerefos, C., and the MACC team: The MACC reanalysis:  
6 an 8 yr data set of atmospheric composition, *Atmos. Chem. Phys.*, 13, 4073-4109,  
7 doi:10.5194/acp-13-4073-2013, 2013.

8 Israelevich, P. L., Levin, Z., Joseph, J. H., and Ganor, E.: Desert aerosol transport in the  
9 Mediterranean region as inferred from the TOMS aerosol index, *J. Geophys. Res.*, 107(D21),  
10 4572, doi:10.1029/2001JD002011, 2002.

11 Israelevich, P. L., Ganor, E., Levin, Z., and Joseph, J. H.: Annual variations of physical  
12 properties of desert dust over Israel, *J. Geophys. Res.*, 108(D13), 4381,  
13 doi:10.1029/2002JD003163, 2003.

14 Israelevich, P., Ganor, E., Alpert, P., Kishcha, P. and Stupp, A.: Predominant transport paths  
15 of Saharan dust over the Mediterranean Sea to Europe, *J. Geophys. Res.*, 117(D2), D02205,  
16 doi:10.1029/2011JD016482, 2012.

17 Jones, T. A. and Christopher, S. A.: A reanalysis of MODIS fine mode fraction over ocean  
18 using OMI and daily GOCART simulations, *Atmos. Chem. Phys.*, 11, 5805-5817,  
19 doi:10.5194/acp-11-5805-2011, 2011.

20 Kabatas, B., Unal, A., Pierce, R. B., Kindap, T. and Pozzoli, L.: The contribution of Saharan  
21 dust in PM10 concentration levels in Anatolian Peninsula of Turkey, *Sci. Total Environ.*, 488-  
22 489(1), 413-421, doi:10.1016/j.scitotenv.2013.12.045, 2014.

23 Kalivitis, N., Gerasopoulos, E., Vrekoussis, M., Kouvarakis, G., Kubilay, N.,  
24 Hatzianastassiou, N., Vardavas, I. and Mihalopoulos, N.: Dust transport over the eastern  
25 Mediterranean derived from Total Ozone Mapping Spectrometer, Aerosol Robotic Network,  
26 and surface measurements, *J. Geophys. Res.*, 112(D3), D03202, doi:10.1029/2006JD007510,  
27 2007.

28 Kanakidou, M., Mihalopoulos, N., Kindap, T., Im, U., Vrekoussis, M., Gerasopoulos, E.,  
29 Dermizaki, E., Unal, A., Koçak, M., Markakis, K., Melas, D., Kouvarakis, G., Youssef, A.  
30 F., Richter, A., Hatzianastassiou, N., Hilboll, A., Ebojje, F., Wittrock, F., von Savigny, C.,  
31 Burrows, J. P., Ladstaetter-Weissenmayer, A. and Moubasher, H.: Megacities as hot spots of

1 air pollution in the East Mediterranean, *Atmos. Environ.*, 45(6), 1223-1235,  
2 doi:10.1016/j.atmosenv.2010.11.048, 2011.

3 Karnieli, A., Derimian, Y., Indoitu, R., Panov, N., Levy, R. C., Remer, L. A., Maenhaut, W.,  
4 and Holben, B. N.: Temporal trend in anthropogenic sulfur aerosol transport from central and  
5 eastern Europe to Israel, *J. Geophys. Res.*, 114, D00D19, doi:10.1029/2009JD011870, 2009.

6 Kaskaoutis, D. G., Kosmopoulos, P., Kambezidis, H. D. and Nastos, P. T.: Aerosol  
7 climatology and discrimination of different types over Athens, Greece, based on MODIS data,  
8 *Atmos. Environ.*, 41(34), 7315-7329, doi:10.1016/j.atmosenv.2007.05.017, 2007.

9 Kaskaoutis, D. G., Kambezidis, H. D., Nastos, P. T. and Kosmopoulos, P. G.: Study on an  
10 intense dust storm over Greece, *Atmos. Environ.*, 42(29), 6884-6896,  
11 doi:10.1016/j.atmosenv.2008.05.017, 2008.

12 Kaskaoutis, D. G., Nastos, P. T., Kosmopoulos, P. G. and Kambezidis, H. D.: The combined  
13 use of satellite data, air-mass trajectories and model applications for monitoring dust transport  
14 over Athens, Greece, *Int. J. Remote Sens.*, 31(19), 5089-5109,  
15 doi:10.1080/01431160903283868, 2010.

16 Kaskaoutis, D. G., Kharol, S. K., Sifakis, N., Nastos, P. T., Sharma, A. R., Badarinath, K. V.  
17 S. and Kambezidis, H. D.: Satellite monitoring of the biomass-burning aerosols during the  
18 wildfires of August 2007 in Greece: Climate implications, *Atmos. Environ.*, 45(3), 716-726,  
19 doi:10.1016/j.atmosenv.2010.09.043, 2011.

20 Kaskaoutis, D. G., Kosmopoulos, P. G., Nastos, P. T., Kambezidis, H. D., Sharma, M. and  
21 Mehdi, W.: Transport pathways of Sahara dust over Athens, Greece as detected by MODIS  
22 and TOMS, *Geomatics, Nat. Hazards Risk*, 3(1), 35-54, doi:10.1080/19475705.2011.574296,  
23 2012a.

24 Kaskaoutis, D. G., Prasad, A. K., Kosmopoulos, P. G., Sinha, P. R., Kharol, S. K., Gupta, P.,  
25 El-Askary, H. M. and Kafatos, M.: Synergistic use of remote sensing and modeling for  
26 tracing dust storms in the mediterranean, *Adv. Meteorol.*, 2012, doi:10.1155/2012/861026,  
27 2012b.

28 Kaskaoutis, D. G., Nastos, P. T., Kosmopoulos, P. G. and Kambezidis, H. D.: Characterising  
29 the long-range transport mechanisms of different aerosol types over Athens, Greece during  
30 2000-2005, *Int. J. Climatol.*, 32(8), 1249-1270, doi:10.1002/joc.2357, 2012c.

- 1 Kaskaoutis, D. G., Kahn, R. A., Pawan Gupta, P., Jayaraman, A., and Bartzokas, A.: Desert  
2 Dust Properties, Modelling, and Monitoring, *Advances in Meteorology*, vol. 2012, ID  
3 483632, 2 pp, 2012. doi:10.1155/2012/483632, 2012d.
- 4 Kaufman, Y. J., Tanré, D., Remer, L. a., Vermote, E. F., Chu, a. and Holben, B. N.:  
5 Operational remote sensing of tropospheric aerosol over land from EOS moderate resolution  
6 imaging spectroradiometer, *J. Geophys. Res.*, 102(D14), 17051, doi:10.1029/96JD03988,  
7 1997.
- 8 Kaufman, Y. J., Koren, I., Remer, L. A., Tanré, D., Ginoux, P. and Fan, S.: Dust transport and  
9 deposition observed from the Terra-Moderate Resolution Imaging Spectroradiometer  
10 (MODIS) spacecraft over the Atlantic Ocean, *J. Geophys. Res. D Atmos.*, 110(10), 1-16,  
11 doi:10.1029/2003JD004436, 2005.
- 12 Kazadzis, S., Bais, A., Amiridis, V., Balis, D., Meleti, C., Kouremeti, N., Zerefos, C. S.,  
13 Rapsomanikis, S., Petrakakis, M., Kelesis, A., Tzoumaka, P., and Kelektoglou, K.: Nine  
14 years of UV aerosol optical depth measurements at Thessaloniki, Greece, *Atmos. Chem.*  
15 *Phys.*, 7, 2091-2101, doi:10.5194/acp-7-2091-2007, 2007.
- 16 Kazadzis, S., Veselovskii, I., Amiridis, V., Gröbner, J., Suvorina, A., Nyeki, S.,  
17 Gerasopoulos, E., Kouremeti, N., Taylor, M., Tsekeri, A., and Wehrli, C.: Aerosol  
18 microphysical retrievals from precision filter radiometer direct solar radiation measurements  
19 and comparison with AERONET, *Atmos. Meas. Tech.*, 7, 2013-2025, doi:10.5194/amt-7-  
20 2013-2014, 2014.
- 21 Kelektoglou, K. and Rapsomanikis, S.: AERONET observations of direct and indirect  
22 aerosol effects over a South European conurbation, *Int. J. Remote Sens.*, 32, 2779-2798,  
23 2011.
- 24 Khaliq, M. N. and Ouarda, T. B. M. J.: On the critical values of the standard normal  
25 homogeneity test (SNHT), *Int. J. Climatol.*, 27(5), 681-687, doi:10.1002/joc.1438, 2007.
- 26 Kloog, I., Sorek-Hamer, M., Lyapustin, A., Coull, B., Wang, Y., Just, A. C., Schwartz, J., and  
27 Broday, D. M.: Estimating daily PM<sub>2.5</sub> and PM<sub>10</sub> across the complex geo-climate region of  
28 Israel using MAIAC satellite-based AOD data, *Atmos. Environ.*, 122, 409-416,  
29 doi:10.1016/j.atmosenv.2015.10.004, 2015.
- 30 Kokkalis, P., Papayannis, A., Amiridis, V., Mamouri, R. E., Veselovskii, I., Kolgotin, A.,  
31 Tsaknakis, G., Kristiansen, N. I., Stohl, A., and Mona, L.: Optical, microphysical, mass and

1 geometrical properties of aged volcanic particles observed over Athens, Greece, during the  
2 Eyjafjallajökull eruption in April 2010 through synergy of Raman lidar and sunphotometer  
3 measurements, *Atmos. Chem. Phys.*, 13, 9303-9320, doi:10.5194/acp-13-9303-2013, 2013.

4 Koren, I., Joseph, J.H., Israelevich P.: Detection of dust plumes and their sources in  
5 northeastern Libya, *Can J Remote Sens*, 29 (2003), pp. 792-796, 2003.

6 Kosmopoulos, P. G., Kaskaoutis, D. G., Nastos, P. T., and Kambezidis, H. D.: Seasonal  
7 variation of columnar aerosol optical properties over Athens, Greece, based on MODIS data,  
8 *Remote Sens. Environ.*, 112, 2354-2366, doi:10.1016/j.rse.2007.11.006, 2008.

9 Koukouli, M., Balis, D., Amiridis, V., Kazadzis, S., Bais, A., Nickovic, S. and Torres, O.:  
10 Aerosol variability over Thessaloniki using ground based remote sensing observations and the  
11 TOMS aerosol index, *Atmos. Environ.*, 40(28), 5367-5378,  
12 doi:10.1016/j.atmosenv.2006.04.046, 2006.

13 Koukouli, M. E., Kazadzis, S., Amiridis, V., Ichoku, C., and Balis, D. S.: Comparisons of  
14 satellite derived aerosol optical depth over a variety of sites in the southern Balkan region as  
15 an indicator of local air quality, *Remote sensing of clouds and the atmosphere XII*, edited by:  
16 Comerón, A., Picard, R. H., Schäfer, K., Slusser, J. R., and Amodeo, A., *Proceedings of SPIE*,  
17 Vol. 67451V, doi:10.1117/12.737681, 2007.

18 Koukouli, M. E., Kazadzis, S., Amiridis, V., Ichoku, C., Balis, D. S. and Bais, A. F.: Signs of  
19 a negative trend in the MODIS aerosol optical depth over the Southern Balkans, *Atmos.*  
20 *Environ.*, 44(9), 1219-1228, doi:10.1016/j.atmosenv.2009.11.024, 2010.

21 Kourtidis, K., Rapsomanikis, S., Zerefos, C., Georgoulas, A. K., Pavlidou E.: Severe  
22 particulate pollution from the deposition practices of the primary materials of a cement plant,  
23 *Environ. Sci. Pollut. Res.*, 21, 9796-9808. doi:10.1007/S12356-014-2969-6, 2014.

24 Kourtidis, K., Stathopoulos, S., Georgoulas, A. K., Alexandri, G., and Rapsomanikis, S.: A  
25 study of the impact of synoptic weather conditions and water vapor on aerosol-cloud  
26 relationships over major urban clusters of China, *Atmos. Chem. Phys.*, 15, 10955-10964,  
27 doi:10.5194/acp-15-10955-2015, 2015.

28 Kubilay, N.: Optical properties of mineral dust outbreaks over the northeastern  
29 Mediterranean, *J. Geophys. Res.*, 108(D21), 4666, doi:10.1029/2003JD003798, 2003.

1 Lehahn, Y., Koren, I., Boss, E., Ben-Ami, Y., and Altaratz, O.: Estimating the maritime  
2 component of aerosol optical depth and its dependency on surface wind speed using satellite  
3 data, *Atmos. Chem. Phys.*, 10, 6711-6720, doi:10.5194/acp-10-6711-2010, 2010.

4 Lelieveld, J., Berresheim, H., Borrmann, S., Crutzen, P. J., Dentener, F. J., Fischer, H.,  
5 Feichter, J., Flatau, P. J., Heland, J., Holzinger, R., Korrmann, R., Lawrence, M. G., Levin,  
6 Z., Markowicz, K. M., Mihalopoulos, N., Minikin, A., Ramanathan, V., De Reus, M.,  
7 Roelofs, G. J., Scheeren, H. A., Sciare, J., Schlager, H., Schultz, M., Siegmund, P., Steil, B.,  
8 Stephanou, E. G., Stier, P., Traub, M., Warneke, C., Williams, J., and Ziereis, H.: Global air  
9 pollution crossroads over the Mediterranean., *Science*, 298(5594), 794-799,  
10 doi:10.1126/science.1075457, 2002.

11 Levelt, P. F., Van den Oord, G. H. J., Dobber, M. R., Malkki, A., Visser, H., de Vries, J.,  
12 Stammes, P., Lundell, J. O. V and Saari, H.: The Ozone Monitoring Instrument, *Ieee Trans.*  
13 *Geosci. Remote Sens.*, 44(5), 1093-1101, doi:Urn:nbn:nl:ui:25-648485, 2006.

14 Levy, R. C.: Evaluation of the Moderate-Resolution Imaging Spectroradiometer (MODIS)  
15 retrievals of dust aerosol over the ocean during PRIDE, *J. Geophys. Res.*, 108(D19), 8594,  
16 doi:10.1029/2002JD002460, 2003.

17 Levy, R. C., Remer, L. A. and Dubovik, O.: Global aerosol optical properties and application  
18 to Moderate Resolution Imaging Spectroradiometer aerosol retrieval over land, *J. Geophys.*  
19 *Res. Atmos.*, 112(D13), doi:10.1029/2006JD007815, 2007a.

20 Levy, R. C., Remer, L. A., Mattoo, S., Vermote, E. F., and Kaufman, Y. J.: Second-  
21 generation operational algorithm: Retrieval of aerosol properties over land from inversion of  
22 Moderate Resolution Imaging Spectroradiometer spectral reflectance, *J. Geophys. Res.*  
23 *Atmos.*, 112(D13), doi:10.1029/2006JD007811, 2007b.

24 Levy, R., Remer, L., Tanré, D., Mattoo, S., and Kaufman, Y.: Algorithm for remote sensing  
25 of tropospheric aerosol over dark targets from MODIS: Collections 005 and 051: Revision 2,  
26 February 2009, MODIS Algorithm Theoretical Basis Document, 2009.

27 Levy, R. C., Remer, L. A., Kleidman, R. G., Mattoo, S., Ichoku, C., Kahn, R., and Eck, T. F.:  
28 Global evaluation of the Collection 5 MODIS dark-target aerosol products over land, *Atmos.*  
29 *Chem. Phys.*, 10, 10399-10420, doi:10.5194/acp-10-10399-2010, 2010.

1 Levy, R. C., Mattoo, S., Munchak, L. A., Remer, L. A., Sayer, A. M., Patadia, F., and Hsu, N.  
2 C.: The Collection 6 MODIS aerosol products over land and ocean, *Atmos. Meas. Tech.*, 6,  
3 2989-3034, doi:10.5194/amt-6-2989-2013, 2013.

4 Li, J., Carlson, B. E., and Lacis, A. A.: A study on the temporal and spatial variability of  
5 absorbing aerosols using Total Ozone Mapping Spectrometer and Ozone Monitoring  
6 Instrument Aerosol Index data, *J. Geophys. Res.*, 114(D9), D09213,  
7 doi:10.1029/2008JD011278, 2009.

8 Li, C., Joiner, J., Krotkov, N. A., and Bhartia, P. K.: A fast and sensitive new satellite SO<sub>2</sub>  
9 retrieval algorithm based on principal component analysis: Application to the ozone  
10 monitoring instrument, *Geophys. Res. Lett.*, 40, 6314-6318, doi:10.1002/2013GL058134,  
11 2013.

12 Li, J., Carlson, B. E., Dubovik, O., and Lacis, A. A.: Recent trends in aerosol optical  
13 properties derived from AERONET measurements, *Atmos. Chem. Phys.*, 14, 12271-12289,  
14 doi:10.5194/acp-14-12271-2014, 2014.

15 Liora, N., Markakis, K., Poupkou, A., Giannaros, T. M. and Melas, D.: The natural emissions  
16 model (NEMO): Description, application and model evaluation, *Atmos. Environ.*, 122, 493-  
17 504, doi:10.1016/j.atmosenv.2015.10.014, 2015.

18 Lyapustin, A., Wang, Y., Xiong, X., Meister, G., Platnick, S., Levy, R., Franz, B., Korkin, S.,  
19 Hilker, T., Tucker, J., Hall, F., Sellers, P., Wu, A., and Angal, A.: Scientific impact of  
20 MODIS C5 calibration degradation and C6+ improvements, *Atmos. Meas. Tech.*, 7, 4353-  
21 4365, doi:10.5194/amt-7-4353-2014, 2014.

22 Mamouri, R. E., Amiridis, V., Papayannis, A., Giannakaki, E., Tsaknakis, G., and Balis, D.  
23 S.: Validation of CALIPSO space-borne-derived attenuated backscatter coefficient profiles  
24 using a ground-based lidar in Athens, Greece, *Atmos. Meas. Tech.*, 2, 513-522,  
25 doi:10.5194/amt-2-513-2009, 2009.

26 Mamouri, R. E., Ansmann, A., Nisantzi, A., Kokkalis, P., Schwarz, A., and Hadjimitsis, D.:  
27 Low Arabian extinction-to-backscatter ratio, *Geophys. Res. Lett.*, 40, 4762-4766,  
28 doi:10.1002/grl.50898, 2013.

29 Mamouri, R. E. and Ansmann, A.: Estimated desert-dust ice nuclei profiles from polarization  
30 lidar: methodology and case studies, *Atmos. Chem. Phys.*, 15, 3463-3477, doi:10.5194/acp-  
31 15-3463-2015, 2015.

1 Mangold, A., De Backer, H., De Paepe, B., Dewitte, S., Chiapello, I., Derimian, Y.,  
2 Kacenelenbogen, M., Léon, J.-F., Huneus, N., Schulz, M., Ceburnis, D., O'Dowd, C.,  
3 Flentje, H., Kinne, S., Benedetti, A., Morcrette, J.-J. and Boucher, O.: Aerosol analysis and  
4 forecast in the European Centre for Medium-Range Weather Forecasts Integrated Forecast  
5 System: 3. Evaluation by means of case studies, *J. Geophys. Res.*, 116(D3), D03302,  
6 doi:10.1029/2010JD014864, 2011.

7 Marey, H. S., Gille, J. C., El-Askary, H. M., Shalaby, E. A., and El-Raey, M. E.: Aerosol  
8 climatology over Nile Delta based on MODIS, MISR and OMI satellite data, *Atmos. Chem.*  
9 *Phys.*, 11, 10637-10648, doi:10.5194/acp-11-10637-2011, 2011.

10 Mateos, D., Antón, M., Toledano, C., Cachorro, V. E., Alados-Arboledas, L., Sorribas, M.,  
11 Costa, M. J., and Baldasano, J. M.: Aerosol radiative effects in the ultraviolet, visible, and  
12 near-infrared spectral ranges using long-term aerosol data series over the Iberian Peninsula,  
13 *Atmos. Chem. Phys.*, 14, 13497-13514, doi:10.5194/acp-14-13497-2014, 2014.

14 Mélin, F., Zibordi, G. and Djavidnia, S.: Development and validation of a technique for  
15 merging satellite derived aerosol optical depth from SeaWiFS and MODIS, *Remote Sens.*  
16 *Environ.*, 108(4), 436-450, doi:10.1016/j.rse.2006.11.026, 2007.

17 Mishra, A. K., Klingmueller, K., Fredj, E., Lelieveld, J., Rudich, Y., and Koren, I.: Radiative  
18 signature of absorbing aerosol over the eastern Mediterranean basin, *Atmos. Chem. Phys.*, 14,  
19 7213-7231, doi:10.5194/acp-14-7213-2014, 2014.

20 Morcrette, J.-J., Boucher, O., Jones, L., Salmond, D., Bechtold, P., Beljaars, A., Benedetti, A.,  
21 Bonet, A., Kaiser, J. W., Razinger, M., Schulz, M., Serrar, S., Simmons, A. J., Sofiev, M.,  
22 Suttie, M., Tompkins, A. M. and Untch, A.: Aerosol analysis and forecast in the European  
23 Centre for Medium-Range Weather Forecasts Integrated Forecast System: Forward modeling,  
24 *J. Geophys. Res.*, 114(D6), D06206, doi:10.1029/2008JD011235, 2009.

25 Moulin, C., Lambert, C. E., Dayan, U., Masson, V., Ramonet, M., Bousquet, P., Legrand, M.,  
26 Balkanski, Y. J., Guelle, W., Marticorena, B., Bergametti, G. and Dulac, F.: Satellite  
27 climatology of African dust transport in the Mediterranean atmosphere, *J. Geophys. Res.*  
28 *Atmos.*, 103(D11), 13137-13144, doi:10.1029/98JD00171, 1998.

29 Nabat, P., Solmon, F., Mallet, M., Kok, J. F., and Somot, S.: Dust emission size distribution  
30 impact on aerosol budget and radiative forcing over the Mediterranean region: a regional

1 climate model approach, *Atmos. Chem. Phys.*, 12, 10545-10567, doi:10.5194/acp-12-10545-  
2 2012, 2012.

3 Nabat, P., Somot, S., Mallet, M., Chiapello, I., Morcrette, J. J., Solmon, F., Szopa, S., Dulac,  
4 F., Collins, W., Ghan, S., Horowitz, L. W., Lamarque, J. F., Lee, Y. H., Naik, V., Nagashima,  
5 T., Shindell, D., and Skeie, R.: A 4-D climatology (1979-2009) of the monthly tropospheric  
6 aerosol optical depth distribution over the Mediterranean region from a comparative  
7 evaluation and blending of remote sensing and model products, *Atmos. Meas. Tech.*, 6, 1287-  
8 1314, doi:10.5194/amt-6-1287-2013, 2013.

9 Nikitidou, E. and Kazantzidis, A.: On the differences of ultraviolet and visible irradiance  
10 calculations in the Mediterranean basin due to model- and satellite-derived climatologies of  
11 aerosol optical properties, *Int. J. Climatol.*, 33(13), 2877-2888, doi:10.1002/joc.3638, 2013.

12 Nisantzi, A., Mamouri, R. E., Ansmann, A., Schuster, G. L., and Hadjimitsis, D. G.: Middle  
13 East versus Saharan dust extinction-to-backscatter ratios, *Atmos. Chem. Phys.*, 15, 7071-  
14 7084, doi:10.5194/acp-15-7071-2015, 2015.

15 Papadimas, C. D., Hatzianastassiou, N., Mihalopoulos, N., Querol, X., and Vardavas, I.:  
16 Spatial and temporal variability in aerosol properties over the Mediterranean basin based on  
17 6-year (2000-2006) MODIS data, *J. Geophys. Res.*, 113(D11), D11205,  
18 doi:10.1029/2007JD009189, 2008.

19 Papadimas, C. D., Hatzianastassiou, N., Mihalopoulos, N., Kanakidou, M., Katsoulis, B. D.,  
20 and Vardavas, I.: Assessment of the MODIS Collections C005 and C004 aerosol optical depth  
21 products over the Mediterranean basin, *Atmos. Chem. Phys.*, 9, 2987-2999, doi:10.5194/acp-  
22 9-2987-2009, 2009.

23 Papadimas, C. D., Hatzianastassiou, N., Matsoukas, C., Kanakidou, M., Mihalopoulos, N. and  
24 Vardavas, I.: The direct effect of aerosols on solar radiation over the broader Mediterranean  
25 basin, *Atmos. Chem. Phys.*, 12(15), 7165-7185, doi:10.5194/acp-12-7165-2012, 2012.

26 Papayannis, A. and Balis, D.: Study of the structure of the lower troposphere over Athens  
27 using a backscattering Lidar during the MEDCAPHOT-TRACE experiment: Measurements  
28 over a suburban area, *Atmos. Envi.*, 32, 12, 2161-2172, 1998.

29 Papayannis, A., Balis, D., Amiridis, V., Chourdakis, G., Tsaknakis, G., Zerefos, C., Castanho,  
30 A. D. A., Nickovic, S., Kazadzis, S., and Grabowski, J.: Measurements of Saharan dust  
31 aerosols over the Eastern Mediterranean using elastic backscatter-Raman lidar,



1 spectrophotometric and satellite observations in the frame of the EARLINET project, *Atmos.*  
2 *Chem. Phys.*, 5, 2065-2079, doi:10.5194/acp-5-2065-2005, 2005.

3 Papayannis, A., Mamouri, R. E., Amiridis, V., Kazadzis, S., Pérez, C., Tsaknakis, G.,  
4 Kokkalis, P., and Baldasano, J. M.: Systematic lidar observations of Saharan dust layers over  
5 Athens, Greece in the frame of EARLINET project (2004-2006), *Ann. Geophys.*, 27, 3611-  
6 3620, doi:10.5194/angeo-27-3611-2009, 2009.

7 Pey, J., Querol, X., Alastuey, A., Forastiere, F., and Stafoggia, M.: African dust outbreaks  
8 over the Mediterranean Basin during 2001-2011: PM10 concentrations, phenomenology and  
9 trends, and its relation with synoptic and mesoscale meteorology, *Atmos. Chem. Phys.*, 13,  
10 1395-1410, doi:10.5194/acp-13-1395-2013, 2013.

11 Pozzer, A., de Meij, A., Yoon, J., Tost, H., Georgoulias, A. K., and Astitha, M.: AOD trends  
12 during 2001–2010 from observations and model simulations, *Atmos. Chem. Phys.*, 15, 5521-  
13 5535, doi:10.5194/acp-15-5521-2015, 2015.

14 Rea, G., Turquety, S., Menut, L., Briant, R., Mailler, S., and Siour, G.: Source contributions  
15 to 2012 summertime aerosols in the Euro-Mediterranean region, *Atmos. Chem. Phys.*, 15,  
16 8013-8036, doi:10.5194/acp-15-8013-2015, 2015.

17 Remer, L. A., Tanre, D., Kaufman, Y. J., Ichoku, C., Mattoo, S., Levy, R., Chu, D. A.,  
18 Holben, B., Dubovik, O., Smirnov, A., Martins, J. V., Li, R. R., Ahmad, Z.: Validation of  
19 MODIS aerosol retrieval over ocean, *Geophys. Res. Lett.*, 29(12), 2-5,  
20 doi:10.1029/2001GL013204, 2002.

21 Remer, L. A., Kaufman, Y. J., Tanré, D., Mattoo, S., Chu, D. A., Martins, J. V., Li, R.-R.,  
22 Ichoku, C., Levy, R. C., Kleidman, R. G., Eck, T. F., Vermote, E. and Holben, B. N.: The  
23 MODIS Aerosol Algorithm, Products, and Validation, *J. Atmos. Sci.*, 62(4), 947-973,  
24 doi:10.1175/JAS3385.1, 2005.

25 Remer, L., Kaufman, Y., and Kleidman, R.: Comparison of three years of terra and aqua  
26 MODIS aerosol optical thickness over the global oceans, *IEEE Geosci. Remote S.*, 3, 537-  
27 540, doi:10.1109/LGRS.2006.879562, 2006.

28 Remer, L. A., Kleidman, R. G., Levy, R. C., Kaufman, Y. J., Tanré, D., Mattoo, S., Martins,  
29 J. V., Ichoku, C., Koren, I., Yu, H. and Holben, B. N.: Global aerosol climatology from the  
30 MODIS satellite sensors, *J. Geophys. Res.*, 113(D14), D14S07, doi:10.1029/2007JD009661,  
31 2008.

1 Retalis, A. and Sifakis, N.: Urban aerosol mapping over Athens using the differential textural  
2 analysis (DTA) algorithm on MERIS-ENVISAT data, *ISPRS J. Photogramm. Remote Sens.*,  
3 65(1), 17-25, doi:10.1016/j.isprsjprs.2009.08.001, 2010.

4 Rudich, Y., Kaufman, Y. J., Dayan, U., Yu, H., and Kleidman, R. G.: Estimation of  
5 transboundary transport of pollution aerosols by remote sensing in the eastern Mediterranean,  
6 *J. Geophys. Res.*, 113, D14S14, doi:10.1029/2007JD009601, 2008.

7 Sayer, A. M., Hsu, N. C., Bettenhausen, C. and Jeong, M. J.: Validation and uncertainty  
8 estimates for MODIS Collection 6 “deep Blue” aerosol data, *J. Geophys. Res. Atmos.*,  
9 118(14), 7864-7872, doi:10.1002/jgrd.50600, 2013.

10 Sayer, A. M., Munchak, L. A., Hsu, N. C., Levy, R. C., Bettenhausen, C. and Jeong, M.-J.:  
11 MODIS Collection 6 aerosol products: Comparison between Aqua’s e-Deep Blue, Dark  
12 Target, and “merged” data sets, and usage recommendations, *J. Geophys. Res. Atmos.*,  
13 119(24), 13,965-13,989, doi:10.1002/2014JD022453, 2014.

14 Sciare, J., Oikonomou, K., Favez, O., Liakakou, E., Markaki, Z., Cachier, H., and  
15 Mihalopoulos, N.: Long-term measurements of carbonaceous aerosols in the Eastern  
16 Mediterranean: evidence of long-range transport of biomass burning, *Atmos. Chem. Phys.*, 8,  
17 5551-5563, doi:10.5194/acp-8-5551-2008, 2008.

18 Shi, Y., Zhang, J., Reid, J. S., Holben, B., Hyer, E. J., and Curtis, C.: An analysis of the  
19 collection 5 MODIS over-ocean aerosol optical depth product for its implication in aerosol  
20 assimilation, *Atmos. Chem. Phys.*, 11, 557-565, doi:10.5194/acp-11-557-2011, 2011.

21 Shi, Y., Zhang, J., Reid, J. S., Hyer, E. J., and Hsu, N. C.: Critical evaluation of the MODIS  
22 Deep Blue aerosol optical depth product for data assimilation over North Africa, *Atmos.*  
23 *Meas. Tech.*, 6, 949-969, doi:10.5194/amt-6-949-2013, 2013.

24 Sifakis, N. I., Iossifidis, C. and Kontoes, C.: CHRISTINE Code for High Resolution Satellite  
25 mapping of optical Thickness and Ångström Exponent. Part II: First application to the urban  
26 area of Athens, Greece and comparison to results from previous contrast-reduction codes,  
27 *Comput. Geosci.*, 62, 142-149, doi:10.1016/j.cageo.2013.05.011, 2014.

28 Smirnov, A.: Maritime component in aerosol optical models derived from Aerosol Robotic  
29 Network data, *J. Geophys. Res.*, 108(D1), 4033, doi:10.1029/2002JD002701, 2003.

1 Sorek-Hamer, M., Cohen, A., Levy, R. C., Ziv, B. and Broday, D. M.: Classification of dust  
2 days by satellite remotely sensed aerosol products, *Int. J. Remote Sens.*, 34(8), 2672-2688,  
3 doi:10.1080/01431161.2012.748991, 2013.

4 Tanré, D., Kaufman, Y. J., Herman, M. and Mattoo, S.: Remote sensing of aerosol properties  
5 over oceans using the MODIS/EOS spectral radiances, *J. Geophys. Res. Atmos.*, 102(D14),  
6 16971-16988, doi:10.1029/96JD03437, 1997.

7 Torres, O., Bhartia, P. K., Herman, J. R., Ahmad, Z., and Gleason, J.: Derivation of aerosol  
8 properties from a satellite measurements of backscattered ultraviolet radiation: Theoretical  
9 basis, *J. Geophys. Res.*, 103, 17099-17110, 1998.

10 Torres, O., Tanskanen, A., Veihelman, B., Ahn, C., Braak, R., Bhartia, P. K., Veeffkind, P.,  
11 and Levelt, P.: Aerosols and Surface UV Products from OMI Observations: An Overview, *J.*  
12 *Geophys. Res.*, 112, D24S47, doi:10.1029/2007JD008809, 2007.

13 Tsaknakis, G., Papayannis, A., Kokkalis, P., Amiridis, V., Kambezidis, H. D., Mamouri, R.  
14 E., Georgoussis, G., and Avdikos, G.: Inter-comparison of lidar and ceilometer retrievals for  
15 aerosol and Planetary Boundary Layer profiling over Athens, Greece, *Atmos. Meas. Tech.*, 4,  
16 1261-1273, doi:10.5194/amt-4-1261-2011, 2011.

17 Tyrlis, E. and Lelieveld, J.: Climatology and dynamics of the summer Etesian winds over the  
18 Eastern Mediterranean, *J. Atmos. Sci.*, 70, 3374-3396, doi:10.1175/JAS-D-13-035.1, 2013.

19 Varga, G., Ujvari, G., and Kovacs, J.: Spatiotemporal patterns of Saharan dust outbreaks in  
20 the Mediterranean Basin, *Aeolian Res.*, 15, 151-160, doi:10.1016/j.aeolia.2014.06.005, 2014.

21 Vrekoussis, M., Liakakou, E., Koçak, M., Kubilay, N., Oikonomou, K., Sciare, J. and  
22 Mihalopoulos, N.: Seasonal variability of optical properties of aerosols in the Eastern  
23 Mediterranean, *Atmos. Environ.*, 39(37), 7083-7094, doi:10.1016/j.atmosenv.2005.08.011,  
24 2005.

25 Zyrichidou, I., Koukouli, M. E., Balis, D. S., Katragkou, E., Melas, D., Poupkou, A.,  
26 Kioutsioukis, I., van der A, R., Boersma, F. K., van Roozendaal, M., and Richter, A.: Satellite  
27 observations and model simulations of tropospheric NO<sub>2</sub> columns over south-eastern Europe,  
28 *Atmos. Chem. Phys.*, 9, 6119-6134, doi:10.5194/acp-9-6119-2009, 2009.

29

1 **Table 1.** Full name, abbreviation, geolocation, host country and type of the 13 AERONET  
2 cimel sunphotometer sites used for the validation of MODIS Terra and Aqua Collection 051  
3 observations. The common measurement period of MODIS and AERONET data and the  
4 corresponding overpass time of MODIS Terra and Aqua (*Italics*) over each station are also  
5 given.

AERONET Station	Lat (°N)	Lon (°E)	Period of study	Country	Type	TERRA overpass	AQUA overpass
ATHENS-NOA (ATH)	37.988	23.775	05/2008-10/2012	Greece	Urban (coastal)	9:23±22min UT	<i>11:32±22min UT</i>
Bucharest Inoe (BUC)	44.348	26.030	07/2007-09/2012	Romania	Sub-urban (coastal)	9:17±24min UT	<i>11:15±20min UT</i>
CUT-TEPAK (CUT)	34.675	33.043	04/2010-12/2012	Cyprus	Urban (coastal)	8:43±25min UT	<i>10:55±25min UT</i>
Eforie (EFO)	44.075	28.632	09/2009/12/2012	Romania	Rural (coastal)	9:09±21min UT	<i>11:04±21min UT</i>
FORTH Crete (FOR)	35.333	25.282	01/2003-08/2011	Greece	Rural (coastal)	9:12±24min UT	<i>11:25±25min UT</i>
IMS-METU-ERDEMLI (IMS)	36.565	34.255	01/2004-01/2012	Turkey	Rural (coastal)	8:39±23min UT	<i>10:48±22min UT</i>
Lecce University (LEC)	40.335	18.111	03/2003-12/2012	Italy	Sub-urban (coastal)	9:44±25min UT	<i>11:49±25min UT</i>
Nes ziona (NES)	31.922	34.789	02/2000-12/2012	Israel	Sub-urban (coastal)	8:38±24min UT	<i>10:44±25min UT</i>
SEDE BOKER (SED)	30.855	34.782	01/2000-04/2012	Israel	Rural (semi-arid)	8:30±27min UT	<i>10:50±25min UT</i>
Sevastopol (SEV)	44.616	33.517	05/2006-12/2012	Ukr.-Crimea	Urban (coastal)	8:51±21min UT	<i>10:40±21min UT</i>
Thessaloniki (THE)	40.630	22.960	09/2005-12/2012	Greece	Urban (coastal)	9:28±25min UT	<i>11:32±22min UT</i>
TUBITAK UZAY Ankara (TUB)	39.891	32.778	12/2009-04/2012	Turkey	Urban (continental)	8:48±26min UT	<i>10:56±24min UT</i>
Xanthi (XAN)	41.147	24.919	01/2008-10/2010	Greece	Rural (coastal)	9:18±25min UT	<i>11:24±21min UT</i>

7  
8  
9  
10  
11  
12  
13  
14  
15  
16  
17  
18  
19  
20  
21  
22  
23  
24  
25  
26  
27

1 **Table 2.** Results of the comparison of spatially (using a spatial window around each station)  
2 and temporally ( $\pm 30$  min from the MODIS overpass time) collocated MODIS Terra and Aqua  
3 (Italics) Collection 051 level-2 and AERONET sunphotometric (quadratically interpolated)  
4 AOD<sub>550</sub> observations for the Eastern Mediterranean stations. The algorithms used for the  
5 production of the validated MODIS data (DT and DB), the spatial window used for the spatial  
6 collocation (25 x 25 km<sup>2</sup> or 50 x 50 km<sup>2</sup> window around each station) with the AERONET  
7 data, the average MODIS and AERONET AOD<sub>550</sub> and the corresponding  $\pm 1\sigma$  values, the  
8 mean difference between them, the normalized mean bias (NMB) and the corresponding root  
9 mean squared (RMS) error, the percentage of the collocation points that fall within the  
10 expected error (EE) envelope and the pre-launch expected error (pLEE) envelope (Expected  
11 Uncertainty - EU envelope for DB data), the correlation coefficient R, the slope a and the  
12 intercept of the regression line and the number of the collocation points are given in the table.  
13 L10 denotes the use of a collocation window of 50° x 50° as in Levy et al. (2010) while HQ  
14 denotes the use of high quality data only.

15

Alg.	Window	MODIS TERRA MODIS AQUA	AERONET	Mean Diff.	NMB %	RMS err.	in EE %	in pl EE %	R	a	b	Obs
DT	25 km	0.223±0.163	0.200±0.123	0.023±0.106	11.59	0.11	63.28	67.78	0.76	1.007	0.022	6697
<i>DT</i>	<i>25 km</i>	<i>0.247±0.173</i>	<i>0.197±0.121</i>	<i>0.050±0.109</i>	<i>25.18</i>	<i>0.12</i>	<i>57.14</i>	<i>61.87</i>	<i>0.78</i>	<i>1.113</i>	<i>0.027</i>	<i>6283</i>
DT	50 km (L10)	0.204±0.152	0.194±0.124	0.010±0.085	5.10	0.09	70.17	74.64	0.83	1.016	0.007	6054
<i>DT</i>	<i>50 km (L10)</i>	<i>0.224±0.155</i>	<i>0.194±0.125</i>	<i>0.030±0.088</i>	<i>15.34</i>	<i>0.09</i>	<i>66.76</i>	<i>70.45</i>	<i>0.82</i>	<i>1.018</i>	<i>0.026</i>	<i>5557</i>
DB	25 km	0.226±0.177	0.186±0.128	0.040±0.162	21.38	0.17	-	51.90	0.47	0.657	0.104	2580
<i>DB</i>	<i>25 km</i>	<i>0.242±0.217</i>	<i>0.182±0.118</i>	<i>0.06±0.196</i>	<i>33.03</i>	<i>0.20</i>	-	<i>55.30</i>	<i>0.44</i>	<i>0.815</i>	<i>0.094</i>	<i>5345</i>
DB <sub>HQ</sub>	25 km	0.229±0.158	0.186±0.132	0.043±0.141	22.82	0.15	-	52.41	0.54	0.651	0.108	498
<i>DB<sub>HQ</sub></i>	<i>25 km</i>	<i>0.260±0.220</i>	<i>0.186±0.138</i>	<i>0.074±0.204</i>	<i>39.84</i>	<i>0.22</i>	-	<i>52.34</i>	<i>0.42</i>	<i>0.670</i>	<i>0.136</i>	<i>896</i>

16

17

18

19

20

21

22

23

24

25

26

27

28

29

1 **Table 3.** AOD<sub>550</sub> levels, the corresponding  $\pm 1\sigma$  values and the number of gridded values used  
 2 for the calculations over Eastern Mediterranean (EMT), over the land covered part (EML),  
 3 over the oceanic part and over the 9 sub-regions of Eastern Mediterranean appearing in Fig. 1  
 4 based on the MODIS Terra and Aqua (*Italics*) observations.

5

Region	MODIS TERRA AOD <sub>550</sub>	Num. of values	<i>MODIS AQUA</i> <i>AOD<sub>550</sub></i>	Num. of values
EMT	0.215±0.187	61496654	<i>0.217±0.199</i>	<i>49522934</i>
EML	0.219±0.165	25923766	<i>0.239±0.189</i>	<i>21008713</i>
EMO	0.213±0.201	35572888	<i>0.202±0.205</i>	<i>28514221</i>
NBL	0.183±0.163	5563495	<i>0.187±0.162</i>	<i>3853688</i>
SBL	0.197±0.152	7345829	<i>0.207±0.152</i>	<i>5272449</i>
ANL	0.223±0.146	7948817	<i>0.228±0.148</i>	<i>5539261</i>
NAL	0.282±0.192	5065625	<i>0.306±0.238</i>	<i>6343315</i>
BSO	0.198±0.150	6433951	<i>0.183±0.134</i>	<i>5262438</i>
NWO	0.209±0.162	11645069	<i>0.197±0.154</i>	<i>9231630</i>
SWO	0.226±0.266	6202893	<i>0.223±0.310</i>	<i>4925665</i>
NEO	0.214±0.196	4807910	<i>0.199±0.166</i>	<i>3896554</i>
SEO	0.221±0.236	6483065	<i>0.210±0.239</i>	<i>5197934</i>

6

7

8

9

10

11

12

13

14

15

16

17

18

19

20

21

22

23

24

25

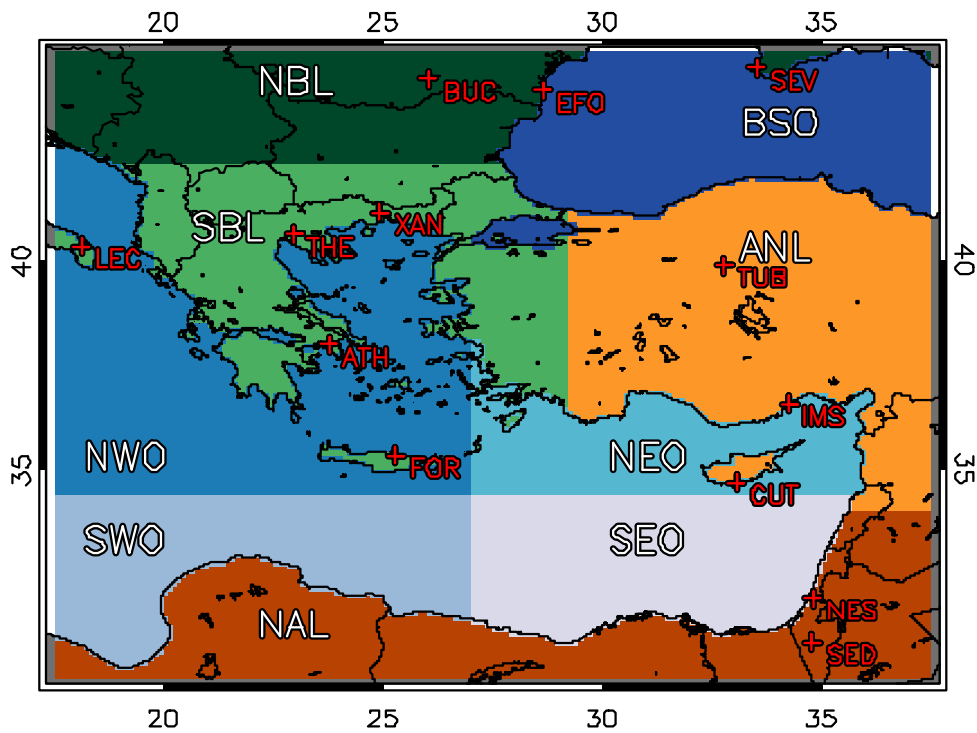
26

27

1 **Table 4.** Relative contribution of anthropogenic aerosols, dust, fine mode natural and marine  
2 aerosols to the total AOD<sub>550</sub> (bold) and the corresponding  $\tau_a$ ,  $\tau_d$ ,  $\tau_n$ ,  $\tau_m$  levels with their  $\pm 1\sigma$   
3 values (in parentheses) over Eastern Mediterranean (EMT), over the land covered part (EML),  
4 over the oceanic part and over the 9 sub-regions of Eastern Mediterranean appearing in Fig. 1  
5 based on the MODIS Terra and Aqua (Italics) observations. The sum of the aerosol type  
6 AODs per region does not necessarily correspond to the total AOD<sub>550</sub> values appearing in  
7 Table 3 as these results were for the total of the days with aerosol retrievals even for days  
8 when our aerosol type separation algorithm was not applicable.

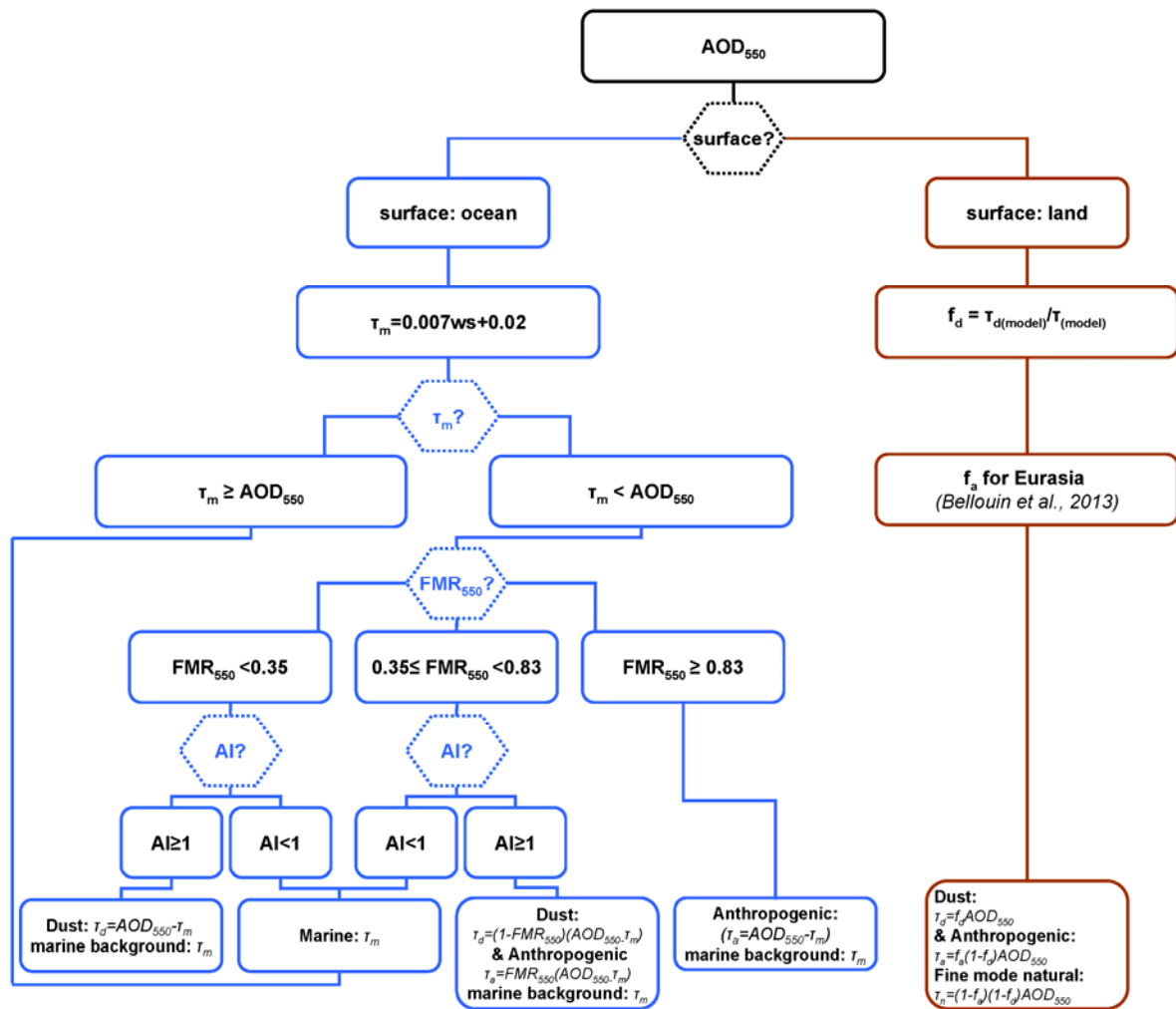
Region	Satellite	Contribution to MODIS TERRA/AQUA AOD <sub>550</sub>			
		Anthropogenic	Dust	Fine mode natural	Marine
EML	TERRA	<b>52 %</b> (0.112±0.087)	<b>32 %</b> (0.074±0.080)	<b>16 %</b> (0.034±0.026)	-
	AQUA	<b>50 %</b> (0.117±0.093)	<b>35 %</b> (0.090±0.102)	<b>15 %</b> (0.035±0.028)	-
EMO	TERRA	<b>41 %</b> (0.086±0.085)	<b>34 %</b> (0.076±0.185)	-	<b>25 %</b> (0.054±0.018)
	AQUA	<b>40 %</b> (0.079±0.080)	<b>33 %</b> (0.070±0.181)	-	<b>27 %</b> (0.054±0.018)
NBL	TERRA	<b>59 %</b> (0.108±0.101)	<b>23 %</b> (0.042±0.046)	<b>18 %</b> (0.032±0.030)	-
	AQUA	<b>59 %</b> (0.110±0.100)	<b>24 %</b> (0.045±0.047)	<b>17 %</b> (0.033±0.030)	-
SBL	TERRA	<b>55 %</b> (0.109±0.088)	<b>28 %</b> (0.056±0.058)	<b>17 %</b> (0.033±0.026)	-
	AQUA	<b>55 %</b> (0.113±0.088)	<b>29 %</b> (0.060±0.060)	<b>16 %</b> (0.034±0.026)	-
ANL	TERRA	<b>51 %</b> (0.113±0.075)	<b>34 %</b> (0.076±0.068)	<b>15 %</b> (0.034±0.023)	-
	AQUA	<b>50 %</b> (0.114±0.075)	<b>35 %</b> (0.079±0.070)	<b>15 %</b> (0.034±0.023)	-
NAL	TERRA	<b>50 %</b> (0.113±0.083)	<b>35 %</b> (0.083±0.085)	<b>15 %</b> (0.034±0.025)	-
	AQUA	<b>48 %</b> (0.118±0.091)	<b>38 %</b> (0.099±0.108)	<b>14 %</b> (0.035±0.027)	-
BSO	TERRA	<b>53 %</b> (0.108±0.103)	<b>22 %</b> (0.044±0.101)	-	<b>25 %</b> (0.051±0.016)
	AQUA	<b>51 %</b> (0.094±0.087)	<b>22 %</b> (0.042±0.085)	-	<b>27 %</b> (0.051±0.016)
NWO	TERRA	<b>41 %</b> (0.087±0.090)	<b>33 %</b> (0.071±0.142)	-	<b>26 %</b> (0.055±0.020)
	AQUA	<b>40 %</b> (0.079±0.083)	<b>32 %</b> (0.066±0.127)	-	<b>28 %</b> (0.055±0.020)
SWO	TERRA	<b>32 %</b> (0.071±0.070)	<b>42 %</b> (0.097±0.257)	-	<b>26 %</b> (0.058±0.018)
	AQUA	<b>32 %</b> (0.093±0.288)	<b>41 %</b> (0.072±0.080)	-	<b>27 %</b> (0.059±0.018)
NEO	TERRA	<b>48 %</b> (0.098±0.094)	<b>28 %</b> (0.061±0.144)	-	<b>24 %</b> (0.050±0.016)
	AQUA	<b>46 %</b> (0.086±0.082)	<b>28 %</b> (0.057±0.115)	-	<b>26 %</b> (0.050±0.016)
SEO	TERRA	<b>36 %</b> (0.079±0.070)	<b>39 %</b> (0.087±0.224)	-	<b>25 %</b> (0.055±0.016)
	AQUA	<b>36 %</b> (0.075±0.071)	<b>38 %</b> (0.080±0.217)	-	<b>26 %</b> (0.055±0.016)

10  
11  
12  
13  
14  
15  
16  
17  
18  
19  
20  
21  
22  
23



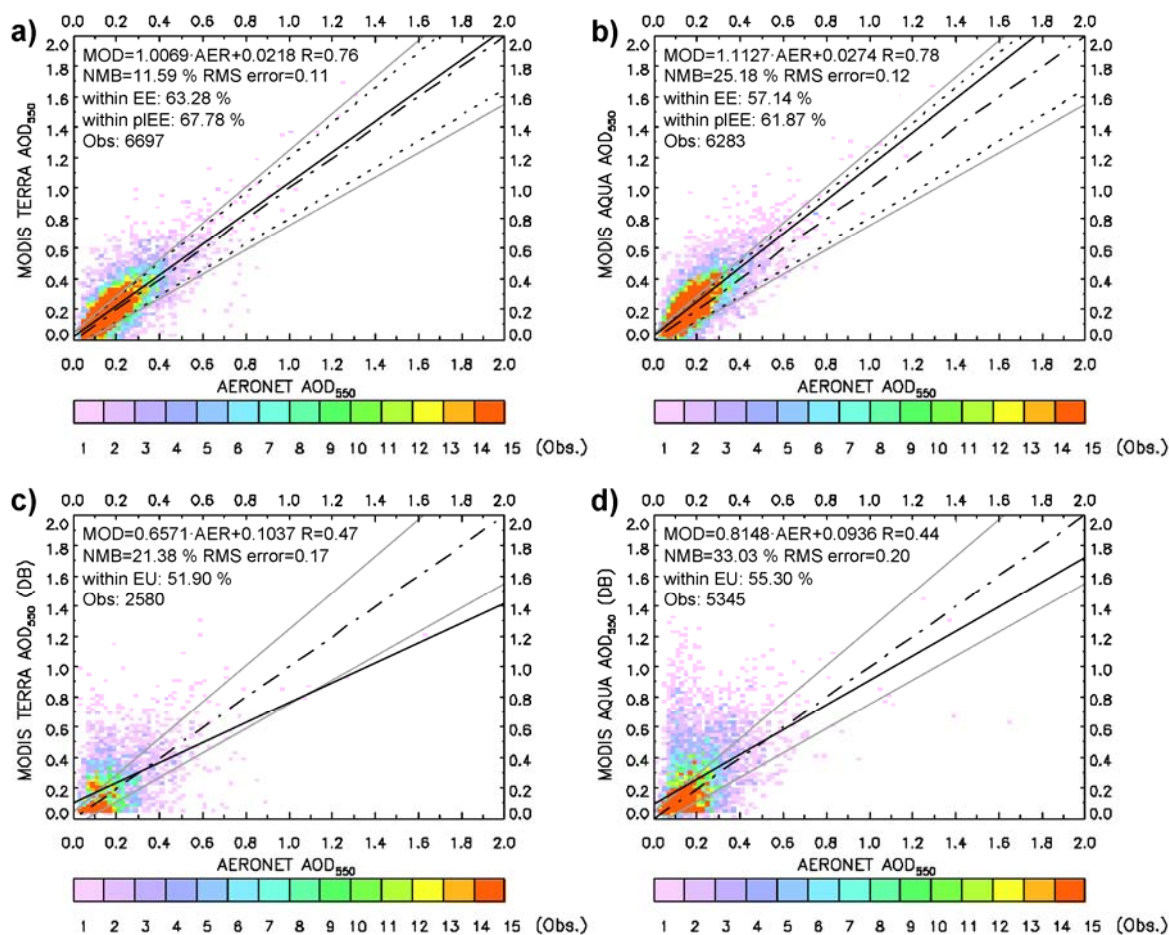
1  
2 **Figure 1.** Eastern Mediterranean map with the 9 sub-regions selected for the generalization of  
3 our results and the location of the AERONET stations used for the validation of MODIS  
4 satellite data. The 9 sub-regions are: NBL (Northern Balkans Land), SBL (Southern Balkans  
5 Land), ANL (Anatolia Land), NAL (Northern Africa Land), BSO (Black Sea Oceanic), NWO  
6 (North-Western Oceanic), SWO (South-Western Oceanic), NEO (North-Eastern Oceanic) and  
7 SEO (South-Eastern Oceanic). The full names and the geolocation of the 13 AERONET  
8 stations appearing in the map are available in Table 1.





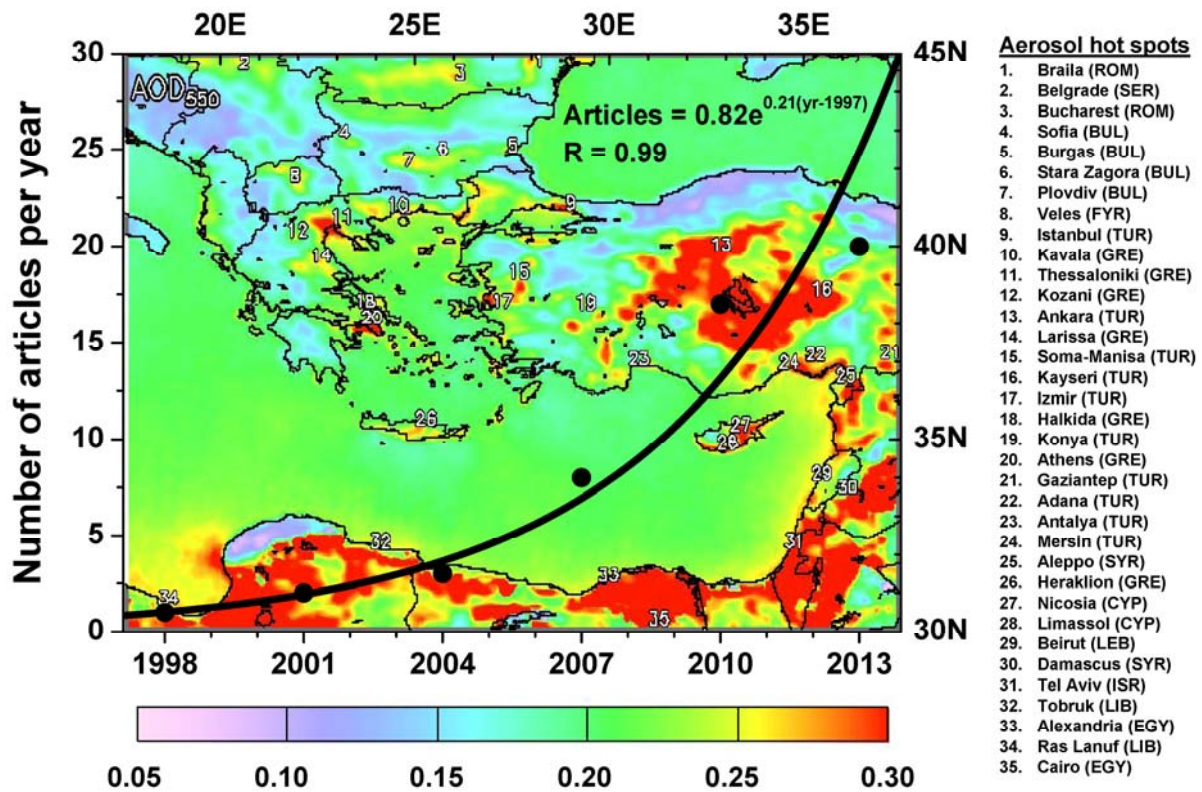
1  
2  
3  
4  
5  
6

**Figure 2.** Flowchart with the methodology followed for the calculation of the anthropogenic aerosol, dust and marine aerosol optical depths ( $\tau_a$ ,  $\tau_d$  and  $\tau_m$ ) over the sea (blue color) and the anthropogenic aerosol, dust and fine mode natural aerosol optical depths ( $\tau_a$ ,  $\tau_d$  and  $\tau_n$ ) over land (brown color).

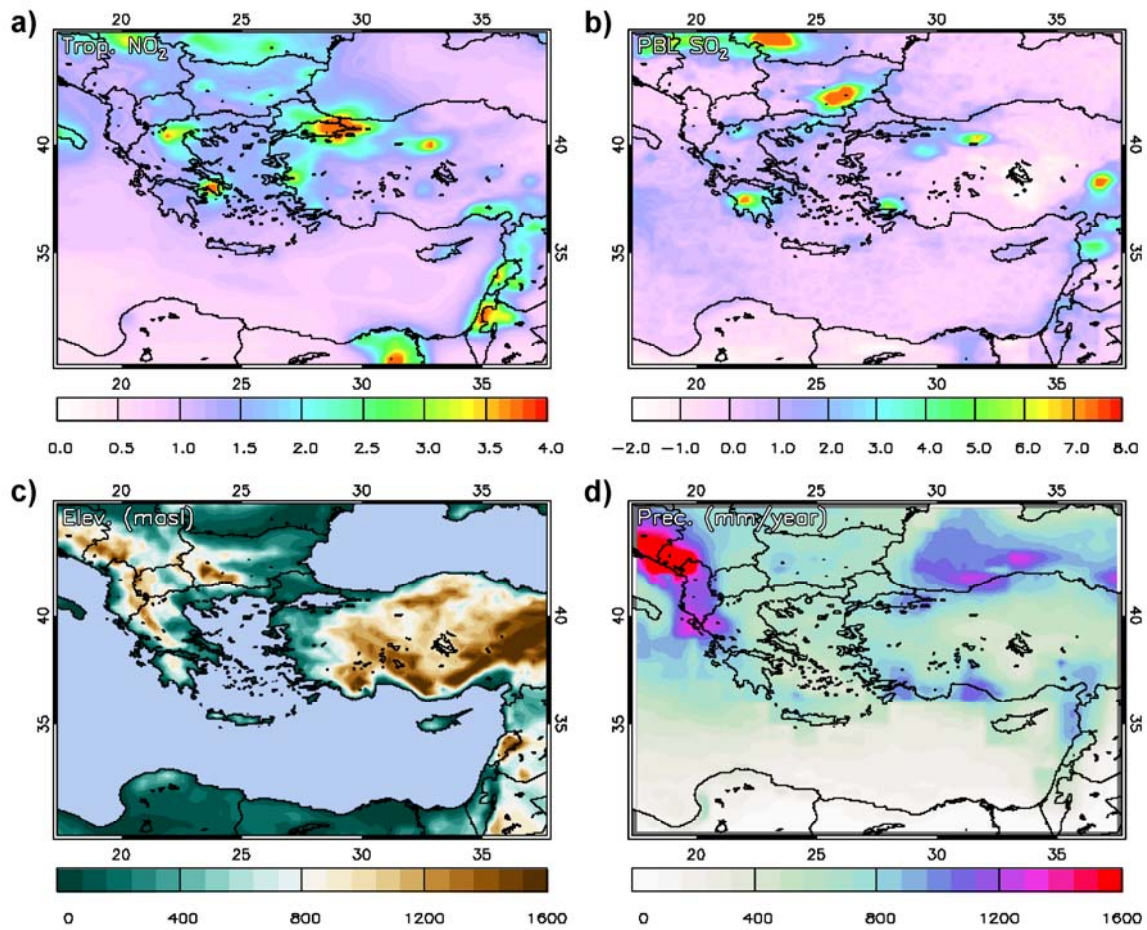


1  
2  
3 **Figure 3.** Comparison of spatially (using a 25 x 25 km<sup>2</sup> window around each station) and  
4 temporally ( $\pm 30$  min from the MODIS overpass time) collocated MODIS Collection 051  
5 level-2 and AERONET sunphotometric (quadratically interpolated) AOD<sub>550</sub> observations for  
6 the Eastern Mediterranean stations: (a) for MODIS Terra DT data, (b) for MODIS Aqua DT  
7 data, (c) for MODIS Terra DB data and (d) for MODIS Aqua DB data. The color scale  
8 corresponds to the number of MODIS-AERONET collocation points that fall within 0.02 x  
9 0.02 grid boxes. The solid line is the regression line of the MODIS-AERONET observations,  
10 the dashed-dotted line is the 1:1 line, the dotted lines represent the expected error (EE)  
11 envelope and the grey lines the pre-launch expected error (pLEE) envelope (Expected  
12 Uncertainty - EU envelope for DB data). The slope and the intercept of the regression line, the  
13 correlation coefficient R, the normalized mean bias (NMB), the root mean squared (RMS)  
14 error, the percentage of the collocation points that fall within the EE and pLEE and the number  
15 of all the collocation points.

16



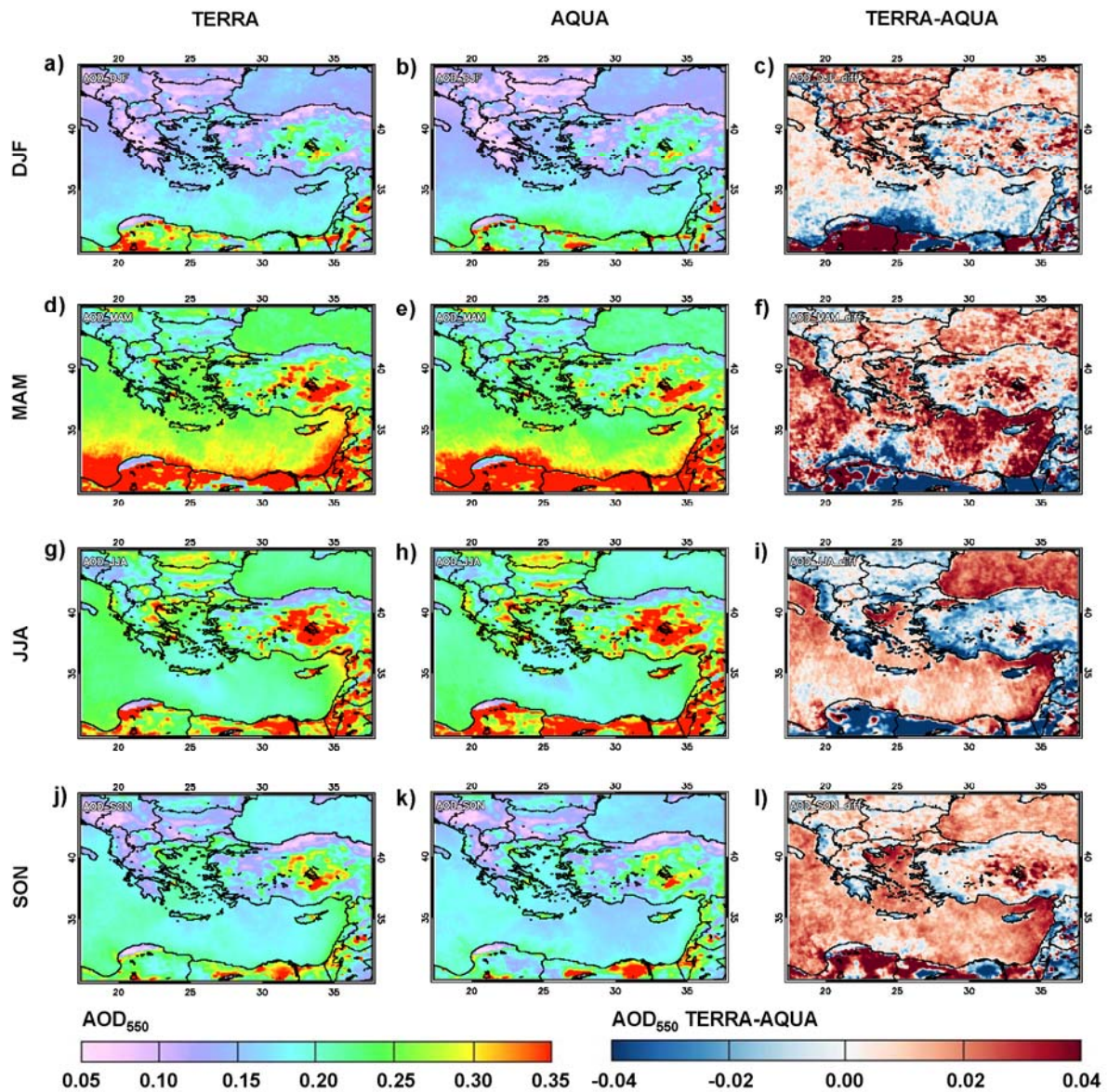
1  
2  
3 **Figure 4.** AOD<sub>550</sub> patterns over Eastern Mediterranean as seen by MODIS Terra during the  
4 period 3/2000-12/2012 (3/2000-12/2007 for regions of North Africa covered by DB data  
5 only). The colorscale corresponds to the AOD<sub>550</sub> levels while the top x-axis and the right y-  
6 axis correspond to the longitude (°E) and latitude (°N), respectively. The position of 35  
7 aerosol hot spots is marked on the map (numbers from 1 to 35) while the names of the places  
8 and the countries where the hot spots are located appear on the right of the map. In the same  
9 figure the exponential growth of the number of satellite-based articles focusing on aerosols  
10 over the greater Eastern Mediterranean from 1997 to 2014 is shown (black line). The black  
11 dots represent the number of articles published within three year intervals. The bottom x-axis  
12 and the left y-axis correspond to the years and the number of published articles, respectively.  
13 The exponential growth corresponds to a near doubling of the publication rate every 3 years.



1  
2

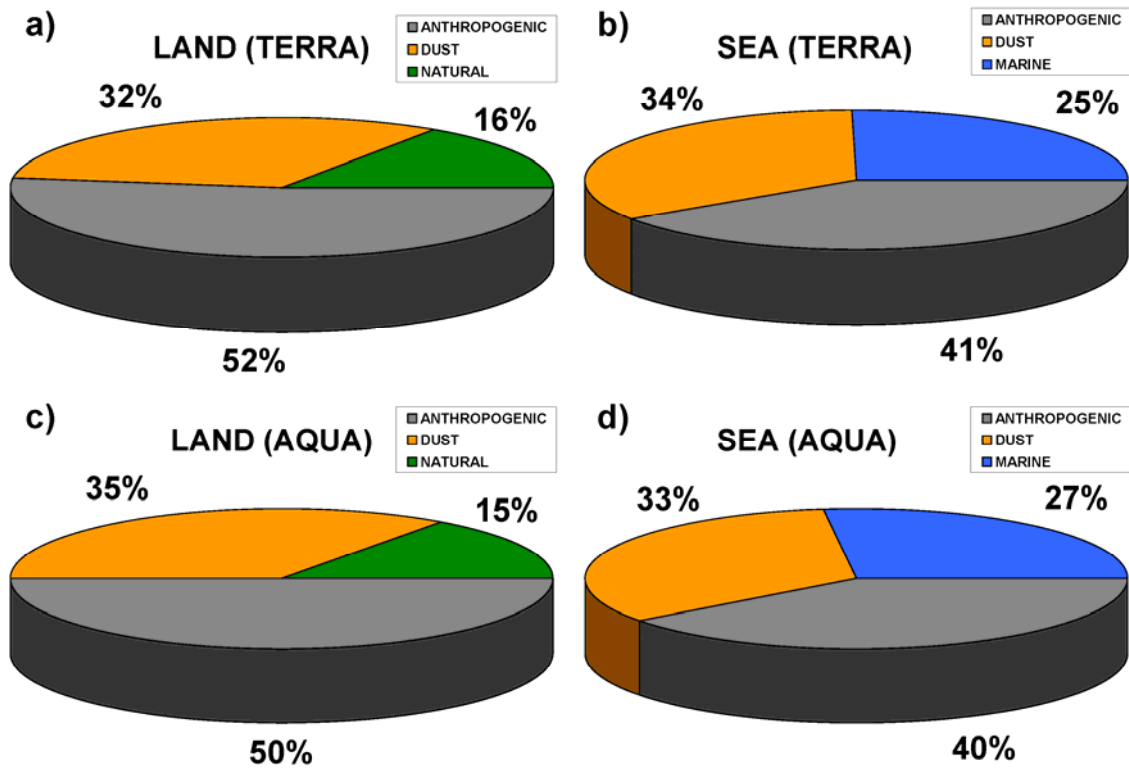
3 **Figure 5.** (a) Tropospheric NO<sub>2</sub> levels and (b) Planetary boundary layer SO<sub>2</sub> levels (in 10<sup>15</sup>  
 4 molecules/cm<sup>2</sup>) over the Eastern Mediterranean as seen from OMI/AURA (2005-2012), (c)  
 5 Topography (GTOPO elevation data in meters above sea level) and (d) Annual precipitation  
 6 levels (in mm/year) from 3B43 TRMM and Other Sources Monthly Rainfall Product (2000-  
 7 2012).





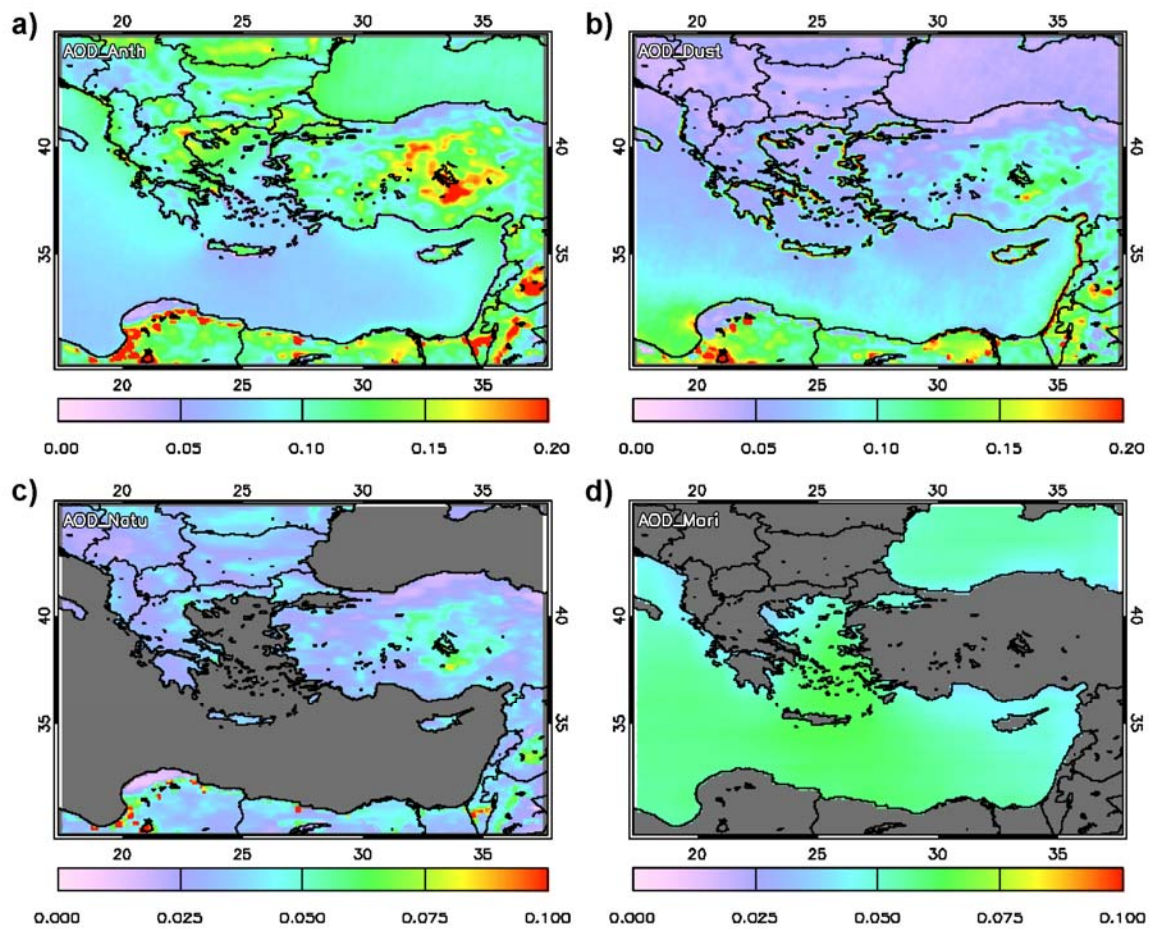
1  
2  
3  
4  
5  
6  
7

**Figure 6.** Seasonal AOD<sub>550</sub> patterns over the Eastern Mediterranean as seen by MODIS Terra (left column) during the period 3/2000-12/2012 (3/2000-12/2007 for regions of North Africa covered by DB data only) and MODIS Aqua (middle column) during the period 7/2002-12/2012. The differences between MODIS Terra and Aqua AOD<sub>550</sub> on a seasonal basis appear on the right column.



1  
2

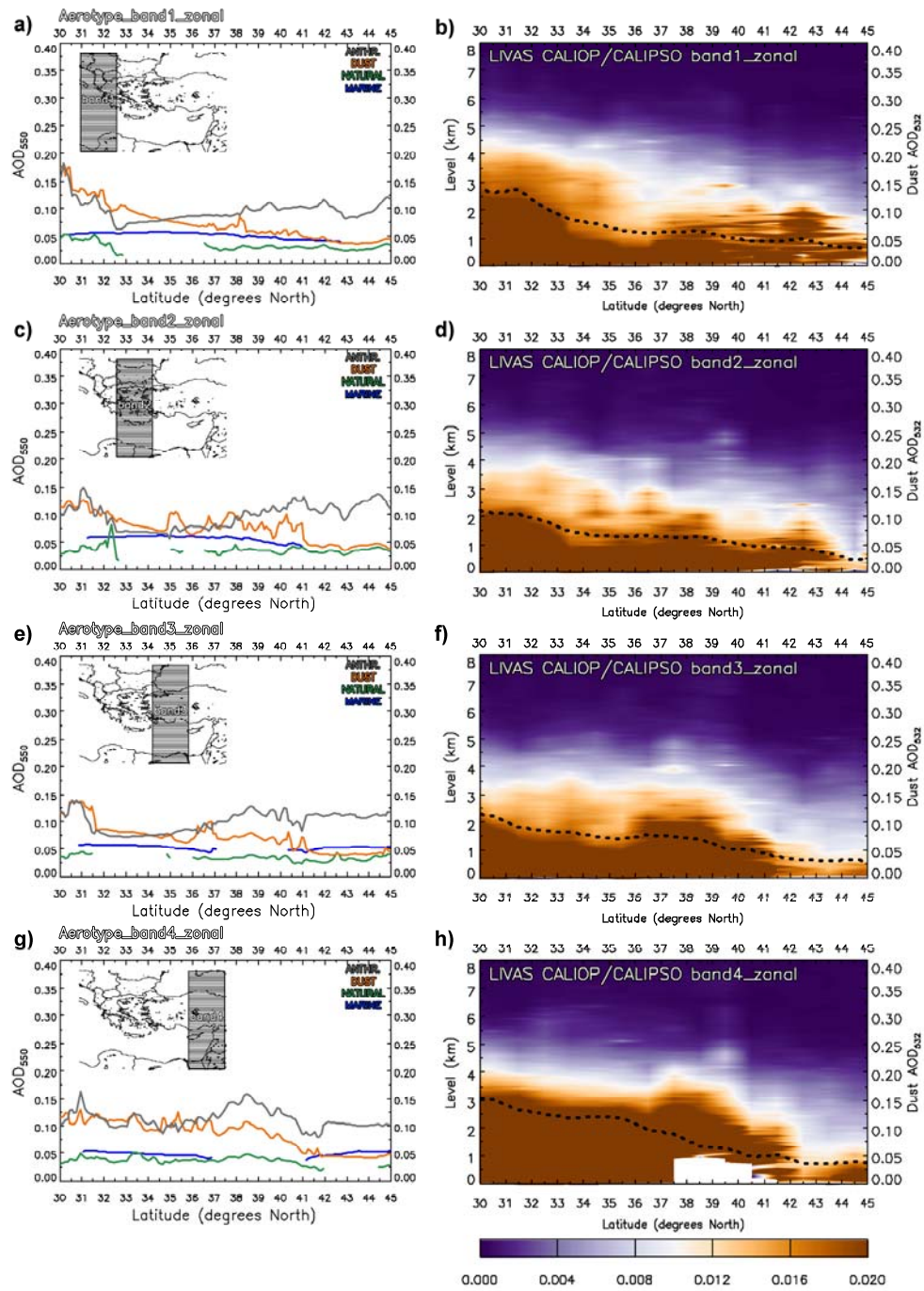
3 **Figure 7.** Relative contribution of anthropogenic aerosols, dust and fine mode natural  
 4 aerosols to the total AOD<sub>550</sub> over the land covered part of Eastern Mediterranean based on  
 5 MODIS Terra (a) and MODIS Aqua (c) observations and relative contribution of  
 6 anthropogenic aerosols, dust and marine aerosols to the total AOD<sub>550</sub> over the oceanic part of  
 7 Eastern Mediterranean based on MODIS Terra (b) and MODIS Aqua (d) observations.



1  
2

3 **Figure 8.** (a) Anthropogenic aerosol ( $\tau_a$ ), (b) dust ( $\tau_d$ ), (c) fine mode natural aerosol ( $\tau_n$ ) and  
 4 (d) marine aerosol ( $\tau_m$ ) patterns over the Eastern Mediterranean based on MODIS Terra  
 5 observations during the period 3/2000-12/2012 (3/2000-12/2007 for regions of North Africa  
 6 covered by DB data only).

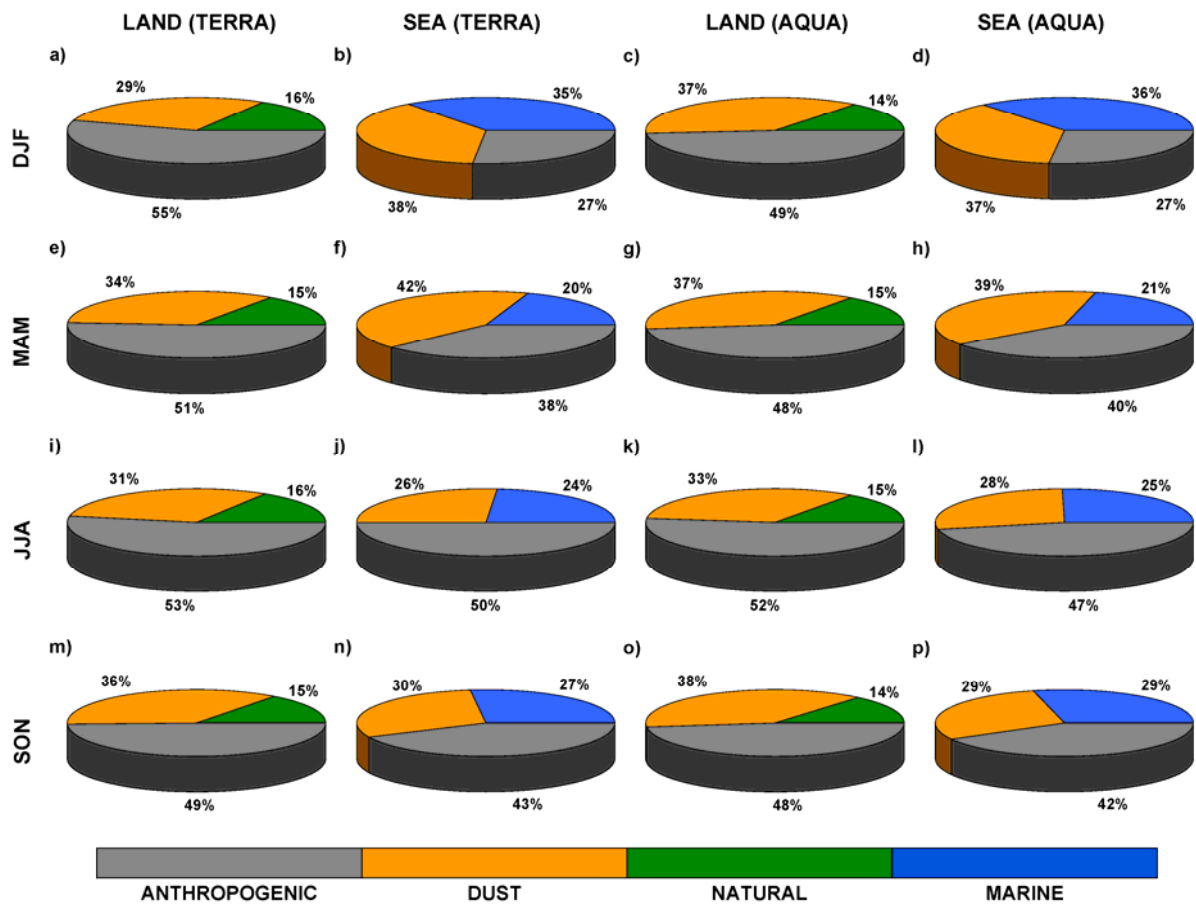




1  
2  
3  
4  
5  
6  
7  
8  
9

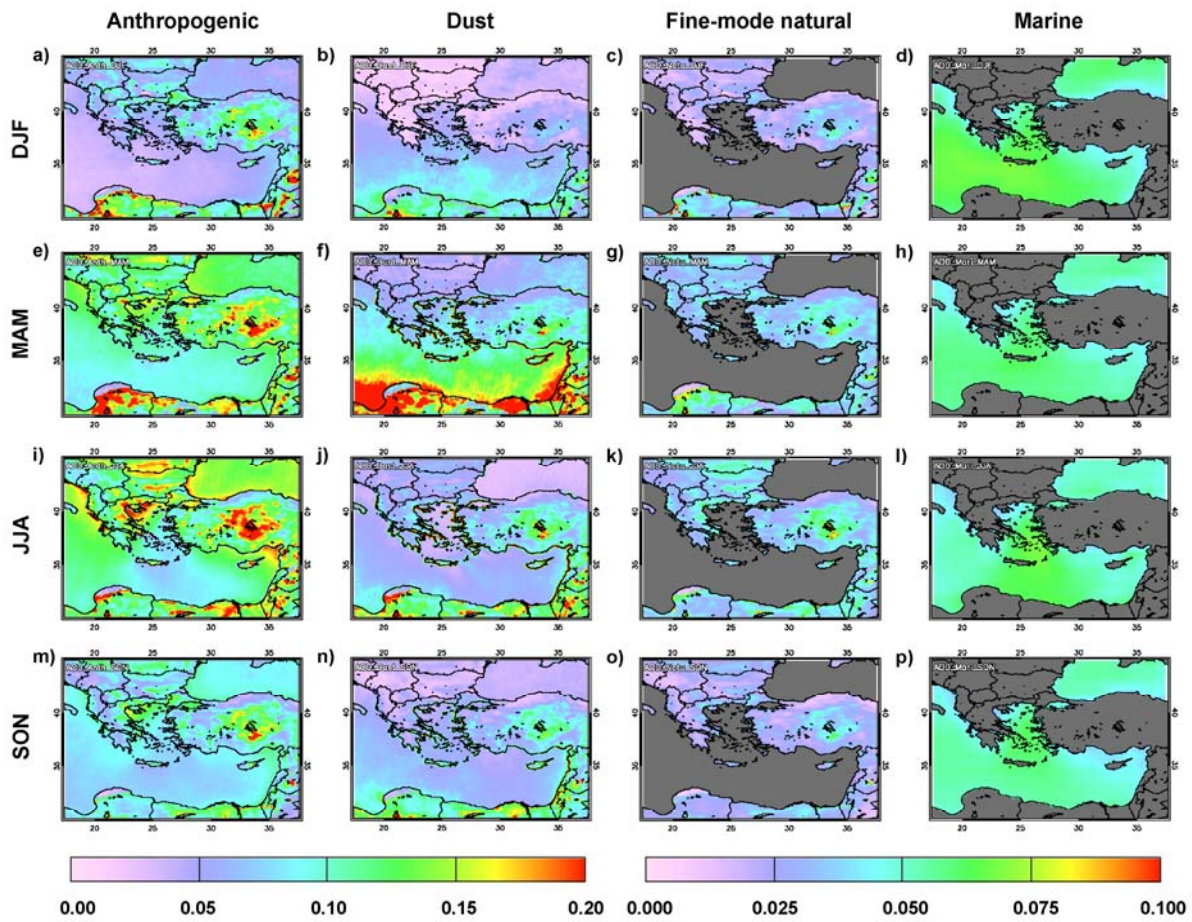
**Figure 9.** Left column: Latitudinal variability of anthropogenic aerosols ( $\tau_a$ ), dust ( $\tau_d$ ), fine mode natural aerosols ( $\tau_n$ ) and marine aerosols ( $\tau_m$ ) for four 5-degree longitudinal bands (see embedded maps) covering Eastern Mediterranean based on MODIS Terra observations. Right column: Latitudinal variability of dust extinction coefficients at 532 nm in  $\text{km}^{-1}$  (colorscale corresponds to the extinction coefficients and left y-axis to the atmospheric levels) and dust aerosol optical depth at 532 nm (dotted line corresponding to the right-y-axis) for the same four bands from LIVAS CALIOP/CALIPSO observations.





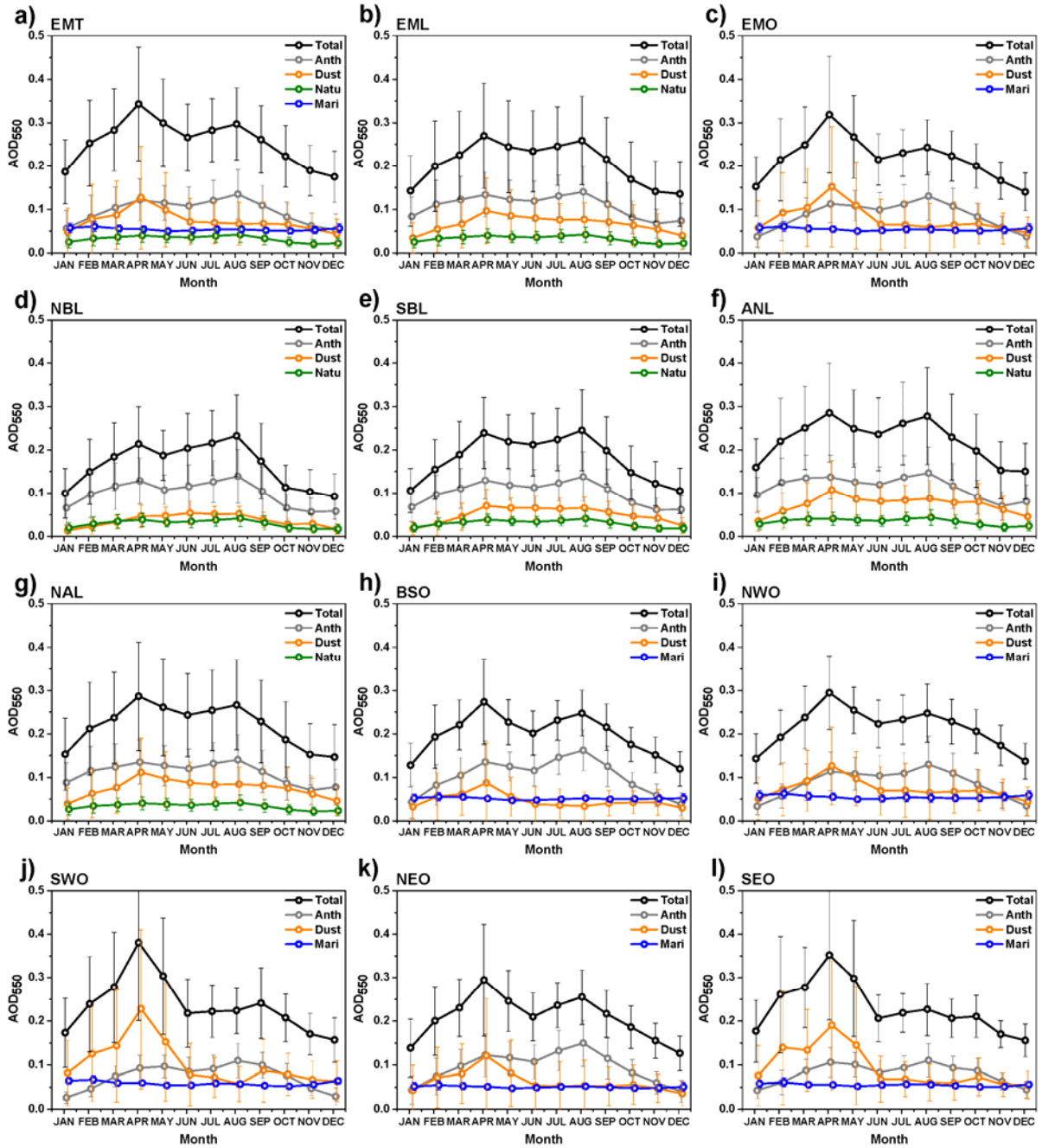
1  
2  
3  
4  
5  
6  
7  
8

**Figure 10.** Seasonal relative contribution of anthropogenic aerosols, dust and fine mode natural aerosols to the total AOD<sub>550</sub> over the land covered part of Eastern Mediterranean based on MODIS Terra (a, e, i, m) and MODIS Aqua (c, g, k, o) observations and seasonal relative contribution of anthropogenic aerosols, dust and marine aerosols to the total AOD<sub>550</sub> over the oceanic part of Eastern Mediterranean based on MODIS Terra (b, f, j, n) and MODIS Aqua (d, h, l, p) observations.



1  
2

3 **Figure 11.** Seasonal (a, e, i, m) anthropogenic aerosol ( $\tau_a$ ), (b, f, j, n) dust ( $\tau_d$ ), (c, g, k, o) fine  
 4 mode natural aerosol ( $\tau_n$ ) and (d, h, l, p) marine aerosol ( $\tau_m$ ) patterns over the Eastern  
 5 Mediterranean based on MODIS Terra observations during the period 3/2000-12/2012  
 6 (3/2000-12/2007 for regions of North Africa covered by DB data only).



1

2

3 **Figure 12.** Seasonal variability of anthropogenic aerosols ( $\tau_a$ ), dust ( $\tau_d$ ), fine mode natural  
 4 aerosols ( $\tau_n$ ) and marine aerosols ( $\tau_m$ ) over Eastern Mediterranean (EMT), over the land  
 5 covered part (EML), over the oceanic part (EMO) and over the 9 sub-regions of the Eastern  
 6 Mediterranean appearing in Fig. 1 based on MODIS Terra observations. The error bars  
 7 represent the  $\pm 1\sigma$  values calculated from monthly gridded data.